Investigating CLIC Proteins on Exosomes as Biomarkers for Ovarian Cancer

Juan Diego Escobar Bermeo

Thesis for the degree of Master of Science (Research)

University of Technology Sydney

February 2023

CERTIFICATE OF ORIGINAL AUTHORSHIP

I, Juan Diego Escobar Bermeo, declare that this thesis is submitted in fulfilment of the requirements for the award of Master of science (Research), in the School of Life Sciences at the University of Technology Sydney.

This thesis is entirely my own work unless otherwise referenced or acknowledged. In addition, I certify that all information sources and literature used are indicated in the thesis. li

This document has not been submitted for qualifications at any other academic institution.

This research is supported by the Australian Government Research Training Program.

Signature:

Production Note:
Signature removed prior to publication.

Juan Diego Escobar Bermeo

ACKNOWLEDGEMENT

I firstly would like to start by thanking my supervisor, Professor Stella Valenzuela, for considering my unconventional initiation and giving me the opportunity to join her research team and carry out my master's degree. It is because of your guidance and boundless kindness that despite all adversities I was able to complete this project.

I also would like to express gratitude to my Lab group colleagues, Rufaka and Amani, for endlessly helping me around the lab; always being eager to provide advice and equally as important, for keeping the most hospitable work environment I have ever experienced.

I would also like to gratefully acknowledge all the academics from the Faculty of Science at UTS for their helpful comments and feedbacks, as well as for their assistance and friendly attitudes in creating a supportive environment. I would like to specifically thank my co-supervisor Professor Deborah Marsh and her group, especially Kristie Dickson for providing an expert eye and critical feedback for my study, as well as access to Human cell lines. I would also like to thank Dr Kristina Warton for allowing me to work outside UTS and helping with access to UNSW facilities.

Lastly, but just as important, I want to thank all the people in my life whose special support made this dream possible. Adrian, Kev & Carmela, Jag, Patrick, Ann, Maddy, Valen, Orlis and Mom I am forever in debt as without your help I could have never even considered this dream a possibility.

With peace and love,

¡Gracias a todos!

Table of Contents

List of Abbreviations

ANOVA	Analysis of Variance
BCA	Bicinchoninic acid assay
BSA	Bovine Serum Albumin
CAFs	Cancer associated fibroblasts
CLIC	Chloride Intracellular Ion Channel
CO2	Carbon Dioxide
DLS	Dynamic Light Scattering
DMEM/F12	Dulbecco's Modified Eagle's Medium Hams F12
DMSO	Dimethyl sulfoxide
DNA	Deoxyribonucleic acid
ECM	Extracellular Matrix
EDTA	Ethylenediaminetetraacetic acid
ESCRT	Endosomal sorting complexes required for transport
FBS	Foetal Bovine Serum
FLAG	DYKDDDDK (where D=aspartic acid, Y=tyrosine, and K=lysine)
FTSECs	fallopian tube secretory epithelium cells
GSH	Glutathione
GST	Glutathione S-Transferase
HCl	Hydrochloric Acid
HGSOC	high-grade serous ovarian cancer
KDa	Kilodaltons
mL	Millilitre
mM	Millimolar
MVBs	Multivesicular Bodies
NaCl	Sodium Chloride
ng	Nanogram

NTA	Nanoparticle Tracking Analysis
PBS	Phosphate Buffer Saline
PBST	Phosphate Buffer Saline+Tween20
pH	Potential of Hydrogen
PVDF	Polyvinylidene difluoride
rcf	Relative Centrifugal Force
RIPA	Radioimmunoprecipitation assay
RNA	Ribonucleic Acid
ROS	Reactive Oxygen Species
rpm	Rotations per Minute
RPMI	Roswell Park Memorial Institute
SDS	Sodium dodecyl sulfate
SDS-PAGE	Sodium Dodecyl Sulphate Polyacrylamide Gel Electrophoresis
SOP	Standard Operating Procedure
TSG101	Tumor Susceptibility 101
UGS	Ultroser™ G Serum
UNSW	The University of New South Wales
UTS	The University of Technology Sydney
V	Volt
WCL	Whole Cell Lysate
µg	Microgram
µl	Microliter

Publications Arising from this Thesis.

- Juan Diego Escobar Bermeo[1, 2], Khondker Rufaka Hossain[1], Kristina Warton[3], Kristie-Ann Dickson[4], Deborah J Marsh[4, 5], Stella M Valenzuela[1, 2]

  1. School of Life Sciences, Faculty of Science, University of Technology Sydney, Sydney, NSW, Australia,

  2. ARC Research Hub for Integrated Device for End-user Analysis at Low-levels (IDEAL), Faculty of Science, University of Technology Sydney, Sydney, NSW, Australia.

  3. Gynaecological Cancer Research Group, Lowy Cancer Research Centre and School of Women's and Children's Health, Faculty of Medicine, University of New South Wales, Sydney, NSW, Australia

  4. Translational Oncology Group, School of Life Sciences, Faculty of Science, University of Technology Sydney, Ultimo, NSW 2007, Australia

  5. Northern Clinical School, Faculty of Medicine and Health, University of Sydney, Camperdown, NSW 2006, Australia

  "CLIC proteins on Exosomes as biomarkers for ovarian cancer"; Contributed to writing of the abstract and prepared the poster to be presented at the 30th ASMR NSW Annual Scientific Meeting, Friday 3rd June 2022

- Khondker Rufaka Hossain [1], Juan Diego Escobar Bermeo[1, 2], Kristina Warton[3] and Stella M Valenzuela[1, 2]

  1. School of Life Sciences, Faculty of Science, University of Technology Sydney, Sydney, NSW, Australia
  2. ARC Research Hub for Integrated Device for End-user Analysis at Low-levels (IDEAL), Faculty of Science, University of Technology Sydney, Sydney, NSW, Australia.
  3. School of Women's and Children's Health, Faculty of Medicine and Health, University of New South Wales, South Wales, NSW, Australia

  Contributed to writing of "New Approaches and Biomarker Candidates for the Early Detection of Ovarian Cancer". submitted to Frontiers in Bioengineering and Biotechnology.

List of Illustrations

List of Tables

Abstract

Ovarian cancer is the ninth most common cancer affecting women in Australia, and early detection is the principal factor for a favourable patient survival outcome. Current diagnosis involves ultrasound examination, alongside CA-125 blood test, which is significantly limited in terms of specificity and sensitivity for patients at early stages; however ultimately, histological examination of the suspected mass remains the gold standard.

Exosomes are a type of extracellular vesicles secreted by most human cells including cancer cells and can be found in a wide range of body fluids. They play a key role in intercellular communication, as the exchange of certain biomolecules that they mediate drive various physiological and pathological pathways. These characteristics as well as their stability in biological fluids make them an attractive candidate for non-invasive diagnostic tests as well as a possible therapeutic target.

One of the protein families that are found as exosome cargo, is the Chloride Intracellular Channel (CLIC) Family, which in recent research have been found overexpressed in a wide range of cancers. Recent studies have demonstrated that CLIC1 and CLIC4 proteins are enriched in exosomes derived from ovarian cancer cells when compared to exosomes derived from healthy control patients. Furthermore, since exosomes are taken up by recipient cells, they potentially partake in progression of the disease, all which suggests that CLIC proteins found on exosomes could serve as useful biomarkers for early detection of ovarian cancer.

Our study found that, CLIC1 is carried by exosomes shed from a range of ovarian cancer cell lines, and that in contrast exosomal levels of the cancerous cell lines, there is a trend for higher levels of CLIC1 compared to those derived from the control cell line. On the other hand, the opposite trend was observed, where exosomal CLIC4 from the control line presented the greatest levels of CLIC4 relative to the ovarian cancer cell lines; by double when compared to PEO1 and PEO4 samples and slightly greatest than Kuramochi and OVCAR3.

In conclusion, CLIC proteins in exosomes represent a potential pathway for early detection and monitoring of ovarian cancer. However, further research involving clinical samples as well as more iterations are necessary to support our findings and to determine the clinical utility of CLIC proteins in exosomes as diagnostic markers for ovarian cancer.

Chapter 1

Literature Review

a) Overview of Ovarian Cancer

Ovarian cancer is the most lethal gynaecologic malignancy (1), of which there are four main types: epithelial, germ cell, sex chord and stromal, with each having different epidemiological statistics. Epithelial ovarian cancer is the most common subtype that accounts for 90% of all cases and primarily occurs in post-menopausal women (2); included are also various histotypes; high-grade serous ovarian cancer (HGSOC), endometrioid ovarian cancer, ovarian clear cell carcinoma, low-grade serous ovarian cancer and mucinous ovarian cancer (3, 4). Surprisingly, more than 80% of patients have symptoms including during early stage; however, the generic nature of these, mean that they are shared with many other common gastrointestinal and gynaecological conditions and don't normally lead to diagnosis (5, 6). As such, early diagnosis isn't common mostly due to the relatively asymptomatic nature of the disease which results in most cases being detected at an advanced stage, when the tumour has already begun to spread to other locations in the body (7); in addition, the lack of established early-stage markers and screening methodologies are also responsible for the low numbers of cases detected at an early stage. For these reasons, identification of new diagnostic markers which allows for detection of the disease at an early stage or to better monitor disease progression, is currently a major focus for this type of cancer research (8).

1.a.1 Burden of Ovarian cancer and Prognosis

The increasing burden of worldwide cancer incidence and mortality is a continuous challenge for research and reflects the increasing aging population (2). A recent review of "Global Cancer Statistics: 2020" which examined the incidence and mortality for various cancers across 185 countries highlighted that in 2020 there were 313,959 new cases and 207,252 deaths attributed to cancer of the ovary (9). In 2022, ovarian cancer was the ninth most diagnosed cancer in Australian women, with 1815 new cases and 1,016 reported deaths (10). About 58% of ovarian cancer patients are diagnosed at advanced stages III or IV which have 5-year survival of 27% and 13% respectively(11). In contrast, the survival rate improves to

70% if diagnosis occurs at earlier stages; unfortunately however, the detection rate for these stages is only approximately 20% (12). These statistics highlight the importance and medical significance that increased early diagnosis can have for patient prognosis (13, 14).

1.a.2 Diagnosis and Treatments

Currently there aren't any screening methods recommended for ovarian cancer, unlike for cervical or breast cancer. The first measure taken is imaging with transvaginal ultrasonography if there is strong suspicion via blood work analysis of the serum biomarker Cancer antigen (CA125) or initial detection of an abdominal mass by examination (1). However, the combination of these examinations can still miss early stages of the disease or lead to misdiagnosis as CA125 can be present in other conditions including endometriosis, liver cancer and gall bladder cancer (15, 16, 17, 18), with the examination of this marker proving most useful in women who are genetically predisposed to developing Ovarian cancer. In addition, around 15-20% of ovarian cancers do not express CA125 (19, 20). Genetic predisposition is another significant indicator of lifetime risk of developing ovarian cancer, accounting for about 10% to 12% of all cases. Specifically, *BRCA1* and *BRCA2* mutations (tumour suppressor genes) are involved in about 10% of cases of ovarian cancer (13, 21, 22, 23). Bilateral salpingo-oophorectomy can be a prophylactic approach in high-risk patients as it reduces ovarian cancer risk by 69% to 100%, however it has significant body image and sexuality impacts on patients (24). Despite significant advances in our understanding of detection of this disease, there remains significant gaps in terms of early diagnosis.

Currently the most common and effective management of the most common histotype of ovarian cancer, high-grade serous ovarian cancer (HGSOC), is a combination of surgery with chemotherapy that consists of a platinum-based drug such as carboplatin and the microtubule inhibitor paclitaxel. Surgical removal of the cancer mass immediately after diagnosis and on occasion, to have it shrunk by neoadjuvant chemotherapy prior to debulking (25); however, this is mostly dependent on the resectability of the tumour as well as patient medical state (26). Furthermore, even though ovarian cancer patients normally respond well to first line chemotherapy, very often patients experience recurrence or chemo-resistance (27), and in the case of recurrent Epithelial Ovarian Cancer there is no cure (12).

A selection of intraperitoneal and intravenous delivery of chemotherapy are available methods of treatment after cytoreduction of tumour (28, 29, 30), while the selection of medications are based on the histological type and stage of ovarian cancer. Platinum containing drugs (carboplatin) and taxane family (docetaxel and paclitaxel) are the most frequent selections. At least 70% of ovarian cancers will respond to a combination of platinum and taxane based chemotherapy administered after surgery, however, nearly half of those patients will have residual treatment resistant cancer that isn't detectable using imaging studies and CA125 analysis after 5 months of treatment (5). Due to the heterogenic nature of ovarian cancer other potential therapeutics that specifically target intrinsic signalling pathways such as the homologous recombination pathway, angiogenesis, hormone receptors, and immunologic factors are now being considered (8, 12), as well as pharmacological inhibition of poly (ADP-ribose) polymerase (PARP) inhibitors, which target homologous recombination deficient mutations such as those in *BRCA1* or *BRCA2* and stops cancer cells from repairing which leads to targeted cell death (31).

1.a.3 Pathogenesis

Multiple genetic and epigenetic abnormalities have been observed across studies of individuals with ovarian cancer (32), the most significant genomic alterations can be observed in late stage cancer patients with histologically differentiated tumours such as HGSOC (33). The most common of these include germline inheritable mutations of BRCA1, BRCA2 and these account for 10 – 15% of ovarian cancers (34).

Most mutations in sporadic ovarian cancer are suspected to arise from spontaneous mutations that occur during cell proliferation (35). Hence, there is increasing evidence of factors that increase the number of ovulatory cycles such as late menopause, leading to an increase in the risk of ovarian cancer (36), however, this is still to be confirmed. One example of cell proliferative activity that increases risk, is the increase in epithelial cell proliferation to repair the ovarian surface which can be ruptured on mature follicles during release of oocytes.

The tumour suppressor p53 is mutated in over 96% of HGSOC which most commonly have the TP53 mutation which inhibits its anti-tumour activity (37, 38) The cellular origin of many high-grade serous ovarian cancers has been shown to be the fimbrial ends of the fallopian

tube (39). This discovery arose from immunohistochemistry analysis of tubular precursor lesions showing p53 overexpression, correlating with gain-of-function *TP53* missense mutations, in the fimbriated ends of the fallopian tube, especially by non-ciliated (secretory) cells (40).

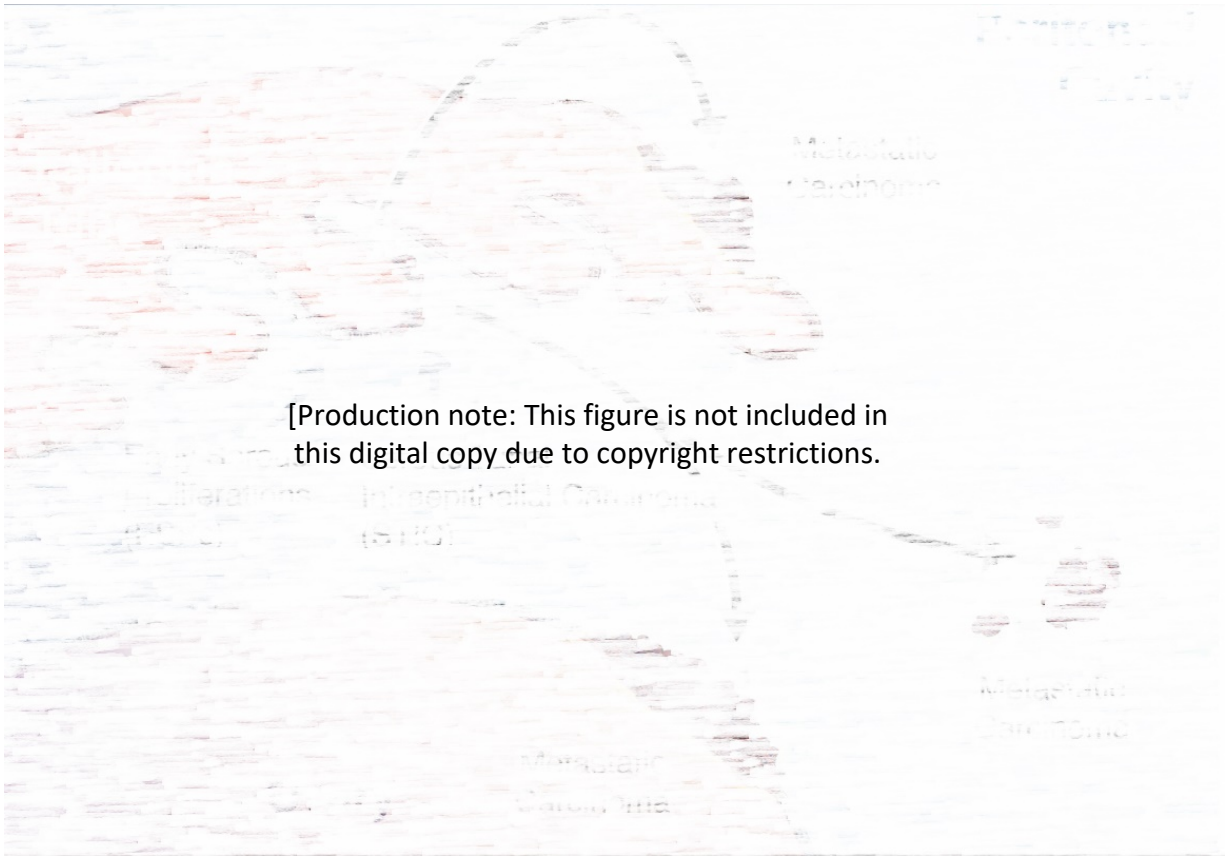

Figure 1. The fallopian tubal theory of high-grade serous ovarian carcinogenesis; Reproduced from (41). *The first step is proposed to entail oxidative stress to the secretory epithelia, that causes DNA damage and initiates Early Serous Proliferations (ESP) leading to a serous Tubal intraepithelial carcinoma (STIC). The final step suggests either the escape of tumour cells via exfoliation into a range of surfaces in the peritoneal cavity or ovarian surfaces or continuous progression and eventual invasion of the fimbria submucosa (41, 42).*

b) Markers used to Detect Ovarian Cancer

Currently, diagnosis of ovarian cancer is initially detected partly by a serum test for cancer antigen 125 (CA125) and is mostly exclusively carried out when symptoms become apparent (43). CA125 levels, however, are understood to not be highly specific for epithelial ovarian cancer as half of patients during early stage and 20% of advanced stage tumours do not present elevated levels; in addition that elevated levels have also been associated with a range of benign diseases including endometriosis, and other malignant cancers such as breast cancer and could lead to an incorrect diagnosis (43, 44). There are multiple markers that can

help with tracking disease progression and prognosis prediction. Some examples include; Osteopontin, which is a glycophosphoprotein secreted by activated T lymphocytes, macrophages, and leukocytes (45) which helps in prognosis determination of later stage patients as presence significantly increases between stages 3 and 4 (46), however, it is also present in endometrial, cervical, breast, non-small cell lung, hepatocellular, colorectal, prostate, and gastric cancer (47). Another example is bikunin, which is a glycoprotein that mediates suppression of cancer cell invasion and metastasis; and high levels have been reported to be a favourable prognostic marker for advanced ovarian cancer patients (48). These examples reinforce the challenge to find more specific biomarkers, that allow for stage I and II diagnosis, to help track progression of the disease during treatment and track accurately for reoccurrence, all which aid in improving our understanding of ovarian cancer pathophysiology.

Vascular endothelial growth factor (VEGF) is a vascular permeability factor that is a key regulator of normal and pathological angiogenesis as well as tumorigenesis (49); its levels are known to be elevated in patients with ovarian cancer and correlate with shorter survival as well as the accumulation of ascites (50). Interestingly, in a hepatocellular carcinoma study, CLIC1 protein (chloride intracellular channel protein 1) expression was significantly correlated with vascular invasion and its knockdown reduced VEGF expression (51). In addition, CLIC4-VEGF signalling pathway, is believed to be significant for vascular development as early as embryonic maturation (52). More recently, other published studies have now directly implicated CLIC1 and CLIC4 and suggested they could serve as potential biomarkers for subtypes of epithelial ovarian cancer (44, 53). Tang et al., 2012 & 2013 have also shown CLIC1 & CLIC4 to be upregulated in EOC patients compared to healthy controls, with further examples included in section 1.c.2. below. Therefore, studying pathways such as the VEGF, and possibly through exosomes as a mechanism for intercellular communication to mediate disease progression, have raised interest in further investigating involvement of members of the CLIC family of proteins, in ovarian cancer progression.

c) Introduction to CLIC proteins

The CLIC (Chloride Intracellular Ion Channel) protein family in vertebrates, consists of six evolutionarily conserved protein members (CLIC1, CLIC2, CLIC3, CLIC4, CLIC5 and CLIC6 in humans) (54). These proteins are unusual, as they exist in cells as both soluble and membrane bound proteins where they exhibit two independent functions; in their membrane bound form, CLIC proteins act as ion channels (55) and in their soluble form, they act as oxidoreductase enzymes, which are believed to likely contribute to cell protective functions like detoxification and/or anti-oxidative roles(56).

The CLICs have been shown to have similar structures to members of the Glutathione-S-Transferase (GST) family and are now included as members of the GST superfamily. The GSTs are well characterised protein enzymes, that enable the reduction of Glutathione (GSH), and are known to remove metabolic by-products, including Reactive Oxygen Species (ROS), generated by oxidative stress (57, 58). In this project, particular focus was placed on CLIC1 and CLIC4, as they have previously been associated with various cancers, including ovarian cancer (51, 52)

1.c.1 Role in cell physiology

The human protein. CLIC1, is found in most human cells. Its intra and intercellular location has classified it as an organelle/cellular transmembrane and as soluble cytoplasmic protein, and as a ubiquitous protein expressed in more than 25 tissues (59). CLIC1 has been shown to have various diverse roles in cell physiology such as a cell content and ionic species homeostasis regulator, via its ability to form chloride ion channels when embedded in membranes (60, 61); while in its soluble form, it demonstrates enzymatic activity and has also been shown to be involved in regulation of the cell cycle (62).

The human protein CLIC4, similarly is expressed across various parts of the body and has been shown to partake in crucial roles in membrane trafficking, cell development, and apoptosis (63, 64, 65). Originally, this family of proteins have been studied for their membrane and ion channel activity, however, more recent research, has focused on their soluble form and their enzymatic activity. CLIC1, CLIC2, CLIC3 and CLIC4 have been shown to have glutathione-dependent oxidoreductase activity (56, 66). Mutation studies have identified the specific

active enzyme site in CLIC1 includes the critical cysteine in position 24, which is responsible for this enzymatic activity. While mutation of Cys24 or that of Cys59, also lead to reduction in CLIC1's ability to form ion channels (56, 67).

1.c.2 Role of CLICs in cancer

Unregulated cell growth can result in tumour development and cancer. Recent studies have shown increasing evidence of involvement by abnormal ion channel function across different cancer cell types (68). Because of this, as well as their widespread expression across many cell types, an increasing number of studies are exploring CLIC proteins' involvement, expression and localization across various types of cancers (69).

CLIC2 has only lately been associated to various cancers. Recently it was shown that healthy cells surrounding tumours show elevated CLIC2 in hepatocellular carcinoma as well as colorectal cancer; and it was then hypothesized that CLIC2 might be involved in the formation of tight junctions between endothelial cells to possibly prevent angiogenesis and metastasis (70). Its elevated expression has also been shown to be a good prognosis marker in breast, lung, liver and gastric cancers (69, 71).

CLIC3 has been established as a driving factor of angiogenesis and tumour invasiveness. A study using microarrays on ovarian tumour tissues found CLIC3 levels to be elevated in 90% of ovarian cancer patients with High Grade Serous Carcinoma, and the highest levels correlated with increased invasiveness and the lowest survival rate (72). Another related study demonstrated the impact that CLIC3 released by cancer cells and proteins released by cancer associated fibroblasts (CAFs) had on the extracellular matrix (ECM) in order to drive invasive activity (66). The study showed that lack of CLIC3, resulted in stiffness of the ECM which impairs motility in the extra cellular microenvironment mediated by CAFs as both matrix stiffness and integrin activation are requirements for cell invasion. It later was concluded that release of protein TGM2 by CAFs in the ECM is mediated by CLIC3 and is required to allow the pseudopod elongation of cancer cells. CLIC3's oxidoreductase activity targets TGM2 which acts to regulate its binding to integrins on cancer cell membranes. TGM2 bound integrins covalently crosslink to fibronectin to mediate communication between intra and extracellular environments, which fundamentally describes CLIC3's role in this invasive behaviour.

CLIC5 and CLIC6 are the members of this family that have been studied or shown to be associated with cancer the least. Increased CLIC6 was correlated with an improved prognosis in breast cancer patients (73). CLIC5 is overexpressed in childhood acute lymphoblastic leukemia as it allows increased resistance to hydrogen peroxide-induced apoptosis (74). A meta-analysis comparing high and low expression of genes showed that elevated CLIC5 was demonstrated as an indicator for poor patient survival in Ovarian cancer, while the opposite was the case for CLIC6 (69).

CLIC1 has previously been found to be overexpressed in several cancers including liver, pancreatic, breast and ovarian cancer (51, 75, 76, 77). In colon cancer cells, it has been demonstrated that CLIC1 partakes in cell migration and metastasis (78, 79). Regarding ovarian cancer, CLIC1 has been found to be differentially elevated in ovarian cancer tissue when metastasis occurs when compared to healthy epithelial ovarian cells (80), in addition elevated CLIC1 expression was observed in more aggressive tumours, so it may aid to predict patient prognosis (53). The other cancer mechanism that CLIC1 has been associated with is angiogenesis, where its overexpression in gastric cancer cells increased ROS in a hypoxia-reoxygenation induced state (81).

Aberrant levels of both CLIC1 and CLIC4 have been described as possible indicators for early-stage disease, as facilitators in diagnosis via staining and as potential therapeutic targets (44). CLIC4 has been studied in breast, uterus, prostate, oesophagus, lung, and ovary cells, where it was reported that expression is downregulated in tumour cells while being elevated in stromal cells and restoration of CLIC4 levels inhibits tumour growth (82). Most recently, knockdown of CLIC4 was linked through its suspected involvement in mitochondrial dysfunction through reactive oxygen species-sensitive signalling pathways (83). These pathways are persistently elevated in many cancer types and are involved in cell proliferation and differentiation, regulating protein synthesis, glucose metabolism, cell survival and inflammation; and have previously been alleged to promote ovarian cancer progression though TGF-ß1-induced fibroblast-to-myofibroblast trans-differentiation (84).

There has also been an increased number of research studies across a range of cancers including ovarian, looking at CLIC proteins within exosomes being transported as cargo to enable disease progression by taking part in pathological intercellular communication (85, 86, 87, 88).

d) Exosomes

Exosomes are a type of extracellular vesicles (EV) that are actively secreted by almost all types of cells such as fibroblasts, endothelial cells, epithelial cells , immune cells, neuronal cells, as well as, cancer cells (89). Soon after their initial discovery, exosomes were thought to have a role in disposal of cellular waste products. However, proteomic studies since revealed the real nature of their cargo, which has sparked an increasing interest from the scientific community regarding their pathophysiological roles and potential for use in more personalised pharmacological applications (90, 91). These particles are now known to have a role in intercellular communication which is fundamental for the correct functioning of eukaryotic multicellular organisms, as they facilitate the exchange of materials such as proteins, metabolites, DNAs (mtDNA, ssDNA, dsDNA), RNAs (mRNA, miRNA, long non coding RNA) and lipids, with these particles secreted by the donor cell can then be taken up by an acceptor cell (92, 93, 94, 95).

1.d.1 Exosome Biogenesis, secretion, and uptake

EVs can be broadly classified into three main groups, based primarily on their size and presumed physiological pathway involvement. The first group includes apoptotic bodies (ABs), ranging in size between 800-5000nm diameter and are released by cells undergoing programmed cell death. Second are microvesicles (MVs), which are large membranous vesicles ranging from 50-1000nm diameter and are produced by budding from the plasma membrane of cells. The third group are much smaller vesicles known as exosomes, which are only 30-150nm in diameter, described as being of endocytic origin (96, 97, 98) thus providing a distinction between exosomes and MVs based on their site of biogenesis and their relative sizes.

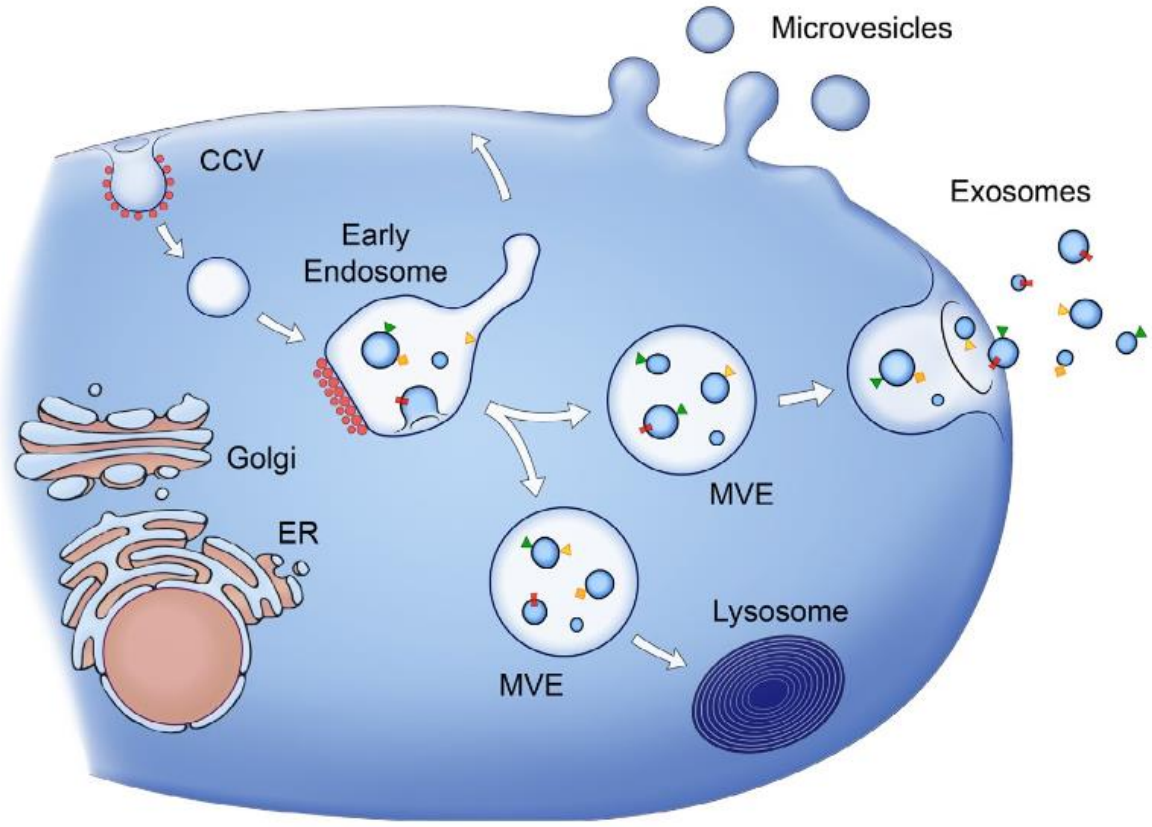

Figure 2 Depiction of differences in biogenesis between Microvesicles and Exosomes. Reproduced from (99). *Biogenesis of exosomes explains that they are formed within early endosomes. First, the plasma membrane invades the cytoplasm as clathrin coated vesicles (CCVs) and then forms a structure that is either independent of or fused to a pre-existing early endosome; next, part of its membrane begins budding within the endosome where cargo (Proteins, nucleic acids and metabolites) has been added by the Endoplasmic reticulum (ER). After this budding stage they are labelled as multivesicular endosomes (MVE). Finally, these may enter the autophagy lysosomal pathway for degradation and repurpose of macromolecules or for energy production; otherwise, they may fuse with the plasma membrane and release their contents (Exosomes) into the extracellular environment.*

1.d.2 Exosomes involvement in diseases and cancer

Exosomes and microvesicles are shed by both healthy and diseased cells and have been found in various body fluids (100). Since exosomes obtain their cargo profile from the host cell from which they originate, it is not surprising that exosomes released by cancer cells have been shown to aid in tumour progression including cellular proliferation, angiogenesis, migration, invasion, metastasis, and drug resistance (101).

One of the most critical roles in which exosomes have been studied across various cancers is metastasis. With their involvement in cell-to-cell communication, exosomes and microvesicles are implicated in the transfer of bioactive molecules between tumour cells and distal potential metastatic sites, that are capable of changing or impacting on the

microenvironment, leading to pre-metastatic niche formation, which permits growth of disseminated tumour cells upon arrival into secondary tumours in metastasis. This phenomenon has been studied in various cancers including, melanoma and pancreatic cancer (102, 103, 104).

Differential and selective protein contents of cancer derived exosomes can help differentiate between cancers of different origins (102). However other cargo types such as nucleic acids also have been demonstrated to mediate pathological progression. Transfer of MMP1 mRNA by ovarian cancer exosomes to mesothelial cells *in vitro* and *in vivo* induced destruction of the peritoneal mesothelium barrier and promoted cancer spread (105).

1.d.3 Clinical interest of Exosomes in cancer

Nowadays, ovarian cancer diagnostics ultimately rely on histological analysis of biopsies. The potential uses of exosomes have the advantage of being a sensitive and non-invasive method, allowing the diagnosis at an early stage. Cancer exosomes have previously been studied for the detection of many types of cancers such as prostate, breast, ovarian cancer, and melanoma, among others (106, 107, 108, 109). Exosomes collected from liquid biopsies are an advantageous method for cancer monitoring and diagnosis in contrast to biopsies as it is less invasive, more economical and provide a more robust transport method for vulnerable biological molecules (101)

A comparable study to the one presented in this thesis, studied the number of exosomes shed by epithelial breast cancer cell lines. The exosomes were purified via ultracentrifugation, with 50% more exosomes collected from the cancer cell line compared to the regular human breast epithelial cell lines (110). In another study, similar results were observed, where the ovarian cancer cell line OVCAR3 was shown to have 50% more exosome yield when compared to a control cell line (HOSEPiC) (111).

The detection of tumour-derived exosomes in body fluids provide not only an option for early detection but also better management by monitoring of disease progression as the exosome can be found in circulation, which allows for minimally invasive sample retrieval of exosomes which protect information carrying molecules from degradation of the potentially therapeutic target cells (112).

Understanding exosome release and the ability to control their circulation has great potential for therapeutic and preventive drug development. Some recent studies using pancreatic and ovarian cancer cells (113, 114, 115) diminished exosome secretion via depletion of Rab27a in the tumour cells (116), and use of pharmacological inhibition of exosomal uptake at sites of future metastases, were demonstrated as potential mechanisms that impaired pre-metastatic niche formation and therefore prevention of formation of metastasis in mice (104, 115, 116).

In summary many studies have associated CLIC1 and CLIC4 upregulation in ovarian cancer, particularly the most common histological subtype of epithelial ovarian cancer, when compared to their healthy controls (44, 53, 80, 117, 118). These trends were detected in serum(117, 118), whereas in tissue, combinations of CLIC1, CLIC4 and CA125 have resulted in improved sensitivity for histological detection over CA125 individually; in addition this same study implicated elevated CLIC4 expression with decreased patient survival, while the knockdown of CLIC1 or CLIC4 resulted in the decreased ovarian cancer cell proliferation which suggests a role of CLICs in cell proliferation and cell migration (44). These findings correlate with other studies which showed a similar trend in CLIC1 and CLIC4 expression and disease progression (44, 53, 80). Elevated CLIC3 levels have also been detected in epithelial ovarian cancer, while in breast tissue have been demonstrated to drive cancer cell invasiveness (66). Exosome associated CLIC proteins could provide cancer-specific signatures for epithelial ovarian cancer, in conjunction with promising technologies allowing for exosome profiling, could lead to early, non-invasive and more specific detection of ovarian cancer.

e) New Approaches and Biomarker Candidates for the Early Detection of Ovarian Cancer (Opinion Piece)

During the COVID19 NSW lockdowns across 2021, my access to UTS laboratories was significantly disrupted. Firstly, I was residing in a suburb of Sydney where special permission was required to travel out of the area, I also contracted COVID19 and therefore was unable to leave home. In addition, there were delays in reagent delivery required for my cell culturing, needing me to freeze down and re-establish my cultures several times. In combination, these events resulted in greatly reduced experimental productivity. In order

however to minimise these impacts and to ensure progress of the project, our team embarked on the writing of a critical opinion piece. Under the supervision and guidance of my co-supervisors Drs Khondker Hossain and Kristina Warton, as well as my principal supervisor Prof Stella Valenzuela, an opinion piece for the scientific journal "*Frontiers in Bioengineering and Biotechnology*" was prepared and subsequently accepted for publication (see Figure 3 below – image of front page. Pre-print version is provided in the Appendix and link to the article is provided here: https://www.frontiersin.org/articles/10.3389/fbioe.2022.819183/full).

My significant contribution as a joint first author arose from my work researching, initial drafting of main sections and co-writing of the manuscript, along with subsequent edits and reviews for final publication. In this paper we outline our rationale for the importance of investigating markers such as CLIC proteins on exosomes shed by ovarian cancer. We also discuss possible technologies that provide exciting new ways for detecting biomarkers including CLIC proteins. These technologies range from quartz crystal microbalance, impedance spectroscopy together with tethered membrane technologies and electrochemical assays for detection and tracking of exosomes.

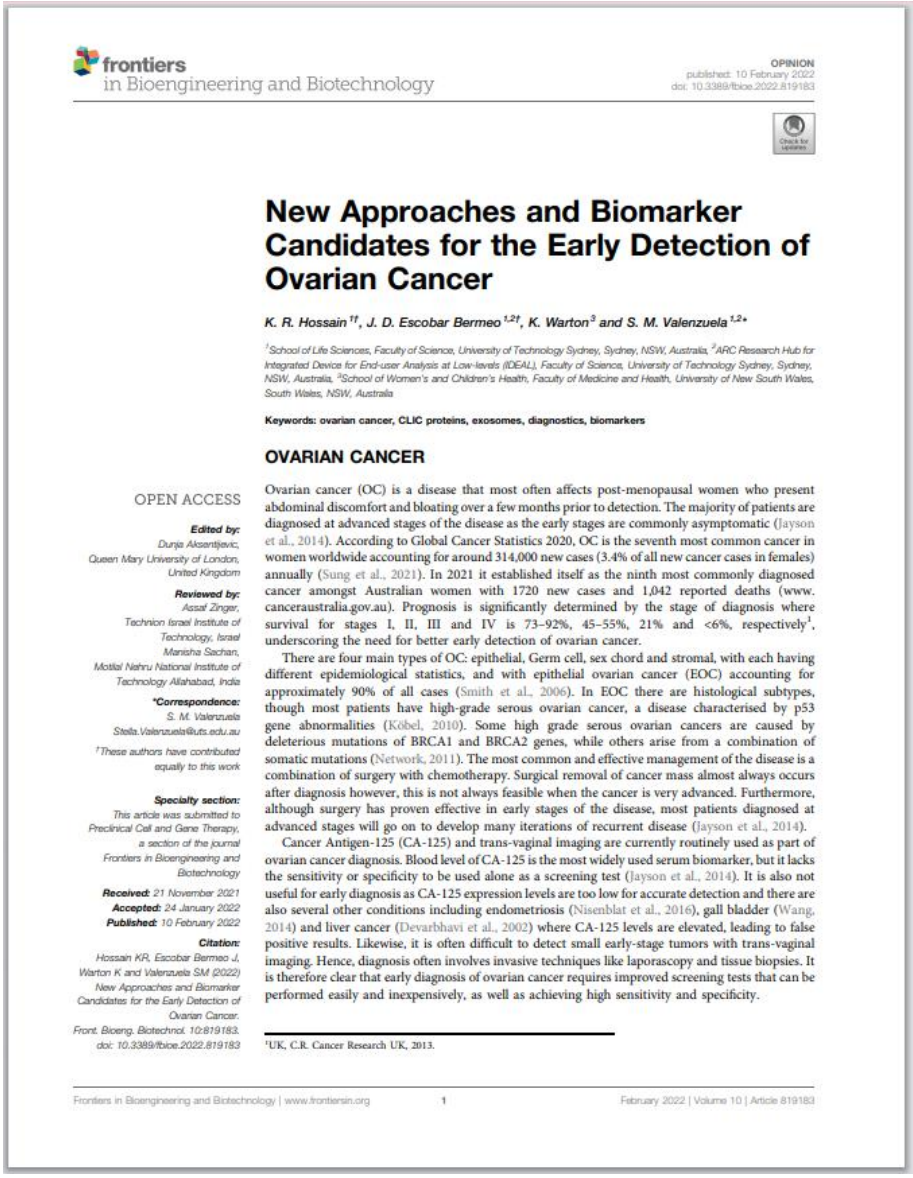

frontiers in Bioengineering and Biotechnology

OPINION
published: 10 February 2022
doi: 10.3389/fbioe.2022.819183

New Approaches and Biomarker Candidates for the Early Detection of Ovarian Cancer

K. R. Hossain [1†], J. D. Escobar Bermeo [1,2†], K. Warton [3] and S. M. Valenzuela [1,2*]

[1]School of Life Sciences, Faculty of Science, University of Technology Sydney, Sydney, NSW, Australia, [2]ARC Research Hub for Integrated Device for End-user Analysis at Low-levels (IDEAL), Faculty of Science, University of Technology Sydney, Sydney, NSW, Australia, [3]School of Women's and Children's Health, Faculty of Medicine and Health, University of New South Wales, South Wales, NSW, Australia

Keywords: ovarian cancer, CLIC proteins, exosomes, diagnostics, biomarkers

OVARIAN CANCER

Ovarian cancer (OC) is a disease that most often affects post-menopausal women who present abdominal discomfort and bloating over a few months prior to detection. The majority of patients are diagnosed at advanced stages of the disease as the early stages are commonly asymptomatic (Jayson et al., 2014). According to Global Cancer Statistics 2020, OC is the seventh most common cancer in women worldwide accounting for around 314,000 new cases (3.4% of all new cancer cases in females) annually (Sung et al., 2021). In 2021 it established itself as the ninth most commonly diagnosed cancer amongst Australian women with 1720 new cases and 1,042 reported deaths (www.canceraustralia.gov.au). Prognosis is significantly determined by the stage of diagnosis where survival for stages I, II, III and IV is 73–92%, 45–55%, 21% and <6%, respectively[1], underscoring the need for better early detection of ovarian cancer.

There are four main types of OC: epithelial, Germ cell, sex chord and stromal, with each having different epidemiological statistics, and with epithelial ovarian cancer (EOC) accounting for approximately 90% of all cases (Smith et al., 2006). In EOC there are histological subtypes, though most patients have high-grade serous ovarian cancer, a disease characterised by p53 gene abnormalities (Köbel, 2010). Some high grade serous ovarian cancers are caused by deleterious mutations of BRCA1 and BRCA2 genes, while others arise from a combination of somatic mutations (Network, 2011). The most common and effective management of the disease is a combination of surgery with chemotherapy. Surgical removal of cancer mass almost always occurs after diagnosis however, this is not always feasible when the cancer is very advanced. Furthermore, although surgery has proven effective in early stages of the disease, most patients diagnosed at advanced stages will go on to develop many iterations of recurrent disease (Jayson et al., 2014).

Cancer Antigen-125 (CA-125) and trans-vaginal imaging are currently routinely used as part of ovarian cancer diagnosis. Blood level of CA-125 is the most widely used serum biomarker, but it lacks the sensitivity or specificity to be used alone as a screening test (Jayson et al., 2014). It is also not useful for early diagnosis as CA-125 expression levels are too low for accurate detection and there are also several other conditions including endometriosis (Nisenblat et al., 2016), gall bladder (Wang, 2014) and liver cancer (Devarbhavi et al., 2002) where CA-125 levels are elevated, leading to false positive results. Likewise, it is often difficult to detect small early-stage tumors with trans-vaginal imaging. Hence, diagnosis often involves invasive techniques like laparoscopy and tissue biopsies. It is therefore clear that early diagnosis of ovarian cancer requires improved screening tests that can be performed easily and inexpensively, as well as achieving high sensitivity and specificity.

[1]UK, C.R. Cancer Research UK, 2013.

OPEN ACCESS

Edited by:
Dunja Aksentijevic,
Queen Mary University of London, United Kingdom

Reviewed by:
Assaf Zinger,
Technion Israel Institute of Technology, Israel
Manisha Sachan,
Motilal Nehru National Institute of Technology Allahabad, India

***Correspondence:**
S. M. Valenzuela
Stella.Valenzuela@uts.edu.au

†These authors have contributed equally to this work

Specialty section:
This article was submitted to Preclinical Cell and Gene Therapy, a section of the journal Frontiers in Bioengineering and Biotechnology

Received: 21 November 2021
Accepted: 24 January 2022
Published: 10 February 2022

Citation:
Hossain KR, Escobar Bermeo J, Warton K and Valenzuela SM (2022) New Approaches and Biomarker Candidates for the Early Detection of Ovarian Cancer. Front. Bioeng. Biotechnol. 10:819183. doi: 10.3389/fbioe.2022.819183

Figure 3: Opinion paper available from https://www.frontiersin.org/articles/10.3389/fbioe.2022.819183/full

f) Aims and Hypotheses of this Research Project

This project aims to distinguish and characterise the expression levels of different CLIC proteins, specifically CLIC1 and CLIC4 on exosomes derived from ovarian cultured cell lines Kuramochi, OVCAR3, PEO1 and PEO4, compared with exosomes derived from FT33-TAg-RAS, a fallopian epithelial cell line, used as a control. In addition, two Hamster ovary epithelial cell lines, one wild type (CHO-K1) and one modified to overexpress the protein CLIC1 (CHO-K1/C4AFBN), were included to more directly interrogate the protein CLIC1 involvement in exosome shedding.

Based on the information summarised in the literature review above, and recent publications implicating CLIC proteins as potential biomarkers for ovarian cancer, we hypothesized that:

A. *Discernible physical differences exist between the number and/or size distribution of exosomes derived from ovarian cancer cell lines compared to exosomes derived from a non-cancerous, control cell line, which correlates with CLIC protein levels on the exosomes.*
B. *Exosomes derived from ovarian cancer cell lines, differentially express the proteins CLIC1 and CLIC4 when compared to exosomes derived from a non-cancerous, control cell line.*

In order to address the hypotheses, the following aims and corresponding methodologies were pursued:

1. Establish cell culture conditions and protocols for the uniform processing and collection of exosomes from a variety of cell lines, including model ovarian cancer cell lines:
    a. all cell lines were grown under controlled settings, with cell counting and detailed monitoring of cell density; cell counts at the time of seeding and at the time of media collection.
    b. exosome collection under equivalent conditions, and purification via differential ultracentrifugation.
2. Characterisation and quantification of purified exosomes, using:
    a. Dynamic Light Scattering (DLS);
    b. Nanoparticle Tracking Analysis (NTA).
3. Protein profiling and characterisation of exosomes:
    a. Establish Western blot protocol for visualising protein expression from exosomes.
    b. Determine appropriate exosome markers for use via Western blotting.
4. Measure CLIC protein levels in exosomes derived from ovarian cancer cell lines compared to exosomes derived from a non-cancerous, control cell line via Western blot analysis.
5. Measure CLIC protein levels in exosomes derived from CHO-K1 cells and CHO-K1 cells overexpressing CLIC1 protein by western blot analysis.

Chapter 2

Exosome purification and characterization from Tissue culture models

Introduction:

This chapter will describe *in vitro* cell studies undertaken in order to establish the growth and maintenance of a variety of cell lines from which exosomes were collected for analysis. It also elaborates on the methodology for purifying and characterising the exosomes and a protocol which was developed that would allow subsequent comparisons of the exosome samples. This necessitated determination of the optimal initial cell seeding densities for each cell line, equivalent cell handling, and final counting of the cells at the point of collecting the exosomes, to allow a determination of final yield of exosomes per cell, and thus also allow for direct comparison of exosomes collected from different cell types.

a) Cell Lines Used in this Study.

The selection of established human cancer-derived cell lines used in this study were readily available to us. These included Kuramochi, NIH: OVCAR3, PE01, PE04. It is appreciated that these cannot be seen to represent a wide population of ovarian cancer patients, or even the sub-type from which the cell line was initially obtained (119) however, they were deemed suitable as tumour models for our initial studies allowing us to compare ovarian cancer cells to a control cell line of epithelial fallopian tube cells, FT33-TAg-RAS.

The Kuramochi cell line is an epithelial cell line derived from a patient of east Asian descent who was diagnosed with high- grade ovarian serous adenocarcinoma. The cell line was retrieved from a metastatic site (ascites) and characterized in 1981 (120). The second cell line that we studied was NIH:OVCAR-3 (OVCAR3); which are epithelial cells isolated from malignant ascites, are a high-grade serous ovarian adenocarcinoma cell line and demonstrate resistance to cyclophosphamide, cisplatin and doxorubicin (121). The OVCAR3 cell line is commonly used to portray increase of ovarian cancer tumour size; and in mice models have been used in the preclinical evaluation of antiangiogenic agents (122, 123). This is because the cell line overexpresses vascular permeability factor VEGF, which has been demonstrated to accelerate the onset of ascites formation, which in turn, allows for metastasis of secondary solid tumours representative of pathogenic progression into stage 4 (124).

In addition to the two cell lines mentioned above, two drug resistant ovarian cancer cell lines were used, in the hope to cover a wider spectrum of real-life tumours within this *in vitro* model. PEO1 and PEO4 are two epithelial cell lines derived from the same patient and first described 1987 (125), which was when they were first characterized and found to be tumorigenic. PEO1 was obtained after commencement of chemotherapy, while PEO4, after the patient developed treatment resistance to a cocktail of cisplatin, 5-fluorouracil and chlorambucil treatment. Since then, these two cell lines have historically been used as models for tumours that have acquired resistance during treatment (125). Both cell lines showed an interesting progression of mutation for expression for protein BRCA2 which has a critical role in DNA damage repair. PEO1 had deleterious mutation c.5193C>G; while PEO4 cells have a different reversion mutation at the same site c.5193C>T, that restores BRCA2 expression (126).

Most importantly, was the need for inclusion of a control non-cancerous cell line, or one that represented a stage prior to carcinogenesis. For this purpose, the cell line FT33-TAg-RAS was used. This cell line was immortalized and derived from fallopian tube secretory epithelium cells (FTSEC) (127). The argument for choosing fallopian epithelial cells rather than ovarian epithelial cell lines as controls is based on current understanding of the progression of ovarian cancer. As previously explained, high-grade serous ovarian cancers are anatomically derived from FTSECs demonstrated by presence of ovarian cancer precursor lesions in the fallopian tube fimbriated ends in patients with inherited BRCA1/2 mutation (127, 128). The FT33 cell lines were immortalised from secretory epithelial cells, as the ciliated cells that are also present, were unable to grow as primary cells on plasticware. In order to immortalize for large scale *in vitro* studies first-passage FTSECs were transduced with a retroviral vector encoding *hTERT*, the catalytic subunit of telomerase, which maintains telomere ends and stalls replicative senescence (129). Finally, in addition to promote growth for expansion, FT33 cells were transduced with SV40 large T plus small T antigens (TAg) which does not transform cells. In a similar manner the FT33-TAg were transduced with *H-Ras*^{V12} (FT33-TAg-Ras) which drastically improved growth rate without genetically resembling HGSOC (127).

In addition to the human cell lines mentioned above, this master's project also included two further mammalian cell lines. The hamster epithelial ovarian cancer cell line CHO-K1 was available in our laboratory. These were Chinese Hamster ovary cell line (CHO-K1) and a CHO-

K1 cell clone, transfected and selected to overexpress the human protein CLIC1 (C4AFBN). From this cell line Prof. Stella Valenzuela previously made stable transformed cell line which overexpresses the protein CLIC1 (ORF of CLIC1 containing the 8 amino acid (DYKDDDDK) FLAG tag at its amino terminus was cloned into the Not1/BamH1 site of the expression vector pIRES1neo (CLONTECH) which will be indicated throughout the thesis as C4AFBN (Clone 4 CLIC1 Amino flag bicistronic neo vector).

These were included as further controls and specifically for exploring CLIC1 involvement in any potential differences or changes that might be revealed given our initial hypothesis and studies published by others, outlined in Chapter 1, which implicate CLIC proteins as potential markers for ovarian cancer.

b) Physical Characterisation of purified exosomes from cells in culture

After producing purified exosome samples, the immediate requirement was to prove the presence of the particles as well as to characterize them. Various conventional techniques for characterisation of extracellular particles were considered including optical methodologies such as Nanoparticle Tracking Analysis (NTA), Dynamic light scattering (DLS) *(See* Figure 3 *and* Figure 6*)* and electron microscopy, while also considering non-optical techniques like Western Blotting as a secondary confirmation method. NTA was selected as the primary method to phenotypically characterize exosome samples as it allows for high resolution analysis at the expected size range of 30-150nm unlike conventional flow cytometry (lower limit ~300 nm). NTA allows for relatively fast measurements with a working range of particles between 10-1000nm providing size and volume distribution of particles as well as their quantification by offering their concentration in suspension (130).

1.b.1 Nanoparticle Tracking Analysis (NTA)

NTA works by measuring light scattering of a laser beam aimed along a clear chamber where the sample suspension flows through; the light scattering caused by the laser is visualised by a microscope that is connected to a video camera which provides a screen live feed of the sample and allows for recording (131) (see).The NTA software tracks particles in the captured video to calculate based on Brownian motion properties, the size distribution of the particles

in suspension, and simultaneously counting the particles in the field of view from the video recordings to calculate the number of particles per millilitre in the sample based on the controlled nature of the chamber (132).

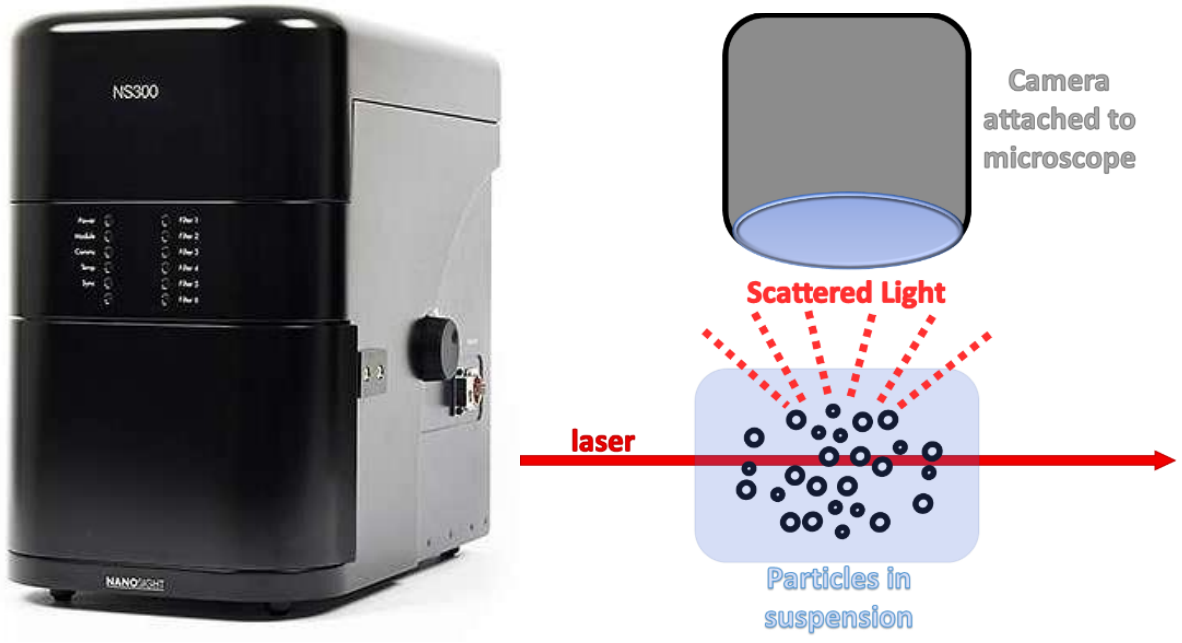

Figure 4 Schema of Nanoparticle Tracking Analysis. On the left is image of the Nanosight NS300 used for experimentation, image obtained from Malvern's website (https://www.malvernpanalytical.com/en/support/product-support/nanosight-range/nanosight-ns300). The figure on the right shows the simplified principle behind NTA; the laser beam runs across the sample which is in suspension in a volume specific chamber. The light reflected from the particles is recorded and visualized by a camera attached to a microscope, and then analysed by NTA software (132).The NS300 allows for the size distribution analysis of all types of particles that range between 0.01µm – 1µm in diameter; while the real-time monitoring, allows to detect subtle changes in particle populations which can be confirmed by visual validation. Particles in liquid suspension are loaded with a syringe into the sample chamber. The laser travels through the sample and the particles in its path scatter the light which can is visualised by the 20X microscope objective and observed as a live feed in the operating software on a computer. A video is recorded with the particles moving under Brownian motion, which the NTA software individually calculates the diameter.

1.b.2 Dynamic light scattering (DLS)

DLS was selected as the initial confirmation method for the presence of exosomes, as significant delays were in place during Covid-19 NSW lockdowns in 2021, which meant that induction to facilities at UNSW were indefinitely put on hold, where the NTA equipment used in this project was located. Dynamic light scattering (DLS) works by using a similar concept to NTA as it also measures the light scattering intensity of a laser beam after hitting suspended particles, while accounting for Brownian motion as a function of time to determine their size; however, it is detected by a photosensor that measures the change in intensity of light

scattered off particles and how it changes overtime to calculate the diameter of the particles; where a more rapid change of intensity is dictated by faster moving particles and correlate to smaller particles.

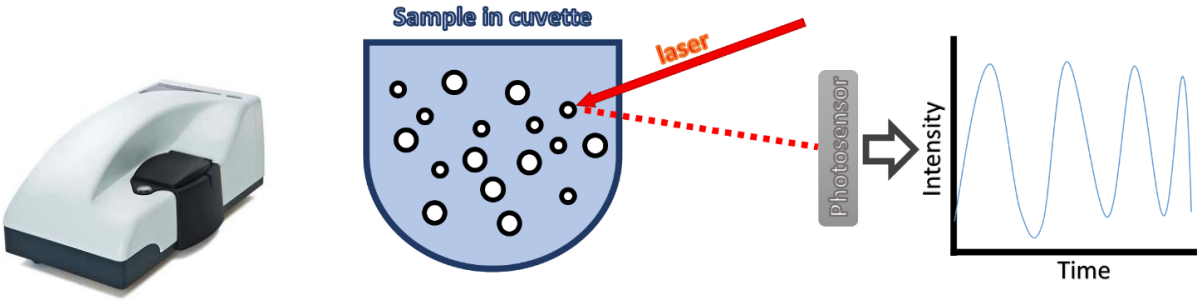

Figure 5 Schema of Dynamic Light Scattering Technique. On the left is image of the Zetasizer nano ZS used for experimentation, obtained from Malvern's website *(https://www.malvernpanalytical.com/en/support/product-support/zetasizer-range/zetasizer-nano-range/zetasizer-nano-zs* and *https://www.malvernpanalytical.com/en/products/product-range/zetasizer-range/zetasizer-advance-range/zetasizer-lab). On the right, the simplified principle behind DLS is shown; where the intensity of the scattered light coming off the particles in suspension, when from a laser beam directed towards the sample is detected by a photosensor that measures over a set period. The sample is illuminated by a laser [He-Ne (633 nm)] and the fluctuations of the scattered light are detected at a known scattering angle of 175°by a fast photon detector. The time over light intensity can then be converted to intensity over size (132). Malvern Zetasizer ZS allows* for *the measurement of particles between 0.3 nm to 10 µm.*

As a method for confirmation for the presence of exosomes, electron microscopy posed as a candidate for this as it can also provide phenotypical information regarding the particle size and morphology, however, this method cannot give quantification of the exosomes present in our sample while another drawback to be considered was the difficulty of sample preparation during which changes to exosome morphology could occur (132). On the other hand, western blot similarly allows identification of EVs marker proteins; and even though it does not provide data regarding particle sizes or their concentration in solution, it allowed for a relatively simplified confirmation method, as well as it is a technique already required to investigate their CLIC protein cargo.

Materials and Methods:

c) Materials for mammalian Cell Culture and Maintenance

The following reagents were purchased from Thermo Fisher Scientific (Sydney, Australia): TrypLE™ Express Enzyme (1X) no phenol red (Catalogue number: 12604013), DMEM/F-12 (Dulbecco's Modified Eagle Medium/Nutrient Mixture F-12) (Gibco)(Catalogue number: 11320033), RPMI 1640 medium with GlutaMAX™ (Catalogue number: 61870036) (Gibco); and the foetal bovine serum (FBS)(United States origin, Catalogue number: 16000044) (Gibco).

The only other reagent was obtained from a different company was from Sartorius Stedim (Victoria, Australia): Ultroser G Serum Substitute 20mL (UGS) (Catalogue Number 15950-017).

d) Cell lines used in this project.

All five of the human cell lines (KURAMOCHI, OVCAR3, PEO1, PEO4 and FT33-Tag-RAS) were provided by Prof Deborah Marsh's Laboratory (UTS). The two hamster cell lines CHO-K1 and C4AFBN were provided by Prof Valenzuela's laboratory (UTS).

e) Generic Protocol for Seeding Cells Prior to Collection of Exosomes from Culture Supernatants

All cell lines were maintained in a humidified incubator at 37 ºC and 5% CO2. All media supernatants that were used for preparation of exosome samples, were collected from flasks that had been seeded with cells and grown over a seven-day period under the previously mentioned conditions.

Each pre-determined cell seeding number, dependent upon the cell line, were seeded into two T-175 tissue culture flasks (SPL Life Sciences, Gyeonggi-do, South Korea) in a final volume of 20mL per flask. For each final exosome sample, two identical T-175 flasks were grown in parallel with equal seeding number of cells over seven days, after which time the media was collected and stored in two 50mL Falcon tubes, each containing an approximate volume of 20mL, labelled and stored at -20°C.

f) Human Ovarian cancer cell lines Tissue culture methodology

The KURAMOCHI, OVCAR3, PEO1 and PEO4 cell lines, were grown in RPMI 1640 medium with GlutaMAX™ supplemented with 10% heat inactivated FBS. In preparation for passaging, media was prepared by placing the heat inactivated FBS and the RPMI 1640 medium with

GlutaMAX in a water bath set to 37°C. Once warm, these were brought into a tissue culture cabinet where 50mL of FBS was filtered through a 0.2µm filter using a 50mL syringe and then added to 450mL of the RPMI media which allowed to make ten lots of 50mL aliquots of the now 10% supplemented media.

1.f.1 Cell passaging of the Kuramochi cell line.

In order to set up Kuramochi cells for subsequent exosome collection, two T-175 flasks were each seeded with 1.8×10^6 cells and grown in 20mL of media for 7 days. On the final day of growth media was collected and the total number of cells in both flasks were calculated for record keeping and subsequent passaging.

To begin, flasks were inspected using the Eclipse Ts2 inverted microscope (Nikon) for possible contamination or cell death. Media was only collected from flasks that had the previously mentioned seeding number of cells and successfully grew to 95% confluency without contamination, otherwise it was discarded. Using thoroughly decontaminated pipette aid and serological pipettes, all the media was drawn from the pair of flasks. Next, cells were gently washed using 5mL of the warmed up RPMI media which next was discarded, to next, add 5mL (3mL if the seeding flask is a T-75) of previously warmed TrypLE™ Express Enzyme (1X) per T-175 flask then placed in the incubator for 7 minutes. After this period, flasks were gently tapped while checking under a Tissue culture microscope in intervals for complete detachment of all cells, which could easily be identified by gently swirling the flask while looking through the microscope. To assure collection of all cells after complete detachment, and hence a more accurate cell count, the flask was stood upwards and 5mL of media were added to each flask, making sure that the side where cells were previously attached was thoroughly washed down. Each of the 10mL of cell media and TrypLE cell suspension were transferred to separate 15mL falcon tubes, which were spun at 1500 RPM for 5 minutes in order to separate cells from the media and TrypLE supernatant; finally, the pellet was resuspended in 10mL of media ready for cell count.

Once all cell counts were recorded and cell concentrations were determined, the next passage of two identical flasks were seeded. For every passage, guided by the calculated cell concentration (cells/mL) from “Flask 1”, the volume of cell suspension required to seed 1.8×10^6 cells were determined with $C1 \times V1 = C2 \times V2$. Prior to aliquoting the seeding volume, cells were thoroughly resuspended with the help of a 5mL serological pipette then

switching to a more appropriately sized serological pipette, normally 1mL; the calculated volume was seeded into two T-175 flasks. As a final step, the volume in every flask was brought up to a total of 20mL with the 10% FBS supplemented media, in order to account for differences in seeding volumes between passages; while also making sure that cells were evenly distributed across the flask surface by using 25mL serological pipettes and drawing and ejecting the flask contents multiple times before examining under the microscope once the media was added. Both flasks were then placed inside the incubator under the same atmospheric conditions as previous passages and grown over 7 days.

1.f.2 Cell passaging of the OVCAR3 cell line.

See *1.f.1 Cell passaging for Kuramochi cell line.* Tissue culture work between Kuramochi and OVCAR3 cell lines was methodically identical; starting with the media that was used and how it was collected, the procedure for detaching, counting and passaging cells for every flask as well as the collected data. The number of seeding cells per T-175 flask was also determined in the same way as the Kuramochi cell line, which was also determined as 1.8×10^6 cells per flask in total volume of 20mL.

1.f.3 Cell passaging for PEO1 and PEO4 Cell lines.

See The KURAMOCHI, OVCAR3, PEO1 and PEO4 cell lines, were grown in RPMI 1640 medium with GlutaMAX™ supplemented with 10% heat inactivated FBS. In preparation for passaging, media was prepared by placing the heat inactivated FBS and the RPMI 1640 medium with GlutaMAX in a water bath set to 37°C. Once warm, these were brought into a tissue culture cabinet where 50mL of FBS was filtered through a 0.2µm filter using a 50mL syringe and then added to 450mL of the RPMI media which allowed to make ten lots of 50mL aliquots of the now 10% supplemented media.

Cell passaging of the Kuramochi cell line. The media used, the detaching protocol and cell count were the same as per the previously outlined protocol in *1.f.1 The KURAMOCHI, OVCAR3, PEO1 and PEO4 cell* lines, were grown in RPMI 1640 medium with GlutaMAX™ supplemented with 10% heat inactivated FBS. In preparation for passaging, media was prepared by placing the heat inactivated FBS and the RPMI 1640 medium with GlutaMAX in a water bath set to 37°C. Once warm, these were brought into a tissue culture cabinet where 50mL of FBS was filtered through a 0.2µm filter using a 50mL syringe and then added to 450mL of the RPMI media which allowed to make ten lots of 50mL aliquots of the now 10% supplemented media.

Cell passaging of the Kuramochi cell line. The main distinction with handling both these cell lines when compared to the other two human lines was during passaging. The passaging protocol for these cells was provided by Prof. Deborah Marsh's group. Firstly, the drastic difference in growth rates were pointed out which later facilitated determining the seeding numbers; but more significantly, while passaging these cell lines, cells were not spun down with a centrifuge to remove the media and TrypLE supernatant and instead cell count and seeding was done using this cell suspension.

1.f.4 Cell passaging of the FT33-Tag-RAS control cell line.

The FT33-Tag-Ras line was chosen and will be referred to as the control cell line as it was not immortalized from a human ovarian cancer patient not it is derived from the ovary; it is derived from immortalized FTSECs. Similar to the human ovarian cancer cell lines, the control cell line was also grown with RPMI 1640 Medium with GlutaMAX; however instead it was supplemented with 2% UGS (SARTORIOUS). UGS was prepared as per manufacturer's instructions twenty 1mL aliquots were produced and were stored at -20°C only to be taken out one at a time every passage. RPMI media and one 1mL aliquot of UGS were warmed up in a water bath at 37°C prior to commencing passaging and once inside the cabinet, 49mL of media were combined with the UGS aliquot.

Significant changes were made to the handling prior to cell count, since unlike FBS, UGS does not neutralize the dissociation agent (TrypLE), so instead it was thoroughly removed during passaging. Media was removed and either stored or discarded accordingly as per previous cell lines. Only 3mL of TrypLE were added per T-175 flask and incubated at 37°C for three and a half minutes. At this stage when examining under the microscope and before tapping the flask, cells should have taken a rounded-up shape appearance. Next, flasks were gently tapped while assuring complete detachment of all cells while examining under the microscope as per previous cell lines. The flasks were brought inside the cabinet and to each 7mL of media were added with the help of a pipette aid and 10mL serological pipettes while making sure the face of the flask where cells were previously attached to, was thoroughly washed. Finally, the cell/media suspension were moved to 15mL falcon tubes and spun for 5 minutes at 1500 RPM, after which the supernatant was completely removed before resuspending the pellet in 10mL of media. Cell counts and passaging remained exact as per previously stated protocols. The seeding number per T-175 flask was 1.2×10^6.

1.f.5 Hamster Cell lines Tissue Culture methodology

Both these cell lines were grown in DMEM/F-12 (Dulbecco's Modified Eagle Medium/Nutrient Mixture F-12) (Gibco) supplemented with 5% FBS. In preparation for passaging, media was prepared by placing a 25mL aliquot of heat inactivated FBS and the DMEM/F-12 in a water bath set to 37°C. The FBS was filtered through a 0.2µm filter using a 50mL syringe and then added to 475mL of the RPMI media which allowed to make ten lots of 50mL aliquots of 5% supplemented media.

g) Cell count protocol and record keeping

A 1:1 dilution was prepared with 20µL of the cell suspension and 20µL of trypan blue, this dilution was then loaded into a haemocytometer for manual counting under the microscope for each individual cell suspension, resulting in two cell counts per passage. Passage number, date of seeding, date of collection, and the total number of cells per flask were recorded every time that media destined for exosome purification was collected.

The concentration in cells per millilitre were calculated for each cell suspension after carrying out the count under the microscope, Firstly by taking the average number of cells per grid section (Labelled letters A-E in "**Figure 6**"), multiplying this by 2, which accounts for the addition of Trypan blue, and finally multiply that by 10000. This calculation gives the c concentration of the cell suspension in cells per millilitre, which was multiplied by 10 (Total volume of cell suspension) to obtain the total number of cells.

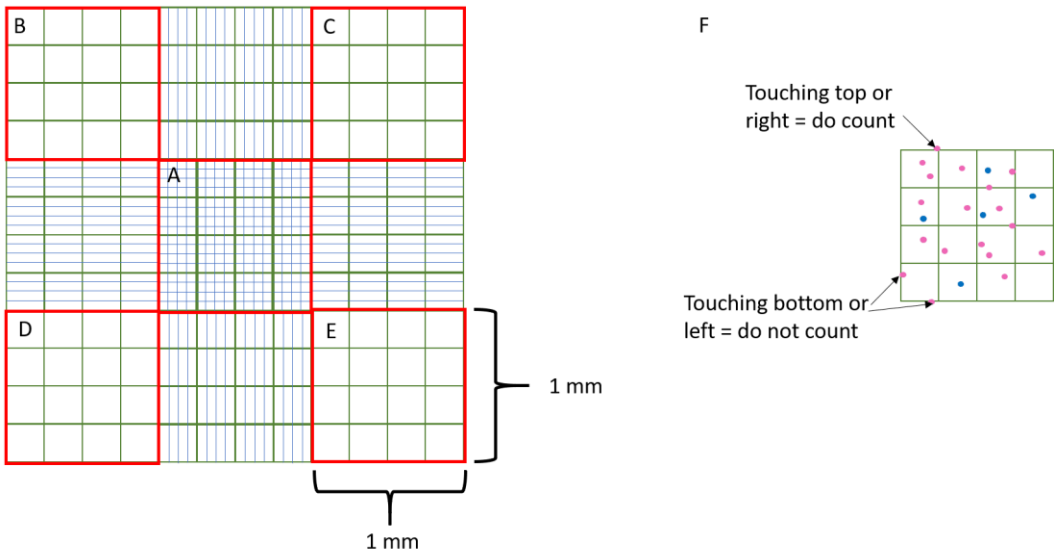

Figure 6 Haemocytometer grid view as viewed though a microscope at 40X magnification Reproduced from: https://bitesizebio.com/wp-content/uploads/2021/04/Haemocytometer.png.

h) Storage of Cells in Liquid Nitrogen

Frozen cells stocks for each cell line were made with the corresponding medium and stored under liquid nitrogen. All media for freezing purposes in this study were supplemented in 10% dimethyl sulfoxide (DMSO) (Sigma) and either 20% of heat inactivated foetal bovine serum (FBS) or in 4% Ultroser G Serum (UGS) the second which was only used for the control cell line. RPMI 1640 medium with GlutaMAX™ was the media used for all human cell lines, while DMEM/F-12 was used for both hamster ovary cell lines. In preparation for creating frozen cell stocks at least one T-75 flask was grown to confluency, after which cells were detached, counted, and resuspended in the prepared freezing down media. A total of 1×10^6 cells were aliquoted per cryo vial from the cell suspension, which then were placed in a Mr. Frosty™ Freezing Container (Thermo Fisher Scientific) and left overnight at -80°C. The next day, vials were placed in the cryo storage facility allocated to the Prof. Stella Valenzuela group.

For thawing, the desired cryo stores were retrieved and brought into the tissue culture room on dry ice. Vials were submerged in a water bath at 37°C for 1 minute to defrost rapidly, then added to 10mL of fresh media which next was centrifuged at 1500 RPM for 5 minutes to separate cells from residual DMSO. Finally, this cell suspension was used to seed two T-25 flasks for incubation and propagation.

i) Exosome Collection and Purification from Cell Culture Supernatants

The exosome purification was modified from reference protocol by Théry, Amigorena (133) this method uses differential centrifugation of incrementing speeds to separate unwanted particles and produce an exosome pellet of relatively high purity extracted from the collected cell media (134) across all cell lines. This method was selected over commercially available purification kits as it can be carried out using the available centrifuges at UTS which made this the most cost-effective option.

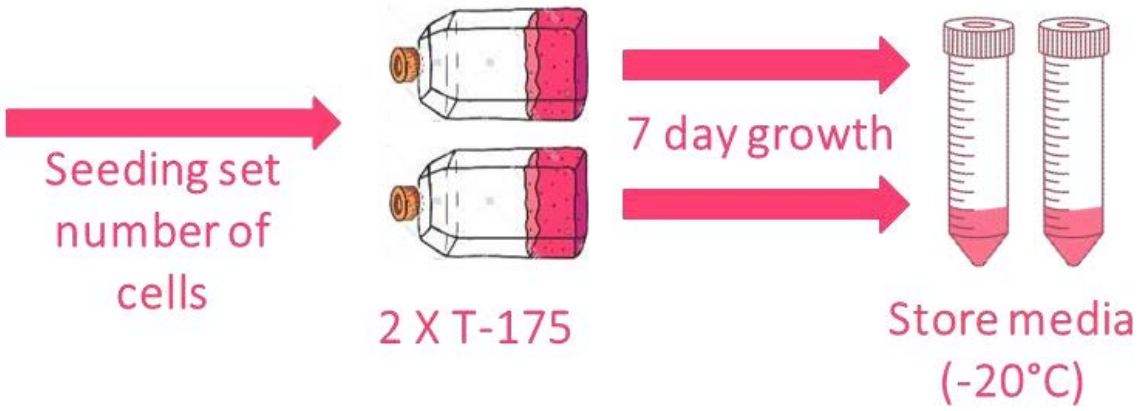

Figure 7 Set up of tissue culture flasks for 7-day incubation of cells and media intended for exosome purification.

A total of two T-175 flasks were grown every passage for all cell lines, collected and stored separately in two different 50mL falcon tubes each containing 20mL of volume; these aliquots weren't pooled together as during initial ultracentrifugation there is a volume limit of 20mL per vial, in addition, smaller aliquots allow for more efficient thawing of the sample. *See Figure 7 above.*

j) Protocol for Exosome purification using differential ultracentrifugation.

In preparation for exosome purification, 1X Phosphate Buffered Saline (PBS) was prepared and autoclaved after which 50mL were filtered through a 0.2µm filter with a syringe; this purified PBS was used for balancing samples throughout the purification protocol.

Each round of purification has an output of four Exosome samples, for which, eight media vials consisting of four pairs were taken out of storage to be purified individually, to eventually pool together the pairs of pellets derived from the same cell line and passage to produce four exosome samples.

First, eight selected falcon tubes of media were taken out the storage freezer to be thawed inside of a water bath set to 37°C. Next, they were Centrifuged for 30 Minutes at 500g using Gyrozen Labogene Scanspeed 1580R and the GRS-G-750-4 Swing-out bucket rotor at 4°C. The supernatants were then transferred to a fresh set of falcon tubes using pipette aid and serological pipettes by drawing slowly especially when nearing the expected location of the pellet. In the same centrifuge the samples were next spun for 10 minutes at 1000g and 4°C.

In a similar manner, the supernatants were transferred to T-865 ultracentrifuge bottles to be centrifuged at 20000g for 30 minutes in the Thermo Scientific™ Sorvall™ WX ultracentrifuge (previously cooled down at 4°C) using a T-865 rotor. Once again, the newly formed pellets were discarded and the supernatants transferred with the same handling care as previous steps, to a fresh set of T-865 bottles to be spun at 100000g for 2 Hours. After this, the supernatant was this time discarded while pellets containing the exosomes were thoroughly resuspended and washed in 1 mL of the ice-cold PBS, previously filter sterilized through a 0.2 µm filter. During this step it is crucial to fully resuspend the exosome pellet to allow for better washing as well as to ease resuspension in the next step.

The final purification step took place in the Beckman-Coulter Optima MAX-XP ultracentrifuge, at 4°C and at 100000 g for 90 minutes, using a TLA-55 rotor. The now washed exosome pellets were then thoroughly resuspended in 100uL ice-cold filter-sterilised PBS, to then be pooled together with the corresponding pair so that to finish, the now 200µL sample could be separated into four 50µL aliquots before being stored at -80°C for quantification and further analysis. Differential centrifugation protocols can be optimised to obtain a high yield and purity of the target population by relying on differences in sedimentation velocities between different populations in a sample. The initial two spins at lower g force (500g and 2000g) sediment out the cells, cell debris and large vesicles from the EVs which remain in the supernatant. This supernatant is then subjected to a third spin at 20,000g which pellets particles smaller than 200nm, and this can be adjusted according to the desired target particle size. The resulting pellet form the third spin is then resuspended in PBS, and then subjected to a final spin at 100,000g, which once again pellets exosomes and washes away residual proteins or smaller contaminants with similar size but lower mobility than exosomes(135, 136). Purification by differential ultracentrifugation is known to “co-separate” non-EV protein complexes and high molecular weight proteins as this method cannot separate solutes if they are similar size and density; the velocity and length of spins, the volumes used and the type of rotor (Fixed angle or Swing out) are factors that dictate the purity of the final sample (137); hence, we utilised an in house, previously trialled purification protocol for which based on later NTA and western blot results, we conclusively determined the presence of isolated exosomes.

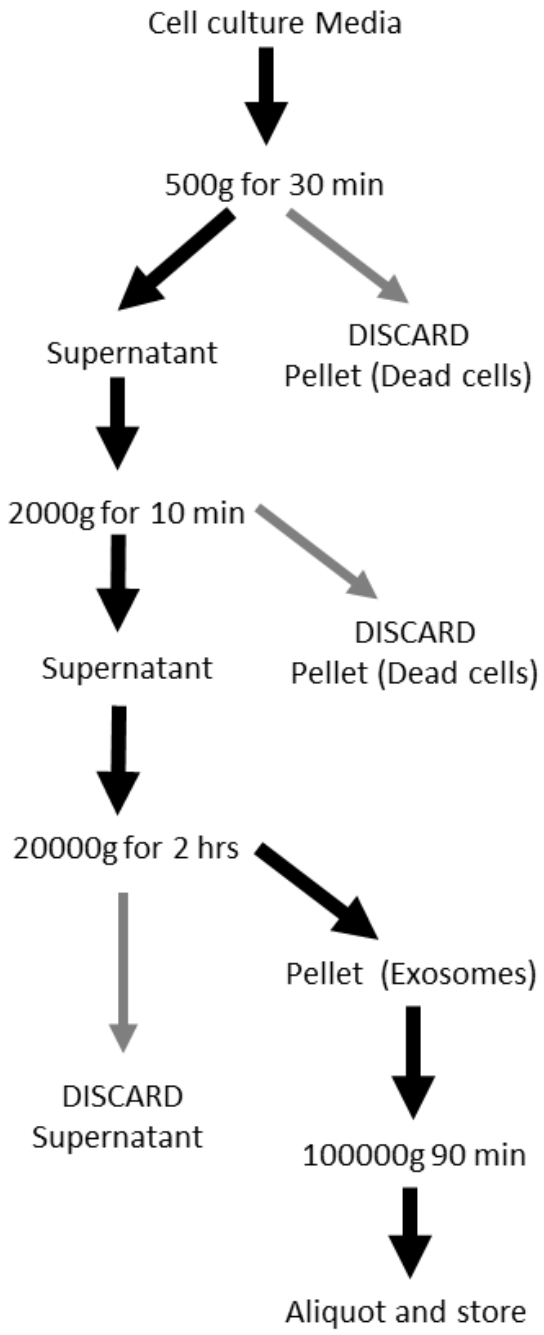

Figure 8 . Flow chart of purification protocol used to obtain exosomes from cell media via ultracentrifugation.

k) Preparation of negative media controls.

Two experimental controls were designed to investigate the presence of exosome or exosome sized particles in supplemented media alone. In order to produce these negative controls "Exosome samples" 20mL of media was incubated in separate T-175 flaks over 7 days

in order to resemble the pair of flasks seeded with cells for normal exosome sample production. The first media control was made with RPMI media supplemented with 10% FBS prepared as per previously described in f) Human Ovarian cancer cell lines Tissue culture methodology, The second media control was prepared with DMEM/F-12 supplemented with 2% UGS prepared as previously stated in 1.f.4 Cell passaging of the FT33-Tag-RAS control cell line.See The KURAMOCHI, OVCAR3, PEO1 and PEO4 cell lines, were grown in RPMI 1640 medium with GlutaMAX™ supplemented with 10% heat inactivated FBS. In preparation for passaging, media was prepared by placing the heat inactivated FBS and the RPMI 1640 medium with GlutaMAX in a water bath set to 37°C. Once warm, these were brought into a tissue culture cabinet where 50mL of FBS was filtered through a 0.2µm filter using a 50mL syringe and then added to 450mL of the RPMI media which allowed to make ten lots of 50mL aliquots of the now 10% supplemented media.

Cell passaging of the Kuramochi cell line. The media used, the detaching protocol and cell count were the same as per the previously outlined protocol in *1.f.1 The KURAMOCHI, OVCAR3, PEO1 and PEO4 cell* lines, were grown in RPMI 1640 medium with GlutaMAX™ supplemented with 10% heat inactivated FBS. In preparation for passaging, media was prepared by placing the heat inactivated FBS and the RPMI 1640 medium with GlutaMAX in a water bath set to 37°C. Once warm, these were brought into a tissue culture cabinet where 50mL of FBS was filtered through a 0.2µm filter using a 50mL syringe and then added to 450mL of the RPMI media which allowed to make ten lots of 50mL aliquots of the now 10% supplemented media.

Cell passaging of the Kuramochi cell line. The main distinction with handling both these cell lines when compared to the other two human lines was during passaging. The passaging protocol for these cells was provided by Prof. Deborah Marsh's group. Firstly, the drastic difference in growth rates were pointed out which later facilitated determining the seeding numbers; but more significantly, while passaging these cell lines, cells were not spun down with a centrifuge to remove the media and TrypLE supernatant and instead cell count and seeding was done using this cell suspension.

Cell passaging of the FT33-Tag-RAS control cell line. After incubating the flasks over 7 days, all media was collected and stored separately in -20°C. These "exosome samples" were

prepared, aliquoted and stored for further analysis in a similar manner to exosome samples as outlined above in i) Exosome Collection and Purification from Cell Culture Supernatants.

l) Exosome Characterisation

1.l.1 Sample preparation for DLS and NTA analysis

Only one 50uL aliquot per exosome sample was needed to carry out both DLS and NTA analysis side by side, the last of which results' were required for further analysis via western blot. The aliquot was retrieved from the -80°C freezer and thawed on ice. Firstly, a dilution with a 1:10 factor was prepared by adding 450µL of previously autoclaved and filtered PBS. It is particularly important to thoroughly mix well when preparing dilutions and resuspending pellets of exosome samples purified by ultracentrifugation to assure the accuracy of quantitative analysis, as compacted exosomes that may have formed during ultracentrifugation, initial freezing and/or thawing of the sample would not be visible (during purification of early samples, we found that exosome pellets that were thoroughly resuspended, resulted in higher quality (monomodal diameter) samples as observed by DLS and NTA, frequently the "exosome pellet" is extremely faint and may not visible to the naked eye). For DLS analysis of exosome samples in the Zetasizer Nano ZS (Malvern Analytical) a 1 in 20 Dilution was made from the already prepared 1 in 10 exosome suspension by taking 50µL from each sample and adding 950µL of Filtered PBS, which makes a 1 in 200 dilution relative to the undilute aliquot. In contrast, for NTA analysis sample was prepared for a 1 in 40 dilution from the initial 1 in 10 dilution, by taking 50µL of diluted exosomes and adding 1950µL of filtered PBS, to make a 1 in 400 dilution relative to the original sample. Once all dilutions to be analysed on the day were prepared, they were placed on ice until they were wanted. The stated exosome dilution for DLS was determined by analysis of numerous pilot samples and their serial dilutions analysis in the DLS, where the most success rate for an acceptable analysis was a dilution of 1:200. Similarly, the 1:400 dilution for NTA of exosomes was determined with pilot samples and their serial dilutions, however, to match 20-100 particles per frame on screen, as stated by the of the nanosight NS300 manual. These concentrations were determined to aliquot samples into fractions intended for DLS and NTA. The goal was to reserve as much sample as possible for protein analysis, eliminating the need to thawing and refreezing the entire sample to avoid degradation of the sample.

1.l.2 Method for analysing Dynamic Light Scattering using the Zetasizer Nano ZS

The samples were loaded in polystyrene 4-side optical pathway 10 mm, cuvettes (Sarstedt). Using a 1mL pipette the sample was resuspended and then the full millilitre prepared was loaded in the cuvette which was placed in the designated chamber making sure the cuvette marking was lined up with the laser trajectory. Next, once the sample has been loaded and the chamber shut, the operating software "Zetasizer Software" is opened. The Standard Operating Procedure was set with "measurement type" for size and had the following parameters:

Dispersant: "1 X PBS" with *RI: 1.332* and *Viscosity (Cp): 1.0203*

Material: "Extracellular vesicles" *RI: 1.38* and *Absorption: 0.010*

Standard Operating Procedure (SOP) Settings: *Temperature: 25°C, Cell type: Disposable Cuvette – DTS 0012; Angle of detection: 173° Backscatter; Measurements: Two measurements of Eleven runs of ten seconds duration*

Once the SOP settings have been selected the readings were carried out and the data was accordingly stored. Readings that were deemed acceptable by the system's "Size Quality Report" (RESULT MEETS QUALITY CRITERIA) which is a summary report detailing whether the result meets the Instruments quality criteria for size measurement.

1.l.3 Method for Nanoparticle Tracking analysis of Exosome samples

Fluorescence NTA is the method selected to quickly phenotype and size nanosized cellular vesicles, utilising the properties of both Brownian motion and light scattering in order to obtain the distribution of the nanoparticles in a liquid suspension. The NanoSight NS300 (available at the University of New South Wales, Malvern Instruments) was used for this project. It utilises a 488 nm laser beam that is aimed at the chamber where the diluted suspension of particles flows through. Light from the laser enters the sample, the beam light scatters after hitting the suspended particles the light in such a way that can be easily detected using a conventional microscopy with a 20X magnification lens which also has a video camera mounted on. The camera works at 30 frames per second and captures the Brownian motion of the particles. The NTA software counts and tracks the motion of every individual vesicle and uses the Stokes-Einstein equation to calculate their diameters.

The instrument was first cleaned from all possible residues by injecting a syringe containing 1mL of 100% ethanol followed by another wash using 1mL of filtered 1XPBS; air bubbles that may cause high background and generation of false data were also carefully removed from syringes before loading them into the system. After the initial cleaning step as well as flushing between samples, on screen there should be no particles left over particles in frame, which depending on the concentration of the previous sample, may require repeated flushes to achieve. In order to determine the number of particles in frame, it is important to set up an initial live image for optimisation during the cleaning steps prior to analysis. The starter settings can be set up as follows; begin by starting the camera live feed and in the Capture tab; set "Screen Gain" to 2.0 and the "Camera Level" to 11, finally, in the "Pumps/Stage" Tab, camera focus should be set to 10. The exosome samples diluted in PBS, previously filtered through a 0.2µm filter, were thoroughly resuspended prior to injection into the system for measurements. Once exosome samples were loaded into the syringe and connected into the NTA system to be injected the Individual measurement, the file for the sample is created within the software interface. Image optimisation had to be individually set per sample, however for every sample the following settings remained constant when creating the individual SOPs:

Standard Measurement: *Number of captures: 3*, *Capture Duration: 30 seconds* and *Target Temperature: 25.0^{o}C*

Once the SOP is created for each individual sample, 0.5mL of the sample was injected into the system before taking the first reading to assure that the first capture taken was of the prepared dilution and not affected by diffusion caused by the liquid already present in the system. Before taking video captures, samples must not be in motion and the number of particles per frame must be approximately 20-100; in addition, focus and camera setting must be individually adjusted per video capture to make sure all particles present could later be detected. Three 30 second video captures were taken for all exosome samples, each separated by an infusion cycle of sample into the system which was stopped at a random set time to take the next video capture. The final part of NTA analysis using the NS300, is the software analysis of the video captures which counts and tracks the particles in suspension. During this stage, the user must make changes to contrast and brightness of the video captures as well as determine a level of threshold which aids the software to distinguish

between actual particles and background noise. There are also no universal analysis settings for this stage and settings must be individually changed per video capture.

Results and Discussion:

m) Establishing Protocol for Collection of Exosomes from Cell Culture Supernatants

In order to yield sufficient exosomes needed for subsequent analyses, the protocol developed by this project required that the cells be left to grow for a seven-day period prior to collection of culture supernatant from which the exosomes were purified. This therefore required that a specific initial cell seeding number be determined for each of the different cell lines. This was required to prevent the cells from becoming too numerous and over-confluent (leading in some cases to cells lifting off and dying) and needed to take into account the different cell growth rates.

Table 1 Seeding number of cells per T-175 Flask for 7-day growth, and the corresponding media for all studied cell lines.

Cell line	Seeding number per T-175 Flask	Growth media	Supplement
KURAMOCHI	1.8×10^6	RPMI 1640 medium with GlutaMAX™	10% Foetal Bovine Serum
OVCAR3	1.8×10^6		
PEO1	1.2×10^6		
PEO4	2×10^6		
FT33-Tag	1.2×10^6		2% Ultroser G Serum
CHO-K1	1×10^6	Dulbecco's Modified Eagle Medium/Nutrient Mixture F-12	5% Foetal Bovine Serum
C4AFBN	1×10^6		

1.m.1 Kuramochi

For the Kuramochi cell line, it had previously been determined that 1.8×10^6 cells per T-175 flask in a total volume of 20mL growth media was an appropriate seeding number to allow growth and approach 100% confluency over the 7-day incubation period. This was determined by seeding four individual T-175 flasks with 1.4×10^6, 1.6×10^6, 1.8×10^6 and 2×10^6 Kuramochi cells and periodically observing the growth over 7 days.

Table 2 Cell count of T-175 flasks per passage for record keeping of the Kuramochi cell line.

PASSAGE NUMBER	DATE SEED	DATE COLLECT	FLASK 1	FLASK 2
P6	19-Aug	26-Aug	15720000	18780000
P7	26-Aug	2-Sep	19540000	17340000
P8	2-Sep	9-Sep	21600000	14480000
P9	9-Sep	16-Sep	25640000	14440000
P10	16-Sep	23-Sep	18560000	19800000

1.m.2 OVCAR3

The first significant difference between OVCAR3 and Kuramochi cell lines was observed over the 7-day growth. Unlike Kuramochi, OVCAR3 only reaches approximately 90% confluency before cell death begins to occur. A second characteristic which resulted in a slight deviation in passaging methodology between the cell lines was distribution and cell morphology (observed in Figure 9 Photo comparison of Kuramochi and OVCAR3 cell lines after 7 days of growth under 40X magnification (Nikon Eclipse Ts2). OVCAR3 grows in a compact clustered manner and to ensure even growth across the flask surface, it was important to ensure even cell distribution during seeding. For the OVCAR3 cell line, immediately before seeding a new passage of cells after re-suspension in 10mL of cell media, the 15mL falcon tube was dragged multiple times over the air grill inside the cabinet to ensure a more thorough break down of compacted cells.

Table 3 Cell count of T-175 flasks per passage for record keeping of the OVCAR3 cell line.

PASSAGE	DATE SEED	DATE COLLECT	FLASK 1	FLASK 2
P6	19-Aug	26-Aug	14080000	21760000
P7	26-Aug	2-Sep	14440000	29640000
P8	2-Sep	9-Sep	16600000	9120000
P9	9-Sep	16-Sep	24680000	18960000
P10	16-Sep	23-Sep	22520000	21160000

Kuramochi 40X	OVCAR3 40X
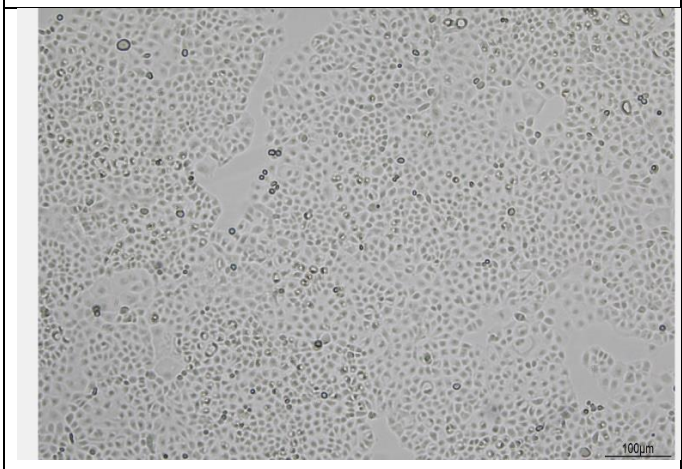	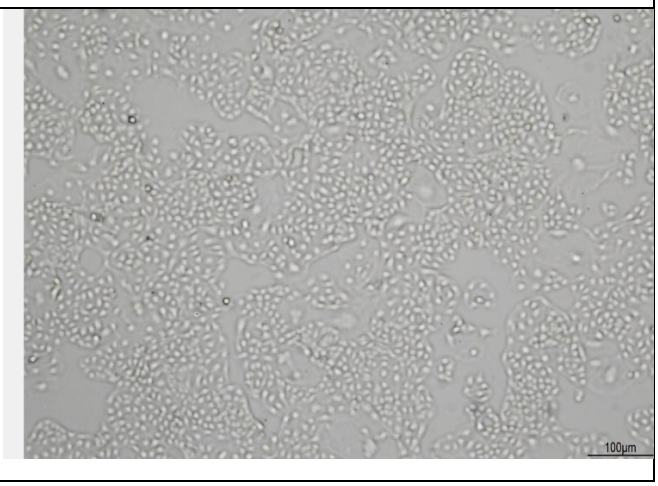

Figure 9 Photo comparison of Kuramochi and OVCAR3 cell lines after 7 days of growth under 40X magnification (Nikon Eclipse Ts2).

1.m.3 PEO1 and PEO4

The seeding number of cells for 7-day growth for PEO4 were determined as mentioned for the Kuramochi and OVCAR3 cell lines; on the other hand, all trial seeding numbers for the PEO1 cell line were too high to allow growth over 7 days and resulted in all T-175 flasks over growing and dying off; as a result I then trialled with 1×10^6 and 1.2×10^6 cells. With this I determined that the seeding numbers were 1.2×10^6 for the PEO1 cell line and 2×10^6 for PEO4.

PEO1 when compared to all other human cell lines showed the fastest growth. The appearance of growth was like the OVCAR3 cells in that they grew compacted, however they neared 100% confluency by the 7th day. PEO4 cells also physically resembled OVCAR3 cells as they grew in tight clusters and the main difference between the two was that PEO4 cells were unable to grow above approximately 70% confluency.

Table 4 Cell count of T-175 flasks per passage for record keeping of the PEO1 cell line.

PASSAGE	DATE SEED	DATE COLLECT	FLASK 1	FLASK 2
P5	19-Aug	26-Aug	25480000	18480000
P6	26-Aug	2-Sep	22340000	27660000
P7	2-Sep	9-Sep	20380000	19380000
P8	9-Sep	16-Sep	11800000	12280000
P9	16-Sep	23-Sep	16700000	17760000
P10	23-Sep	30-Sep	22920000	27240000
p11	30-Sep	7-Oct	12300000	19360000

Table 5 Cell count of T-175 flasks per passage for record keeping of the PEO4 cell line.

PASSAGE	DATE SEED	DATE COLLECT	FLASK 1	FLASK 2
P4	12-Aug	19-Aug	4060000	5320000
P5	19-Aug	26-Aug	18360000	10980000
P6	26-Aug	2-Sep	16600000	11220000
P7	2-Sep	9-Sep	16580000	23120000
P8	9-Sep	16-Sep	24620000	22920000
P9	16-Sep	23-Sep	20960000	17800000
P10	23-Sep	30-Sep	19520000	18720000
P11	30-Sep	7-Oct	7400000	12340000

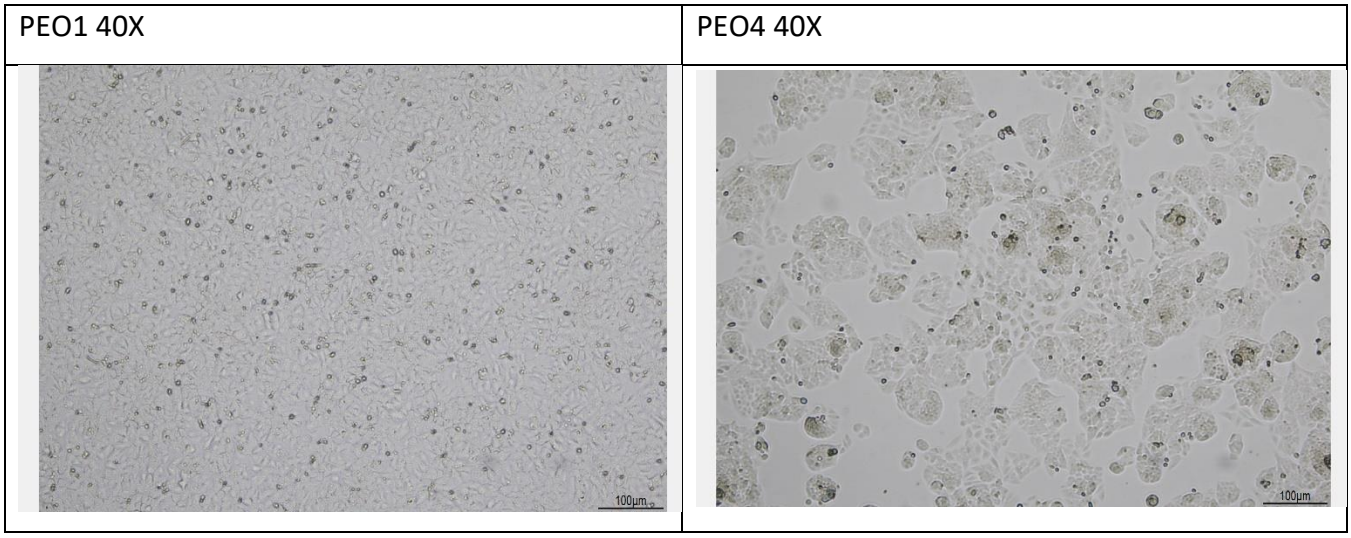

Figure 10 Comparison between PEO1 and PEO4 cell lines after seven days of growth under 40X magnification (Nikon Eclipse Ts2).

1.m.4 Control cell line (FT33-TAg-Ras)

To determine the seeding number for 7-day growth, being aware of the rapid growth rate of the control cell line; I trialled seeding with 1×10^6 , 1.2×10^6 and 1.4×10^6. I determined that 1.2×10^6 cells were the appropriate seeding number of cells for 7 days of growth. In terms of morphology, the control cell line physically resembled the PEO1 cell line and in parallel it was also able to approach 100% confluency after 7 days.

Table 6 Cell count of T-175 flasks per passage for record keeping of the FT33-TAg-RAS cell line.

PASSAGE	DATE SEED	DATE COLLECT	FLASK 1	FLASK 2
P10 I	7-Oct	14-Oct	26520000	17280000
P10 II	7-Oct	14-Oct	29440000	21240000
P11 I	14-Oct	21-Oct	15600000	13760000
P11 II	14-Oct	21-Oct	17680000	14720000
P12 I	21-Oct	29-Oct	32040000	15,040,000

P12 II	21-Oct	29-Oct	23280000	19320000
P13 I	29-Oct	4-Nov	16560000	16280000
P13 II	29-Oct	4-Nov	18350000	20520000

1.m.5 Cell passaging of the Chinese hamster ovary (CHO)-K1 cell line and C4AFBN.

The detaching protocol and cell count were the same as per the previously outlined protocol in 1.f.1 Cell passaging of the Kuramochi cell line. The seeding number of cells for 7-day growth for both CHO-K1 and C4AFBN were determined as mentioned for the PEO1 and the control cell line, since I was also previously aware of the fast growth rate of both cell lines; as a result, I the trialled with 1×10^6 and 1.2×10^6 cells to determine that 1×10^6 was the most appropriate seeding number of cell for 7-day growth.

Both hamster cell lines when compared to all human cell lines studied in this project, grew significantly quicker and at to 100% confluency with little to no cell death once this point was reached; physically both cell lines appeared almost identical when compared to each other under the microscope.

Table 7 Cell count Recording for CHO-K1 cell line

PASSAGE	DATE SEED	DATE COLLECT	FLASK 1	FLASK 2
P9	5-Aug	12-Aug	33560000	28200000
P10	12-Aug	19-Aug	27040000	27600000
P11	19-Aug	26-Aug	32960000	33040000
P12	26-Aug	2-Sep	37840000	28360000
P13	2-Sep	9-Sep	9900000	12100000

Table 8 Cell count Recording for C4AFBN cell line

PASSAGE	DATE SEED	DATE COLLECT	FLASK 1	FLASK 2
P11	22-Jul	29-Jul	17580000	17660000
P12	29-Jul	5-Aug	28560000	31050000
P13	5-Aug	12-Aug	36040000	30680000
P14	12-Aug	19-Aug	42400000	29000000
P15	19-Aug	26-Aug	29480000	22040000

CHO-K1 40X	C4AFBN 40X
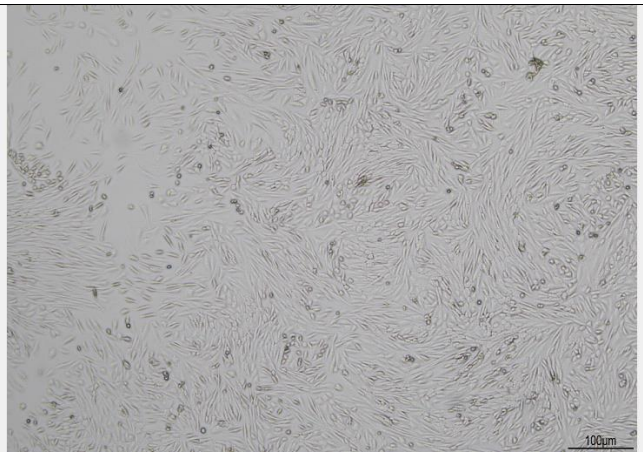	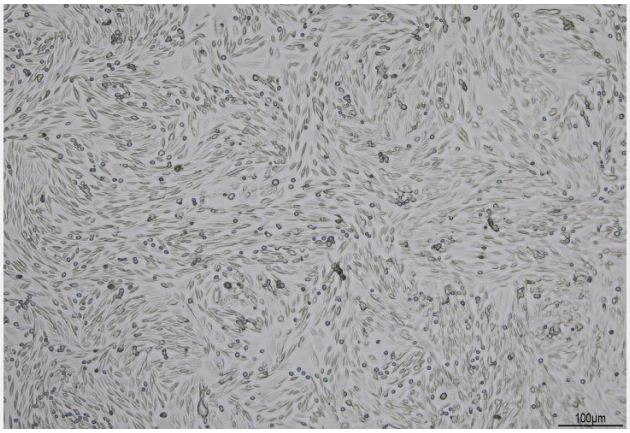

Figure 11 Comparison between CHO-K1 and C4AFBN cell lines after seven days of growth under 40X magnification (Nikon Eclipse Ts2).

n) Exosome Characterisation

After multiple trial runs with both the Nanosight (NTA) and the Zetasizer (DLS) I determined that the majority of samples could successfully be analysed using similar dilutions regardless of the cell line of origin, but instead was dependent upon the desired analysis method. The decision to prepare dilutions ahead of time was ultimately taken to improve efficiency for off-site sample analysis of numerous samples.

The table below (Table 9) contains all the exosome samples that were successfully purified following the protocol outlined above, and were later analysed via Dynamic Light Scattering, Nanoparticle Tracking Analysis as well as analysed by Western Blot (covered in Chapter 3).

Table 9 List of all passages for each cell line from which exosomes were purified via ultracentrifugation and qualitatively and quantitatively analysed downstream.

KURAMOCHI	OVCAR3	PEO1	PEO4	CHO-K1	C4AFBN	FT33-Tag-RAS
		Passage 5				
Passage 6	Passage 6	Passage 6	Passage 6			
Passage 7	Passage 7	Passage 7	Passage 7			
Passage 8	Passage 8	Passage 8	Passage 8	Passage 8		
Passage 9	Passage 9	Passage 9	Passage 9	Passage 9		
Passage 10	Passage 10	Passage 10	Passage 10	Passage 10		Passage 10
		Passage 11	Passage 11	Passage 11	Passage 11	Passage 11
			Passage 12	Passage 12	Passage 12	Passage 12
				Passage 13	Passage 13	Passage 13
					Passage 14	
					Passage 15	

1.n.1 DLS Results

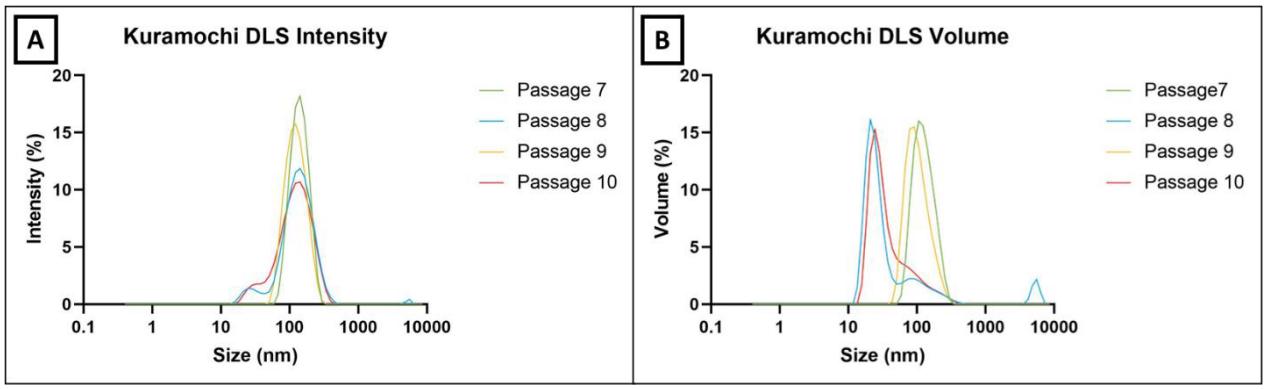

Figure 12 Dynamic Light Scattering analysis across exosome samples purified via ultracentrifugation from 4 different Kuramochi passages. *Graph A shows the measured Intensity by percentage of particles of different diameters and compares them between passages 7-10 which are represented as different coloured lines. B shows the calculated total volume distribution by percentage of all present particles of the same passages as A. The data for each passage line is an average of 2 technical duplicates. Both intensity and volume analysis of the purified exosome dilutions suggest that most of the particles in all four passages fall within the expected 30-150nm. In graph B two different populations of particles can be observed, a smaller population of approximately 50nm in size for passages 8 and 10, while the larger sized population nearing 100nm for passages 7 and 9.*

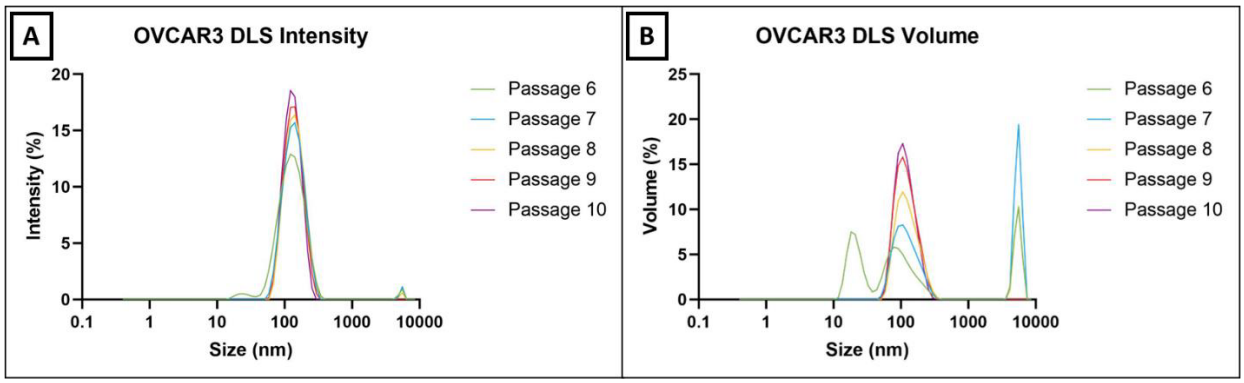

Figure 13 Dynamic Light Scattering analysis across exosome samples purified via ultracentrifugation from 5 different OVCAR3 passages. *Graph A shows the Intensity by percentage of particles of different diameters and compares them between 5 passages which are represented as different coloured lines. B shows the calculated total volume distribution by percentage of all present particles of the same passages as A. The data for each passage line is an average of 2 technical duplicates. The intensity shown by all 5 passages, suggest that majority of particles are at the expected size between 30-150nm; the exception being a small peak close to the 10000nm mark for passages 6 and 7. This peak is better observed in graph B as the volume that the small intensity signal embodies is relatively large, compared to the rest of smaller sized particles.*

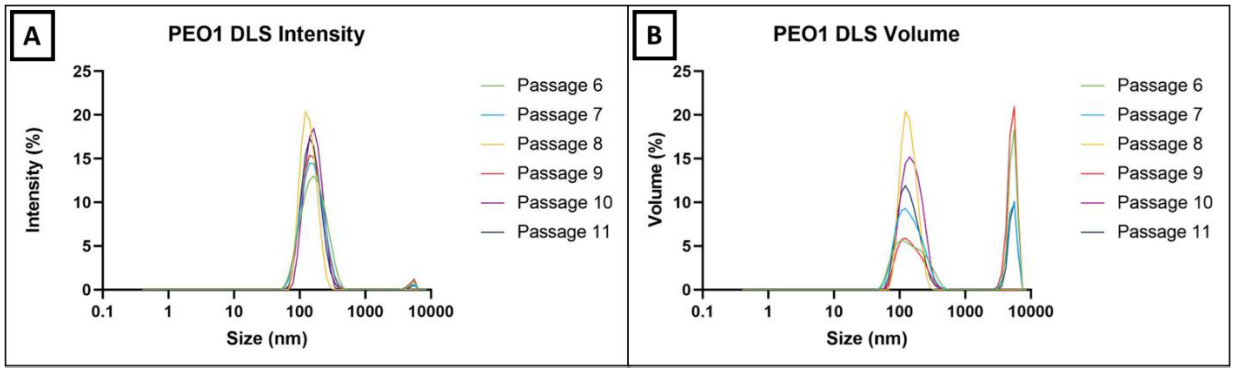

Figure 14 Dynamic Light Scattering analysis across exosome samples purified via ultracentrifugation from 6 different PEO1 passages. *Graph A shows the Intensity by percentage of particles of different diameters and compares them between passages which are represented as different coloured lines. B shows the calculated total volume distribution by percentage of all present particles of the same passages as A. the data for each passage line is an average of 2 technical duplicates as per protocol. Both Intensity and volume analysis of the purified exosome dilutions suggest that majority of the particles in all four passages fall within the expected 30-150nm. The intensity shown by all 6 passages, suggest that majority of particles are at the expected size between 30-150nm, however it is noted the presence of a small peak close to the 10000nm mark on passages 6,7 and 9. The volume percentage these large sized particles represent is significant, as the peaks of the overshadow the peaks at the exosome sized range.*

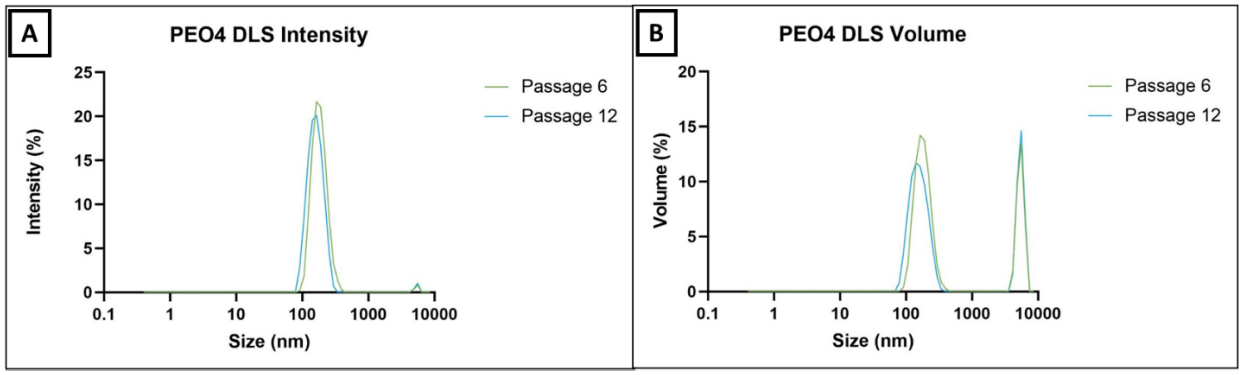

Figure 15 Dynamic Light Scattering analysis across exosome samples purified via ultracentrifugation from 2 different PEO4 passages. *Graph A shows the Intensity by percentage of particles of different diameters and compares them between passages which are represented as different coloured lines. B shows the calculated total volume distribution by percentage of all present particles of the same passages as A. The data for each passage line is an average of 2 technical duplicates as per protocol. Both intensity and volume analysis of the purified exosome dilutions suggest that majority of particles present are within the expected exosome size range. Both passages demonstrate the presence large sized particle nearing 10000nm in diameter portrayed as small intensity peak, which can be better observed in graph B as it accounts for approximately half of total volume in both passages.*

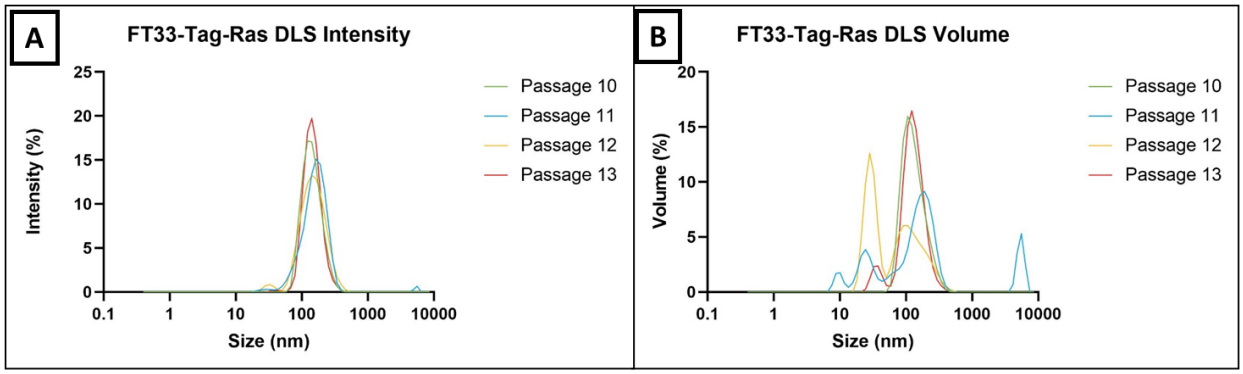

Figure 16 Dynamic Light Scattering analysis across exosome samples purified via ultracentrifugation from 4 different Control cell line passages. *Graph A shows the Intensity by percentage of particles of different diameters and compares them between passages which are represented as different coloured lines. B shows the calculated total volume distribution by percentage of all present particles of the same passages as A. The data for each passage line is an average of 4 readings obtained from 2 technical replicates of 2 samples, as the control cell line was grown as sample duplicates and 2 samples were produced per passage. Intensity analysis of the purified exosome dilutions suggest that majority of the particles in all four passages fall within the expected 30-150nm, with the exception for passage 11 where a small peak can be seen near the 10000nm mark. The volume analysis for this cell lines show that there are two populations of exosome sized particles: one nearing 50nm diameter and the other 150nm.*

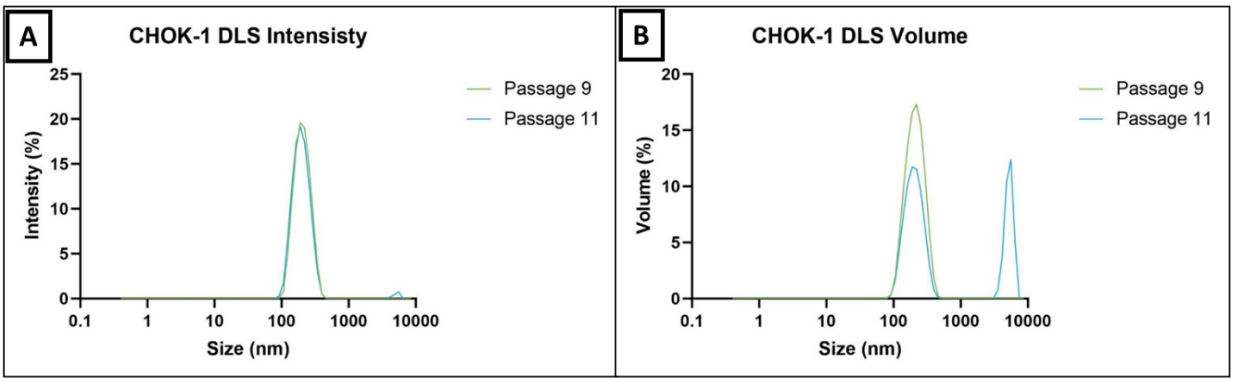

Figure 17 Dynamic Light Scattering analysis across exosome samples purified via ultracentrifugation from 2 different CHO-K1 passages. *Graph A shows the Intensity by percentage of particles of different diameters and compares them between passages which are represented as different coloured lines. B shows the calculated total volume distribution by percentage of all present particles of the same passages as A. The data for each passage line is an average of 2 technical duplicates as per protocol. Both Intensity and volume analysis of the purified exosome dilutions suggest that majority of the particles in both passages fall within the expected 30-150nm with the exception for passage 11 where a small peak can be seen near the 10000nm mark. In graph B the two different population of particles can be better observed for passage 11 where close to half of the total volume is by an unknown particle population located near the 10000nm mark. Only two passages met the equipment's self-analysis criteria and are being shown for this cell line, while all other samples were successfully analysed via NTA and will be further discussed.*

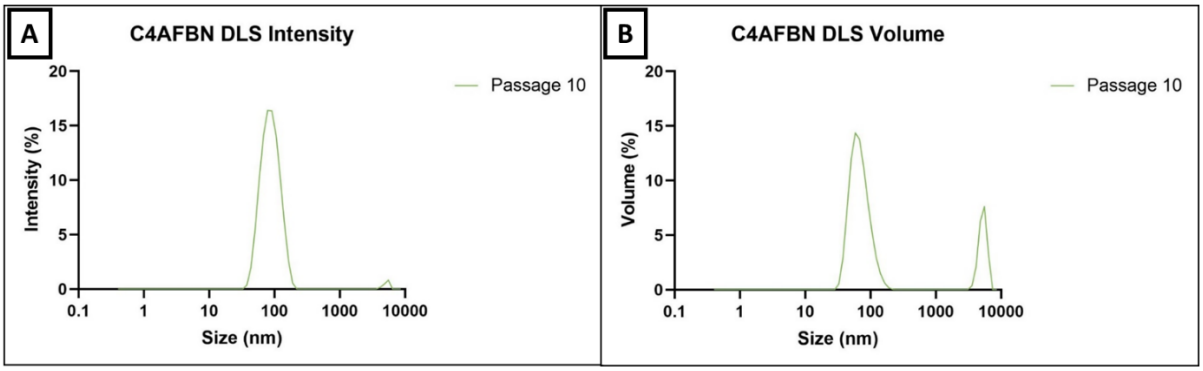

Figure 18 Dynamic Light Scattering analysis across exosome samples purified via ultracentrifugation from a C4AFBN passage. *Graph A shows the Intensity by percentage of particles of different diameters which are represented as a coloured line. B shows the calculated total volume distribution by percentage of all present particles of the same passage as A. The data for the passage line is an average of 2 technical duplicates as per protocol. Both Intensity and volume analysis of the purified exosome dilution suggest that majority of the particles fall within the expected 30-150nm. In graph B the two different population of particles can be better observed where approximately one third of the total volume is by an unexpected particle population located near the 10000nm mark. Only one passage is being presented as for this cell line this was the only DLS analysis of passages between 11 and 15 that met the equipment's self-analysis criteria, other samples were instead analysed via NTA and will be further discussed.*

Figures 10 to 16 show the DLS analysis of all cell lines with each Figure showing two graphs labelled A and B. Graph A shows the particle size distribution as a percentage from the total number of particles, differentiating them by their intensity, to present them as particles of different diameters and compares them between passages which are presented as different coloured lines. Graph B shows the total volume distribution by percentage, of the same particles and passages as A. The data for each passaged line is an average of 2 technical duplicates as described in 1.l.2. Method for analysing Dynamic Light Scattering using the Zetasizer Nano ZS.

Figure 12 shows the DLS analysis of exosomes collected from four different passages of Kuramochi cell lines (passage 7- passage 10 as mentioned in Table 9). Both Intensity and volume analysis of the purified exosome dilutions suggest that majority of the particles in all four passages fall within the expected 30-150nm with a peak value of 118.7nm except for a small peak close to the 10000 nm mark for passage 8. In Figure 10 B, two different population of particles can be observed, a smaller population of approximately 50nm in size for passages 8 and 10; while the larger sized population nearing 100nm for passages 7 and 9. Similar results were observed for other cell lines too where DLS analysis of exosomes collected from

different passages of OVCAR3, PEO1, PEO4, FT33-Tag-Ras and the CHOK1 and C4AFBN cell lines, as seen in Figure 11A, Figure 12A, Figure 13A, Figure 14A, Figure 15A and Figure 16A respectively, suggest that majority of the particles in all the cell lines used in this study fall within the expected 30-150nm range. However, there were slight differences in the total volume distribution amongst the different passages from the same cell line and also differences between the different cell lines as seen in Figures 10B to 16B; which could be caused by either the presence of vesicle aggregates, or the suspension being too concentrated for the DLS to differentiate between individual exosomes and instead measure them as an oversized single unit.DLS analysis of different passages from OVCAR3 shows a small peak close to the 10000nm mark for passages 6 and 7 (Figure 11A). This peak is better observed in Figure 11B as the volume that the small intensity signal embodies at 10000nm is relatively large and can be attributed to the presence of either cellular contaminant or aggregation of exosomes that is quantitively low compared to the number of exosome particles. Similar results were also obtained for exosomes collected from passages 6,7 and 9 of PEO1 cell line where a peak near 10000nm representing a large volume percentage of larger sized particles could be seen (Figure 12B). On the other hand, the volume analysis for FT33-Tag-Ras cell lines show that there are two populations of exosome sized particles: one nearing 50nm diameter and the other 150nm (Figure 14B). In comparison to other cell lines, only one to two passages were being compared for PEO4, CHOK-1 and C4AFBN cell lines (See Figures 13, 15 and 16 respectively) as DLS analysis of exosomes collected from the other passages (see Table 9) did not meet the equipment's self-analysis criteria, and rather than testing concentrations other than 1:200 as per protocol; the samples were instead analysed via NTA analysis and will be further discussed below.

From the above results we can conclude that one of the limitations of Dynamic Light Scattering is its utility in analysing exosomes; particularly when trying to establish the validity of the purification protocol in a similar manner to that of this project, where samples were purified by ultracentrifugation. DLS may not be helpful to initially determinate the size distribution of the particles present in a biological sample since the technique is limited to monomodal samples and the broader the dispersity of diameter the more likely the determined mean size may differ from the true value as noted in the Zetasizer Nano Zs manual. In addition, since the volume distribution of the exosomes (Graphs B in figures 10-

16) (volume of a sphere is equal to $\frac{4}{3}\pi r^3$), as well as other additional measurements, are calculated from the initial intensity measurement (Graph A in figures 10-16); then the calculated volume distribution of the particles is only as accurate as the intensity reading. Because of these reasons, the statistical significance of the data obtained were not calculated, and rather, will later be contrasted with the data obtained by NTA in "q) Comparison between DLS and NTA results"; however, below we have presented the average and standard deviation from all the results presented in figures 10-16

Table 10 Average size particle from particles detected by DLS of previously mentioned samples for all cell lines.

	Kuramochi	OVCAR3	PEO1	PEO4	FT33-TAg-RAS	CHO-K1	C4AFBN
Average Diameter (nm)	118.7	132	152.4	187	145.8	203.3	94.15
Standard Deviation (nm) (+/-)	20.2	12.8	8.7	18.1	19.5	9.6	4.1

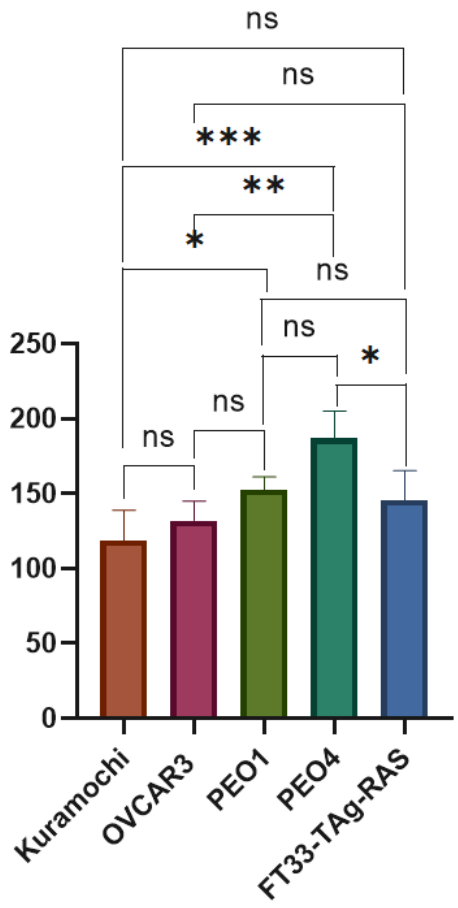

Figure 19 Analysis of variance of DLS measurements from all Human cell lines presented in Table 10. *The passages used in this analysis include Kuramochi passage 7-10; OVCAR3 passage 6-10; PEO1 passage 6-11, PEO4 passage 6 and 12 and FT33-TAg-RAS passage10-13.*

Figure 19 does not present strikingly strong results when contrasting the average size of exosomes between the human cells lines. PEO4 is the cell line that differed significantly the most from the other cell lines. The greatest difference can be observed with Kuramochi and OVCAR3 cell lines, followed by a slight difference with the control cell line. A small difference can also be observed between Kuramochi and PEO1. In summary, the N value for Kuramochi is 4, for OVCAR is 5, PEO1 is 6, PEO4 is 2 and FT33-Tag-RAS is 4; and due to this variance between the cell lines, we will compare these DLS results against their corresponding NTA results rather than gathering conclusion from this data. This comparison will be presented and discussed in section "q) Comparison between DLS and NTA results.".

1.n.2 Nanosight Results

Nanoparticle Tracking Analysis was carried out using the Nanosight NS300. Each exosome sample was prepared and analysed as outlined in 1.l.1 Sample preparation for DLS and NTA analysis and 1.l.3 Method for Nanoparticle Tracking analysis of Exosome samples. Every exosome sample was analysed at least once and for each analysis a total of three video captures were analysed by the Nanosight NTA 3.2 Software.

Below is an example of NTA and data collection of a Kuramochi sample (Passage 10) previously listed above in Table 9 List of all passages for each cell line from which exosomes were purified via ultracentrifugation and qualitatively and quantitatively analysed downstream. Media from this passage was purified and stored at -80°C until taken out for DLS analysis and NTA. The 50µL aliquot was thawed and for NTA purposes a 1:400 dilution was prepared as per protocol.

	DATE SEED	DATE COLLECT	Flask 1	Flask 2
Passage 10	16-Sep	23-Sep	18560000	19800000

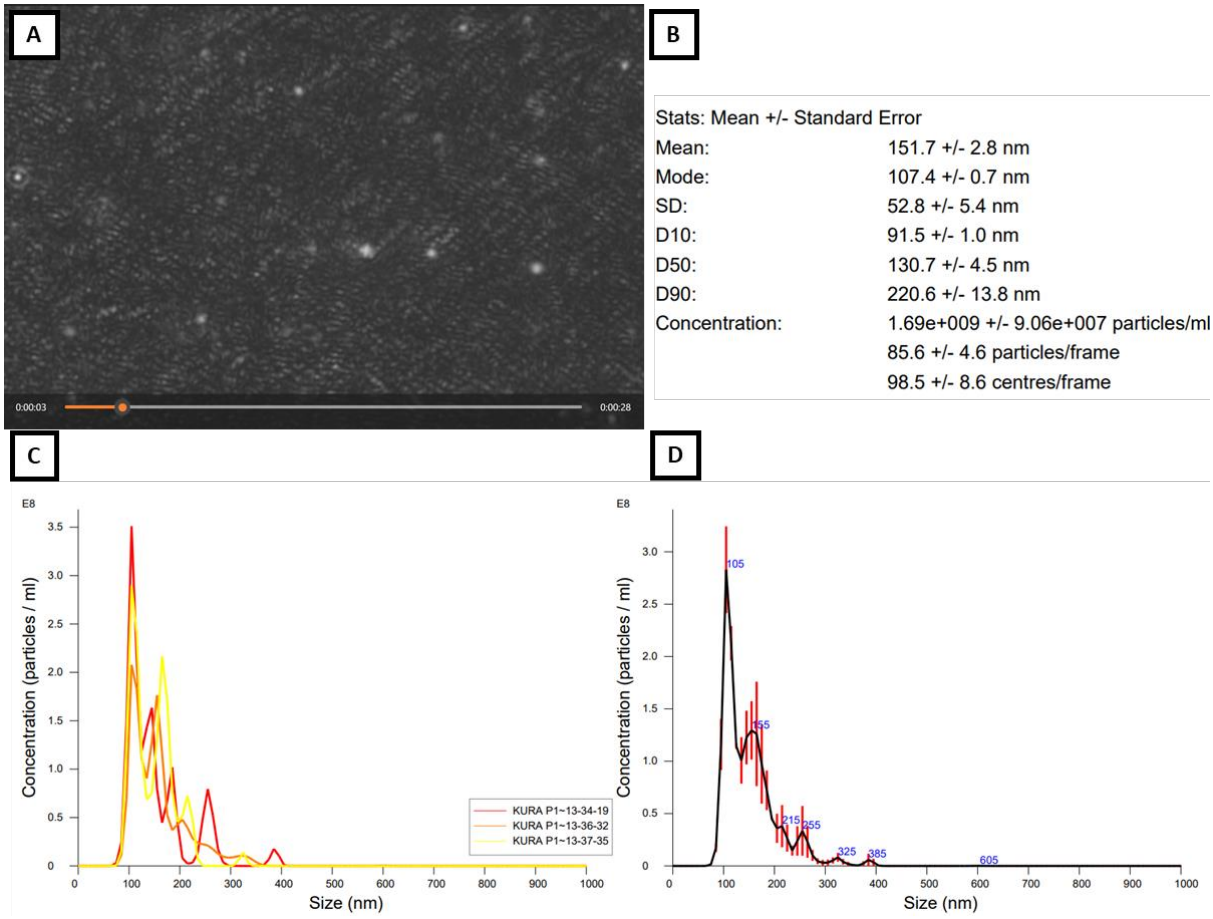

Figure 20 NTA analysis of Passage 10 of the Kuramochi cell line. *A) shows a screenshot from 1 of the 3 video captures taken for this exosome sample, the particles can be observed as differently sized white dots, however they are better observed in video format as particles aren't static but are in Brownian motion which helps distinguish them from background noise. B) section of the summary report document obtained from the NTA analysis where the summary of size distribution, the mean, mode and particle concentrations. C) Shows the Particles measured for each of the three video captures shown as different coloured lines. D) Average data with error bars for the three-reading shown on graph C.*

Once the particle concentration for all exosome samples listed inAfter multiple trial runs with both the Nanosight (NTA) and the Zetasizer (DLS) I determined that the majority of samples could successfully be analysed using similar dilutions regardless of the cell line of origin, but instead was dependent upon the desired analysis method. The decision to prepare dilutions ahead of time was ultimately taken to improve efficiency for off-site sample analysis of numerous samples.

The table below (Table 9) contains all the exosome samples that were successfully purified following the protocol outlined above, and were later analysed via Dynamic Light Scattering, Nanoparticle Tracking Analysis as well as analysed by Western Blot (covered in Chapter 3).

Table 9 were determined by NTA, these concentrations were corrected for the dilution required when preparing samples for NTA, which in the case of this study including the example (Passage 10), dilutions were multiplied by 400. The corrected concentration for the example was calculated to be 6.76E+11 (See Table 11). Next the same was done for all other Kuramochi passages; using these data, the averages for Kuramochi and other cell lines were calculated (See example of corrected data for Kuramochi cell line below in Table 11).

Table 11 NTA data collected for all passages from the Kuramochi cell line and its corresponding dilution correction as well as their calculated averages.

Kuramochi					
NTA determined concentration	Passage 6	Passage 7	Passage 8	Passage 9	Passage 10
	8.39E+08	1.14E+09	2.08E+09	1.59E+09	1.69E+09
Corrected for 1:400	Passage 6	Passage 7	Passage 8	Passage 9	Passage 10
	3.36E+11	4.56E+11	8.30E+11	6.36E+11	6.76E+11

For all cell lines, the NTA values of the last three passages purified were corrected for dilution, then these values were used to create bar graphs which will be discussed following this section (See Figure 21 and Figure 24). Averages for those three passages of human cell lines were calculated and put together in a separate bar graph (see Figure 22) to aid visualize differences in NTA values as well as media only samples (see Table 12). Finally, the calculated averages in particles/mL were next divided by their corresponding cell counts at the time of media collection to produce a graph displaying number of particles collected per cell (See Figure 25), which should provide a more accurate way of comparing the exosome yields between the different cell lines.

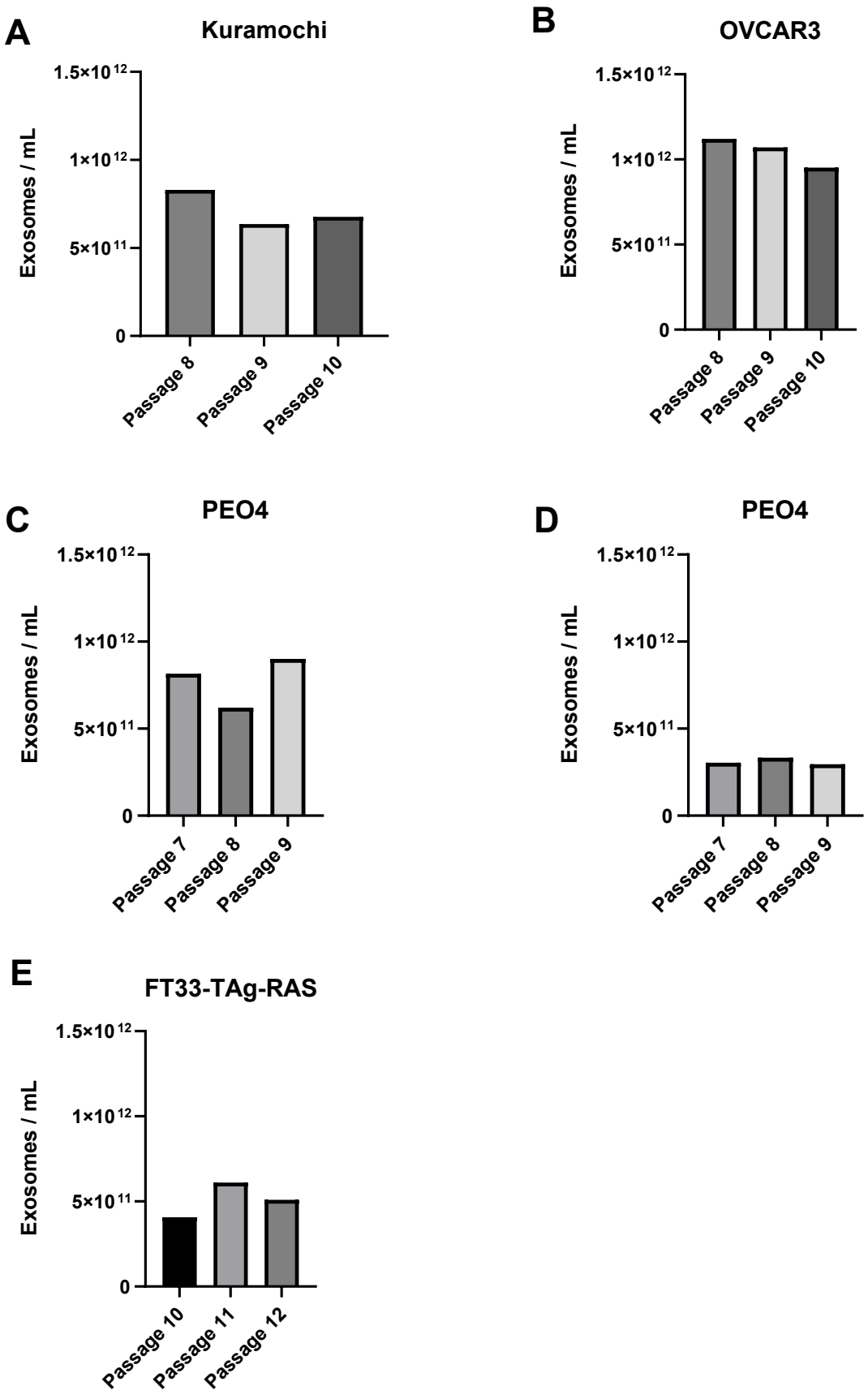

Figure 21 Nanoparticle Tracking Analysis of three passages of human cell lines. *Graph A shows the concentration output for exosome samples purified from passages 8 to 10 of the Kuramochi cell line, corrected for 1:400 dilution. Graph B shows the same for passages 8 to 10 of OVCAR3 corrected for*

1:400 dilution. Graph C shows the concentration output for passages 7 to 9 of PEO1 corrected for 1:400 dilution. Graph D shows the concentration output for passages 7 to 9 of PEO4 corrected for 1:400 dilution; finally, Graph E shows the concentration output for passages 10 to 12 of FT33-TAg-RAS corrected for 1:400 dilution.

Figure 21 presents NTA results for exosomes from various passage ranges of all human cell lines and are labelled A-E in order from Kuramochi, OVCAR3, PEO1, PEO4 and FT33-TAg-RAS. The data shows that there is consistency in samples from different passages across all human cell lines in terms of number of exosomes. Passages from the OVCAR3 cell line show the greatest number of particles detected by NTA values averaging at 1.05E+12; while in contrast exosome samples from the cell line with the lowest number of particles were from PEO4 which averaged at 3.24E+11 particles/mL. Kuramochi, PEO1 and the control cell line had relatively similar values as the averaged at 7.43E+11, 8.57E+11 and 5.96E+11 particles per millilitre correspondingly.

Table 12 Average concentration of exosome samples including cell media controls, determined by NTA and corrected for dilutions.

Cell Line/Exosome sample	Average NTA determined Particles/mL	Concentration corrected for Dilution. Particles/mL
KURAMOCHI	1.86E+09	7.43E+11
OVCAR3	2.62E+09	1.05E+12
PEO1	2.14E+09	8.57E+11
PEO4	8.09E+08	3.24E+11
FT33-TAg-RAS	1.49E+09	5.96E+11
CHO-K1	6.08E+08	2.43E+11
C4AFBN	6.11E+08	2.44E+11
RPMI + FBS	1.57E+08	3.13E+09
DMEM + UGS	3.46E+08	6.92E+09

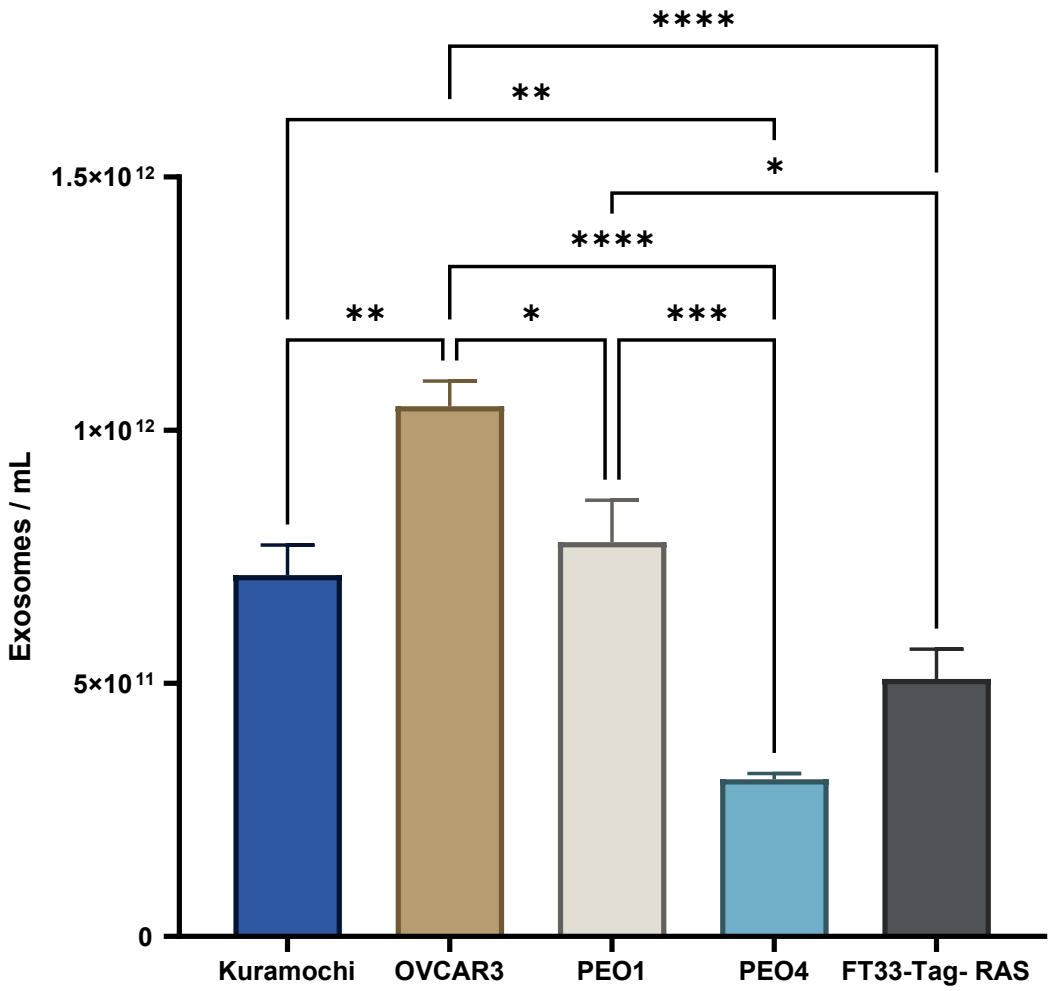

Figure 22 Graph showing Analysis of variance (ANOVA) of the average yield of exosomes from human cell lines form passages discussed in Figure 21. *The figure displays the average concentration of the human exosome samples after purification via ultracentrifugation from the passages described in Figure 21, corrected for 1:400 and compared by ANOVA. The average concentrations were calculated from Kuramochi and OVCAR3 from passages 8 to 10, PEO1 and PEO4 from passages 7 to 9; and finally passages 10 to 12 for the control cell line.*

As seen in Figure 22 samples from the control cell line had fewer number of particles when compared to samples from Kuramochi, OVCAR3 and PEO1 cell lines, the exception to the trend were samples from PEO4, which had significantly fewer particles than all other cell lines including the control cell line. Studying the number of exosomes secreted by different types of cells has been discussed not only in ovarian, but other cancers as well as other human diseases. In cancers, both have been demonstrated, where distinct rates of net exosome production by noncancerous versus cancerous cells have been higher for either of these. For example, a single cell study on breast epithelial cells found that cancer cell consistently secreted exosomes at a decreased rate to the normal cells (138). In the other hand, a wide

number of studies have shown the overexpression in exosomes production components in many pathways including ESCRT in across pancreatic, breast, gastric and thyroid cancer (139, 140, 141). In addition to cellular intrinsic changes, modifications to the microenvironment have also been demonstrated to result in a variations to numbers in exosome secretion; for example, hypoxia has been demonstrated to lead to increase exosomes secretion in breast and oral squamous cancers (142, 143).

A published study that examined and contrasted an epithelial breast cell line with its cancer cell line equivalent for their exosome yield (purified by ultracentrifugation), showed that they were able to collect 1.2×10^{10} exosomes/mL samples from T-25 cell flasks for the cancer cell line (undisclosed media volume), while their healthy counterpart exosome samples only had approximately half the concentration; they also confirmed the presence of exosome markers via western blot (110). Their findings differ from the exosome concentrations we were able to obtain from our ovarian cell lines as we do not see such drastic differences except for the PEO4 cell line; however, the cell lines we used are from a different anatomical origin, and exclusively comparing the number of exosomes might not be ideal regardless of cancerous or non-cancerous state. Of more interest, another study comparing ovarian cancer cell lines (Including OVCAR3) with a control cell line (epithelial ovarian cell line) to presented differences in their exosome yield (111), they were able to collect OVCAR3 samples with concentrations of 1.2×10^{9} exosomes/mL (undisclosed volume of media) after they also purified their exosomes via ultracentrifugation. Interestingly, exosome samples from their control cell line had and average concentration of 8.94×10^{8} exosomes/mL, which made the control consistently the lowest number of particles when compared to OVCAR3 and the other two ovarian cancer cell lines they used; IGROV1 and ES-2 which had exosomes samples of 1.02×10^{9} and 1.19×10^{9} particles/mL respectively. They too were able to obtain successful western blot results for all cell lines from exosome marker TSG101. Their findings align with most of what could be observed in Figure 22, where PEO4 consistently remains the exception, but the number of exosomes secreted by cancer cell lines is slightly larger than that of the control; it however would be interesting to see number of exosomes from a cancerous epithelial cancer cell lines as well as a second control cell line from ovarian origin.

We were able to collect samples with an average concentration of 1.05×10^{12} exosomes/mL for OVCAR3 meaning that our sample concentration was significantly greater when compared

to Zhang, Peng (111), and even though they collected from smaller media flask sizes they interestingly presented their number of particles loaded into the western blot analysis was sufficient to detect TSG-101. The high number of exosomes we obtained is likely due to the greater sized flasks used (T-175), and the modifications made to the standard exosome purification protocol by differential centrifugation found from a published method which suggested swapping out to smaller serological pipettes when approaching the bottom of spun tubes during removal of supernatants (137) as doing so immediately resulted in more robust exosome pellets that were visible throughout steps of ultracentrifugation during our purification protocol.

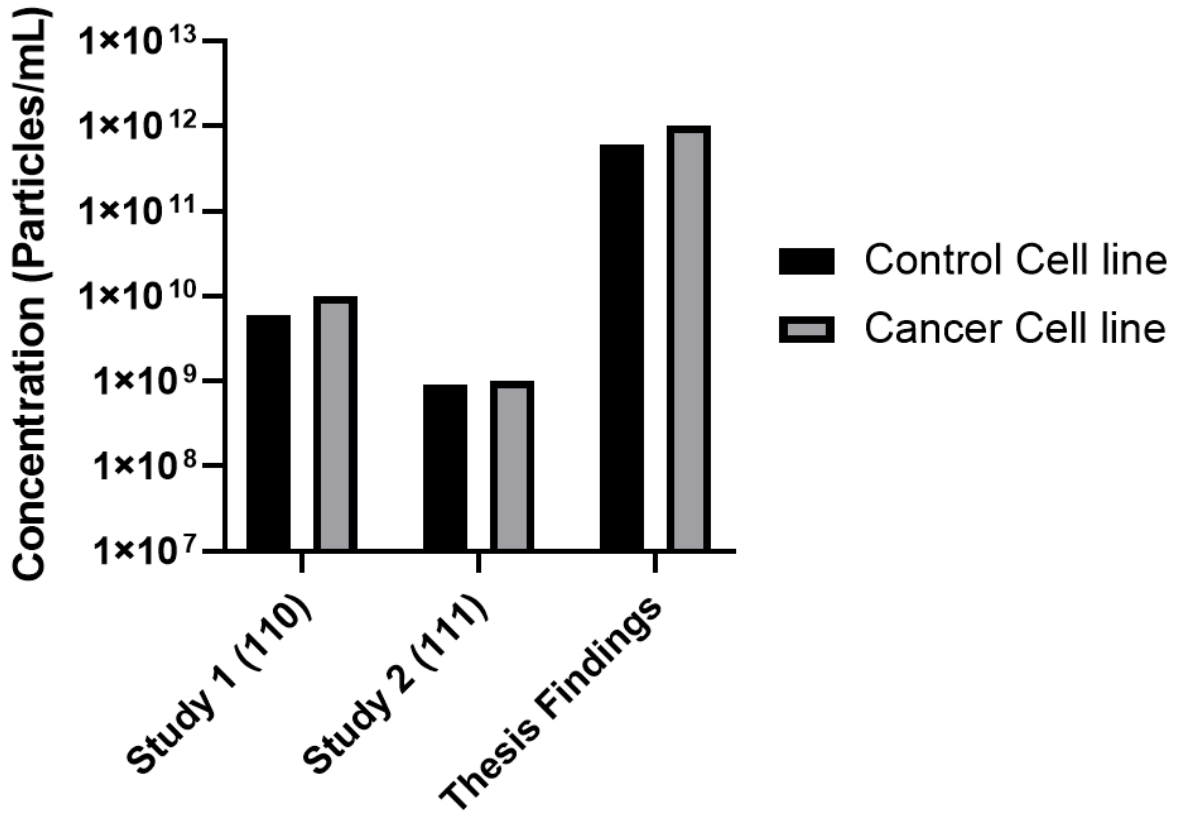

***Figure 23 Exosome Concentrations comparison between previous studies and Thesis findings**, "Study 1" Presents the exosome sample concentrations from an epithelial breast cancer cell line and its healthy counterpart cell line (110). "Study 2" purified exosomes from OVCAR3 and an ovarian epithelial control cell line (111). The "Thesis findings" data set shows the average concentration exosomes obtained from OVCAR3 and the control cell line presented in Table 12.*

Ultimately, it is difficult to do cross study comparisons where the isolation or detection methods of exosomes differs. Secondly, the heterogeneity of the exosome cargo should be individually studied for different cancer types and other diseases, especially since the nature

of exosomal intake differs between receiving cell types (144). There is a clinical significance in investigating the number of exosomes secretion, as cases where increased number of exosomes correlate to disease progression, it presents the possibility of blocking their production as a therapeutic target (144).

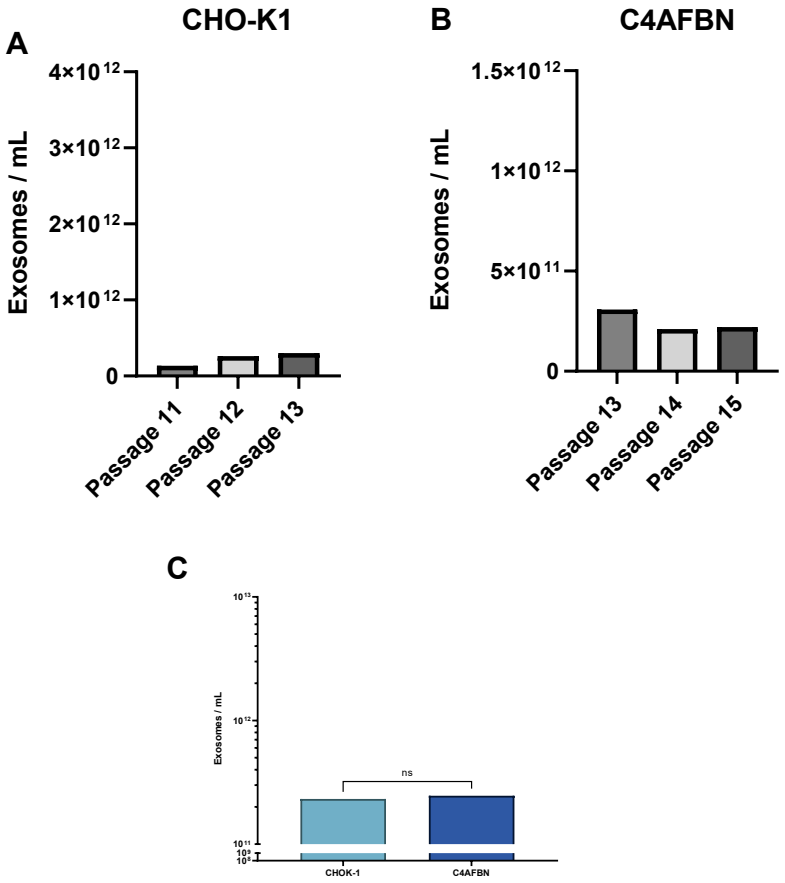

Figure 24 Nanoparticle Tracking Analysis of various passages and their average particle concentrations for both hamster ovarian cell lines. *Graph A shows the NTA concentration output for passages 11 to 13 of CHO-K1 corrected for 1:400 dilution. Graph B shows the concentration output for passages 13 to 15 of C4AFBN corrected for 1:400 dilution; Graph C shows the calculated averages for exosome samples from cell lines CHO-K1 and C4AFBN from the passages described in graphs A and B.*

Similar to Figure 21, Figure 24 Shows the last three passages analysed by NTA for both hamster cell lines which are correspondingly labelled A for CHO-K1 and B for C4AFBN. Their averages were calculated and compared in graph C, which prove that there are no significant differences between these values determined by ANOVA. The averages for CHO-K1 and C4AFBN were correspondingly 2.43E+11 and 2.44E+11.

As presented in chapter 1 of this thesis, previous studies of CLIC1 have demonstrated it to be elevated in breast, liver, pancreatic and ovarian cancers (51, 75, 76, 77); this overexpression has been demonstrated as a prognosis marker indicating poor outcome for 5-Year survival in gastric and ovarian cancers (53, 145). In more detail, an increased CLIC1 has been shown to be a marker for angiogenesis and metastasis in gastric cancer and the latter in colon and gall bladder cancers (78, 79, 81, 146). There is abundant evidence regarding CLIC1 overexpression and its role in cancer stage progression and migration, however the mechanisms by which metastasis is facilitated remains unclear.

The objective of looking at a CLIC1 overexpressing cell line and its wild type, was to examine CLIC1's possible role in rate of exosome production, which would propose this extracellular communication pathway as a possible metastasis driver. However, based on the obtained results, we are unable to draw this conclusion based on the similarity of exosomes (number and size distribution) collected from both cell lines, even when corrected with the cell counts at the time of media collection in figure 24 graph C where ANOVA analysis showed no significant variation.

Since our findings indicate that elevated expression of CLIC1 does not seem to affect the total number of secreted exosomes, it is worth investigating if the rate of exosome shedding may be affected by carryout NTA quantification on exosomes collected at different time intervals, to compare the rate of exosome shedding. Doing this would allow to see if the secretion of exosomes is influenced by CLIC1 overexpression without affecting the uptake rate; otherwise support the idea that CLIC1 is not involved in exosomes production mechanisms.

o) Nanoparticle Tracking Analysis of media only experimental controls.

In order to check for the presence of contaminating exosomes from the serum supplements added to our cell growth media, aliquots from each of the two media only "exosome" controls, were subjected to NTA analysis, per the regular protocol outlined above in 1.l.3 The samples were loaded in polystyrene 4-side optical pathway 10 mm, cuvettes (Sarstedt). Using a 1mL pipette the sample was resuspended and then the full millilitre prepared was loaded in the cuvette which was placed in the designated chamber making sure the cuvette marking was lined up with the laser trajectory. Next, once the sample has been loaded and the

chamber shut, the operating software "Zetasizer Software" is opened. The Standard Operating Procedure was set with "measurement type" for size and had the following parameters:

Dispersant: "1 X PBS" with *RI: 1.332* and *Viscosity (Cp):* 1.0203

Material: "Extracellular vesicles" *RI: 1.38* and *Absorption: 0.010*

Standard Operating Procedure (SOP) Settings: *Temperature: 25°C, Cell type: Disposable Cuvette – DTS 0012; Angle of detection: 173° Backscatter; Measurements: Two measurements of Eleven runs of ten seconds duration*

Once the SOP settings have been selected the readings were carried out and the data was accordingly stored. Readings that were deemed acceptable by the system's "Size Quality Report" (RESULT MEETS QUALITY CRITERIA) which is a summary report detailing whether the result meets the Instruments quality criteria for size measurement.

Method for Nanoparticle Tracking analysis of Exosome samples. It is to note that due to the low number of particles present in both these samples, only a 1:20 dilution was made rather than the 1:400 stated in the method for regular exosome samples.

Table 13 Nanoparticle Tracking Analysis of media only negative controls purified via ultracentrifugation and corrected for dilution.

MEDIA	SUPPLEMENT	Particles/mL
RPMI	10% Foetal Bovine Serum	3.13E+09
DMEM/F12	2% Ultroser G Serum	6.92E+09

Table 13 presents the NTA data collected for both the media controls (10%FBS and 2%UGS) corrected for the stated dilution in k) Preparation of negative media controls. However, in order to contrast these relative number of particles already present in media to the average number of particles collected from all cell lines, we calculated the corresponding NTA values and displayed it as a percentage in Table 14.

Table 14 Relative percentage of particles detected by NTA from Cell media additives compared to their corresponding average number of particles per cell line.

Average particles/mL Corrected for dilution

Media Supplement	10% FBS				2% UGS	5%FBS	
Cell line	Kuramochi	OVCAR3	PEO1	PEO4	FT33	CHO - K1	C4AFBN
Corrected (Particle/mL)	5.87E+11	9.24E+11	1.15E+12	3.18E+11	6.34E+11	2.60E+11	3.65E+11
Percentage of particles from media Supplement	**0.53%**	**0.34%**	**0.27%**	**0.98%**	**1.09%**	**0.60%**	**0.43%**

To the number of particles for all ovarian cancer, cell lines which were grown with 10% FBS, less than 1% of all particles can be attributed to being already present in the media. Similarly, for the control cell line, particles obtained from 2%UGS represent only 1.09% from its average number of collected particles. Both Hamster cell lines were grown in 5% FBS, hence, we compared their average number of particles and took the percentage of media present particles against half of the obtained value from the samples prepared with 10%FBS; and in a similar trend to other cell lines, particles detected in media represent less than 1% of that of samples incubated with cells. However, it is important to highlight that an alternative method to completely prevent contamination of exosomes derived from FBS, is simply to change to media only (no additives) in the days prior to collection, however, the viability for each cell line needs to be evaluated individually under the new conditions.

p) Correlation of shed exosomes per cell between cell lines.

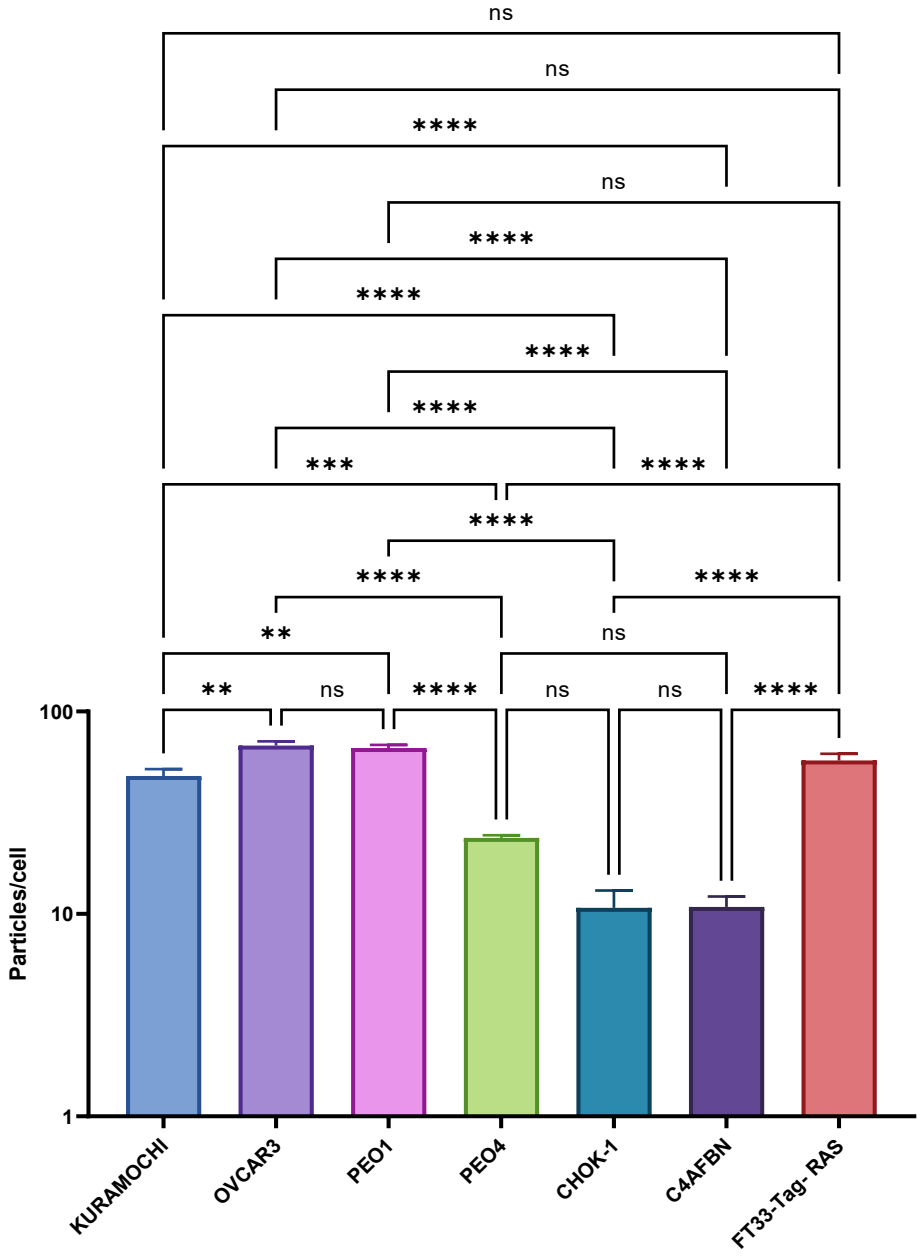

Figure 25 Analysis of Variance (ANOVA) of the last three passages for all cell lines, corrected for the number of cells at the time of media collection. *The graph contrasts data obtained from the last three passages for each cell line (Table 12) where the number of exosomes determined via NTA were corrected to the number of cells counted at the time of media collection prior to purification via ultracentrifugation, and is presents in unit of particles per cell. The data was analysed by ANOVA to highlight differences between cell lines.*

Each bar in Figure 25 are representative of exosomes from a different cell line and show the number of particles determined by NTA divided by each corresponding number of cells

counted at the time of media collection, along with significance in variance between each other.

ANOVA results shows marked difference in exosomes/cell between human and hamster cell lines except for PEO4. Similarly, the control cell line only significantly differed from PEO4 but not from all 3 other ovarian cancer cell lines. OVCAR3 and PEO1 had the highest number of particles/cell lines secretion and had a marked difference when compared to PEO4 as well as a recorded difference when compared to the Kuramochi cell line.

The clearest distinction in exosome yield between cell lines could be observed when comparing human and Hamster cell lines; whereas comparison of the human ovarian cancer cell lines against the human control cell line did not show a significant difference, except in the case of the PEO4 cells, which shed significantly fewer exosomes compared to the human control cell line and the other three human ovarian cancer cell lines. These finding don't align completely with previously published study that compared the number of exosomes secreted by breast cancer cells and their healthy analogue which showed an approximate 10X difference in exosome numbers shed from cancerous versus control cell lines (110). One distinction between this study and others looking to quantify exosomes from cancer cell lines, was choosing the time of media collection at confluency rather than time intervals as this controls for differences of growth rates between cell lines (110, 111)

q) Comparison between DLS and NTA results

All exosome samples were analysed via both DLS and NTA and to streamline analysis of multiple samples, set dilutions were prepared at UTS prior to carrying out analysis at UNSW where the equipment was located. A significant number of samples did not pass the DLS self-analysis report. Aside from rerunning the same sample and in order to carry on with the rest of the samples, new dilutions were not prepared and DLS data was not obtained from a number of samples. The results from samples available for both analyses were compiled together and will be discussed below.

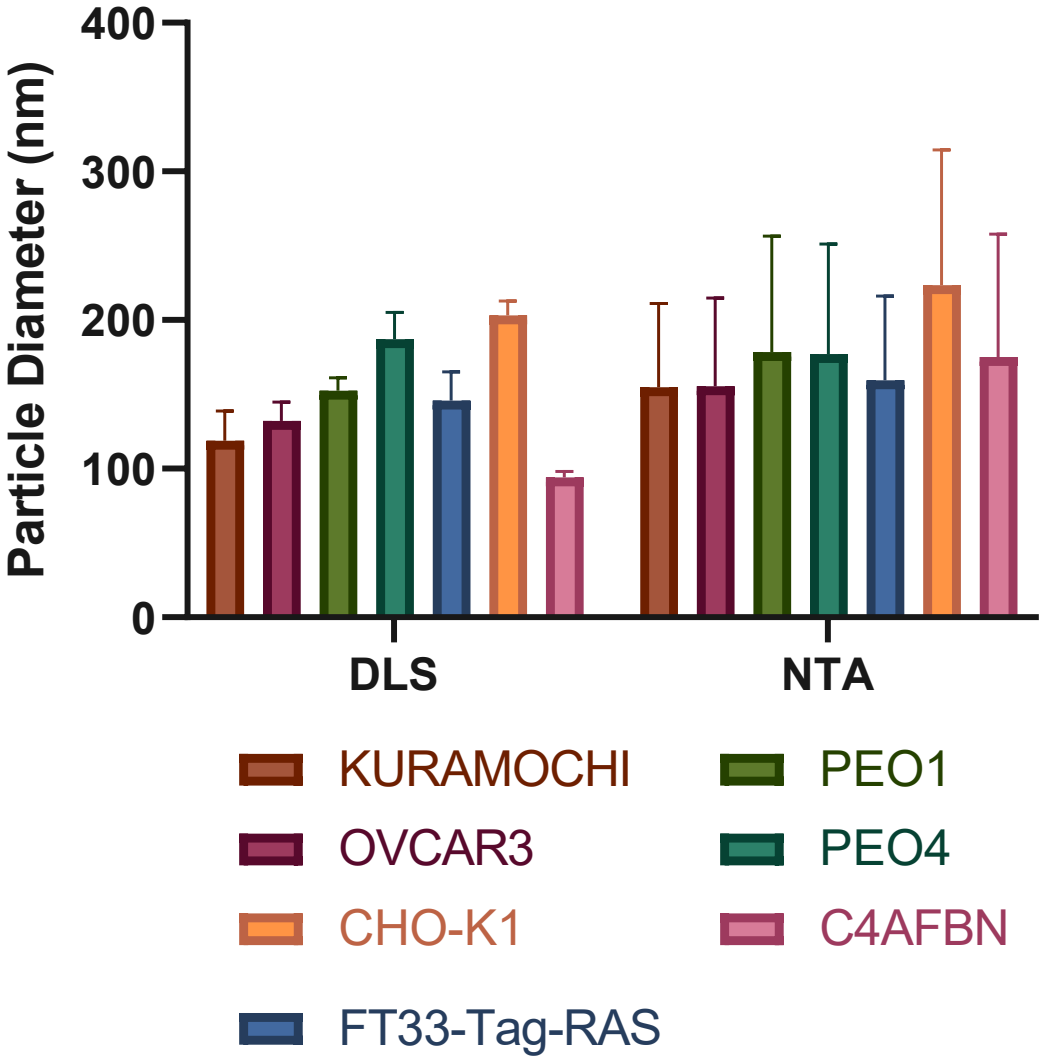

Figure 26 Comparison Between DLS and NTA analysis determination of average particle size for all cell lines. *Represented by different colours are the average diameter size obtained from an average of the same passages by DLS and NTA. Only NTA results from passages where DLS results were available were used to produce this graph; they are the following: Kuramochi passage 7-10; OVCAR3 passage 6-10; PEO1 passage 6-11, PEO4 passage 6 and 12; FT33-TAg-RAS passage10-13; CHO-K1 passage 9 and 11 and C4AFBN passage 10.*

Observed in Figure 26, the Kuramochi average particle size NTA results are 148nm while DLS presented a slightly smaller result of 118nm. This trend of slightly larger average diameter for NTA results can be seen across all cell lines, except for PEO4 where the NTA determined diameter was 177nm while the DLS was slightly larger with 187nm. These results concur that quantity of the size distribution differs between the two analyses; however, they contradict that of previous comparative study for measurements of nanoparticles using both NTA and DLS where the overall trend was that DLS comparatively showed larger diameters (147). The first main difference between our and their study is that they used commercially available 1-palmitoyl-2-oleoyl-glycero-3-phosphocholine (POPC) and prepared a range of polydisperse

samples by filtering them though different sized filters. DLS results for samples that had more polydisperse samples (bigger filter sizes) were relatively smaller and closer to NTA results for the same samples. DLS seems to be an significant tool for rapid characterization of the particles as it provides a wider size range of analysis between 1 nm to 6µm, however it becomes more difficult to obtain DLS results in samples that are too polydisperse (148).

Finally, the obtained NTA and DLS results support that most particles present in our samples are of the expected diameter for exosomes which suggest for acceptable sample purity, however, differential centrifugation is limiting in the ability to minimise contaminating proteins and other membranous particles (149); meaning that further support this purity claims, further exosome characterization by western blot were carried out and will be discussed in the following chapter.

Utilizing both techniques can provide complementary results for investigating exosomes, however, individually each has advantages over the other. DLS won't destroy your sample and provides a very rapid analysis which facilitates analysis of numerous samples, facilitated by its usage of disposable cuvettes, contrary to the continuous flow state requiring flushing between samples of NTA. On the other hand, NTA measured particle size more accurately as it analyses particles individually, rather than calculating a curve; as well providing concentration of particles in sample. One shared limitation between both assays is that diameter is calculated under the assumption that the particles have the diffusional properties of a solid sphere (150), which although should not impact the analysis of exosomes, should still be a consideration.

With these points in mind as well as their size working ranges (NTA 0.01µm – 1µm, DLS 0.3 nm to 10 µm), I suggest that DLS is used first to examine the quality of a sample, the fine tuning of the purification process, and to assess overtime deterioration of a sample after freezing and defrosting in order to carry out a correctly controlled NTA. However, once a consistent sample and handling protocol is established, NTA should be the assay of preference as it provides overall more in-depth results for exosomes.

Conclusions:

This chapter aimed to contrast the yield of exosomes shed by all cell lines by growing them under comparable settings. Based on these previous studies and the western blot results discussed in Chapter 3 of this thesis, it can be determined that the yield of exosomes we obtained were robust and more numerous than that of previous studies. Although, we saw consistency in the number of particles collected across passages, one can speculate that due to the lengthy manual nature of the purification protocol, it is difficult to obtain precise number of exosomes if data is collected from only a few passages, and for this reason more iterations would help solidify our findings.

The preliminary results found in this study justify that the tissue culture arrangement allows to produce a sufficient yield of exosome samples as determine by quantified NTA results, and that in contrast, particles present in media and their corresponding additive prior to seeding cells are not significant in contrast with the final number of particles collected. DLS proved to be a successful quick alternative for determining particle diameter of exosome samples; however, samples need to at least double the concentration of samples run in the NTA; and since this equipment doesn't provide concentration values for the samples, it ultimately results in preparing various dilution with the aim to meet the equipment's parameters.

Finally, to further investigate any role of CLIC1 in exosome secretion, it would be of interest further investigating, using both the hamster cell lines we studied to contrast the rate at which these cell lines reach maximum yield of exosomes. In addition, use of CLIC1 knockdown cell lines may be more appropriate to determine role of CLIC1 in exosome shedding processes.

Chapter 3

Protein expression on exosomes and whole cell lysates

Introduction

This chapter presents the protein profiling using Western Blot analysis of whole cell lysates and exosomes derived from the different cell lines, in order to compare expression levels of a set of specific protein markers. This Western blot analysis was also used as an additional means of confirming the presence of purified exosomes extracted from the cell culture media described in the previous chapter, complementing the NTA and DLS analyses.

According to the International Society for Extracellular Vesicles latest update in 2018 for minimal information for studies of extracellular vesicles (151); in order to carry out protein content-based extracellular vesicle characterization, at least one protein from the transmembrane or glycosylphosphatidylinositol-anchored proteins associated to plasma membrane and/or endosomes; and one from the cytosolic proteins recovered in the extracellular vesicle group must be used to confirm the presence of exosomes. For this first category we have selected the non-tissue specific tetraspanin CD63, and for the second category, we selected Tumour Susceptibility Gene 101 (TSG 101).

CD63 protein is particularly enriched in vesicles within multivesicular endosomes; particularly during their formation from early endosomes (152), and is comparatively higher than when compared to its presence in whole cell lysates (153). CD63 has previously been used to assist in verifying the presence of exosomes from ovarian cancer cell lines (154, 155). Coincidentally, TSG 101 has also been used as a marker for exosomes in ovarian cancer (156), and has been shown that as part of its role in the endosomal sorting complex (ESCRT) which regulates exosome biogenesis, its downregulation resulted in a reduced number of secreted exosomes as well as their associated CD63 (157).

Western blotting is the recommended and most common used methodology by which to analyse CD63 and TSG 101 and any other exosome markers, as stated by the MISEV2018 guide (151). In addition, the guide recommends that western blotting also be carried out on the corresponding source lysates to show if the analysed proteins are enriched in the collected exosomes when compared to their producing cells (151). Ultimately, in order to quantitatively

assess protein expression levels of exosome marker proteins and CLIC proteins of interest in both exosome and whole cell lysate samples, we carried out densitometry analysis of the resulting western blot images.

Materials and Methods

a) Preparation of Whole Cell Lysate

Radioimmunoprecipitation assay (RIPA) buffer (10 Mm Tris HCl, 1 Mm EDTA, 0.1% SDS, 140 Mm NaCl, 1% TritonX-100) was prepared and mixed with protease inhibitors (Sigma-Aldrich, NSW, Australia) (Catalogue number: 11697498001). Cells at 90% confluency in T75 flasks were washed 3 times in ice cold PBS after which they were detached from the plate utilising the standard trypsinization procedure as described *in 1.f.1 Cell passaging of the Kuramochi cell line*. Once detached, cells were collected, the cells in suspension were counted as described in g) *Cell count protocol and record keeping* to aliquot equal number of cells for all cell lines. Once equal number of cells have been aliquoted, they were spun down and the supernatant was discarded, the pelleted cells were washed two times in PBS before being resuspended in the RIPA buffer containing the Protease Inhibitors, to be incubated on ice for 15 minutes while shaking. The lysate was then centrifuged for 15 minutes at 13000rpm, in an Eppendorf 5424R benchtop centrifuge previously cooled down to 4°C. The supernatant lysate was then collected and transferred to a new tube without disturbing the pellet. An aliquot of the lysate was set aside for protein quantification via bicinchoninic acid (BCA) assay, while the rest was stored at -80°C for western blot analysis.

b) BCA Assay

Protein concentration of whole cell lysate samples was determined with the BCA assay, using the Pierce™ BCA Protein Assay Kit (Thermo-Fisher) according to the manufacturer's instruction. In summary, 50 µl of working reagent (50 parts of reagent A to 1 part reagent B, supplied in the kit) were mixed with 50 µl of sample, loaded onto a flat bottom 96-well plate, which then was incubated for 30 minutes at 37°C completely covered in foil, and finally the absorbance was measured at 562 nm using the Infinite M1000 PRO plate reader (Tecan). Measurement readings were carried out in triplicate. A calibration curve was created every time the assay was performed with bovine serum albumin (BSA) (also available in BCA kit)

controls of known concentrations of 0 - 2 mg/ml. Using the standard curve, the protein concentration of each sample was determined according to its absorbance.

c) Sodium Dodecyl Sulphate Polyacrylamide Gel Electrophoresis (SDS-PAGE) for protein electrophoresis

Sodium dodecyl sulphate-polyacrylamide gel electrophoresis (SDS-PAGE) was carried out using the Biorad Minigel System (Biorad), where the 4-15% Mini-PROTEAN® TGX™ Precast Protein Gels (Biorad) were used as resolving gels. Two different loading buffers were prepared according to the protein of interest for each gel. Nine parts of 4 X Laemmli sample buffer (Biorad) to 1 part of 2-mercapthoethanol (Sigma-Aldrich) was added for reducing gels (CLIC1, CLIC4 and TSG-101). Gels probed using anti-CD63 antibodies were always run in non-reducing conditions, meaning samples were mixed with 4 X Laemmli sample buffer only. Samples were then incubated at 95°C for 10 minutes to allow protein denaturation prior to being loaded onto the gel. Gels were run in Tris/Glycine/SDS buffer (Biorad) for 45 minutes, at a voltage of 150V and 0.5 mA.

d) Western Blot Analysis

Proteins were transferred from polyacrylamide gels to blotting membranes using Trans-Blot Turbo Transfer System Transfer pack (Biorad) run in the Trans-Blot Turbo Transfer System, Gels were arranged accordingly as per transfer pack instructions and run for 7 minutes 2.5 A constant: up to 25V. The membranes were blocked for 1 hour on a shaker at room temperature in 5% Bovine Serum Albumin (BSA) blocking buffer in Phosphate-buffered saline with Tween-20 (PBST) (137 mM NaCl, 2.7 mM KCl, 10 mM Na_2HPO_4, and 1.8 mM KH_2PO_4, Tween20 0.05%). The protein of interest was visualized by incubating the membrane with primary antibodies diluted in 0.1% BSA in PBST buffer overnight and in a cold room (4°C). The day after the membranes were washed 3 x 10 minutes in PBST, before being incubated for 2 hours at room temperature in anti-mouse or anti-rabbit secondary antibody (both Thermofisher) diluted in 0.1% BSA in PBST buffer at a concentration of 1:2000, after this the membranes were once again washed for 3 x 10 minutes in PBST before being imaged. The antibody staining was visualized at the ChemiDoc Imaging System (Bio-Rad) using the Clarity™ ECL Blotting substrate (Biorad) prepared as per the manufacturer's instructions and the membranes were incubated for 5 minutes. The molecular weight of the target proteins was assessed against those of a Kaleidoscope Precision Plus Protein Standards (BioRad) on which 5µl were loaded onto the minigel.

The primary antibodies and their dilutions used for this work are the following: Santa Cruz CLIC1 (F-9) antibody (sc-374202), 1:250; Santa Cruz CLIC4 antibody (sc135739), 1:250; TSG 101 Antibody (C-2): sc-7964 1:250; CD63 Antibody (MX-49.129.5): sc-5275, 1:250; Abcam CA125, Recombinant Anti-MUC16 antibody (ab168360), 1:1000.

e) Densitometry analysis

Densitometry analysis was carried out on all images obtained from Exosome and Whole cell lysates membranes labelled all 4 of the primary antibodies studied (anti-CLIC1, anti-CLIC4, anti-CD63 and anti-TSG101). ImageJ software is used to obtain raw data of the band signals to contrast results across membranes.

Calculations with the Raw ImageJ data were as follows:

1. **Whole-cell lysate membrane labelled with anti-CLIC antibodies.**
   The raw data from wells 2-8 was divided by the raw data of the recombinant CLIC protein control (well 9 or 10). Then, this value was normalised by the raw data of B-actin.
2. **Exosome membrane labelled with anti-CLIC antibodies.**
   The raw data from wells 2-8 was divided by the raw data of the recombinant CLIC protein control. Then, these values were normalised by the number of exosomes loaded for each membrane. Then an average from all three replicates was used to create the bar graph with error bars.
3. **Whole-cell lysate membrane labelled with exosome markers antibodies.**
   The whole raw cell lysate data were corrected by dividing by the corresponding raw data β-actin signal.
4. **Exosome membrane labelled with exosome markers antibodies.**
   The raw data from wells 2-8 was divided by the number of exosomes loaded for each membrane.

The obtained calculated values were used to create bar graphs to facilitate visualizing differences between cell lines. Calculated densitometry data from 3 membranes of different set of exosome samples were used to create the bar graphs for each of the target proteins and display their average with error bars. In comparison, only data from one membrane of whole cell lysates was used to produce the corresponding graphs.

Results and discussion

f) Western blot and Densitometry analysis

Each set of **Exosome blots** was produced from SDS-gels that had been loaded with equal number of exosome particles per well. In order to do this, the earliest passage of exosome samples available for each cell line was used, and the concentration of particles was known from the corresponding NTA analysis. Important to note that for each Western blot, the sample with the lowest concentration of particles was determined, and the volumes required to match this number of particles for all other exosome samples was calculated and adjustments made; next, all samples were made up to 25µL with PBS, therefore all samples contained the same number of exosomes suspended in 25µL of PBS. Then, 8.3µL of the 4X Loading buffer was added to all samples to allow loading 30µL to each well of an SDS-PAGE gel.

Whole cell lysate gels were loaded with an equal volume of sample (25µL) from protein lysates derived from equal number of cells, across all cell lines; as previously mentioned in a) Preparation of Whole Cell Lysate . To all whole cell lysate samples, 8.3µL of loading buffer was added and 30µL was loaded per well onto the gels. Control CLIC1 and CLIC4 purified recombinant proteins were analysed with BCA assay in order to determine their protein concentration as per b) BCA Assay , for each sample the corresponding volume for 50µg of protein were calculated and the volume was brough up to 25µL with PBS and as all other samples 8.3µL of loading buffer was added to each sample, and 30µL of sample were loaded per well.

Table 15 Example calculation for loading gels with equal number of exosomes (Membrane C). This table contains calculations for sample preparation and loading of 4 gels, for the set of exosome samples labelled as "Membrane C" further discussed below. Separate preparation was calculated for the membrane to be labelled with CD63 antibody, as loading buffer for this sample did not contain reducing agent. Passage 15 of C4AFBN is highlighted for being the lowest concentration of particles in this set of samples; to which the corresponding volume of sample for all other cell lines were calculated to match.

			CLIC1, CLIC4, TSG101		CD63	
			β-Mercaptoethanol		NO β-ME	
PASSAGE	**CELL LINE**	**NTA (Particles/mL)**	Sample (µL)	PBS (µL)	SAMPLE (µL)	PBS (µL)
Passage 9	Kuramochi	1.59E+09	26.08	48.92	8.69	16.31
Passage 9	OVCAR3	2.68E+09	15.48	59.52	5.16	19.84
Passage 9	PEO1	2.25E+09	18.43	56.57	6.14	18.86
Passage 9	PEO4	7.39E+08	56.16	18.84	18.72	6.28
Passage 12	CHO-K1	6.50E+08	63.84	11.16	21.28	3.72
Passage 15	C4AFBN	5.53E+08	75.00	0.00	25.00	0.00
Passage 11 II	FT33 II	9.18E+08	45.18	29.82	15.06	9.94

g) Determining Expression of Control Protein Markers

In order to determine the most appropriate exosome markers to use for our purposes, various antibodies against a variety of known exosome markers were tested, with some preliminary experiments described here. Below Figure 31, the blot was probed with primary antibody Anti-CD81, with the commercial antibody verified for western blotting of cellular and exosomal CD81 antigen, having a molecular weight of ~25 kDa.

CD81 is another tetraspanin transmembrane protein present in extracellular vesicles (158). This protein in prostate tissue has been observed to be overexpressed and drastically elevated in cancerous tissues (159). Interestingly a similar trend has been witnessed in exosomes secreted from breast, prostate and lung cancer cell lines that have undergone corresponding effective drug treatments(160, 161) these results suggest CD81's use as an indicator of prognosis, as they correlate to efficacy of response to cancer treatments. Relating to ovarian cancer, CD81 has previously been demonstrated to be present in exosomes collected from ovarian cancer cell lines (162, 163). However, its use as a potential prognostic determinant in ovarian cancer has yet to be studied, it would be interesting to investigate if a similar trend of elevated CD81 can be observed in susceptible cancer cell lines when compared against resistant cell lines.

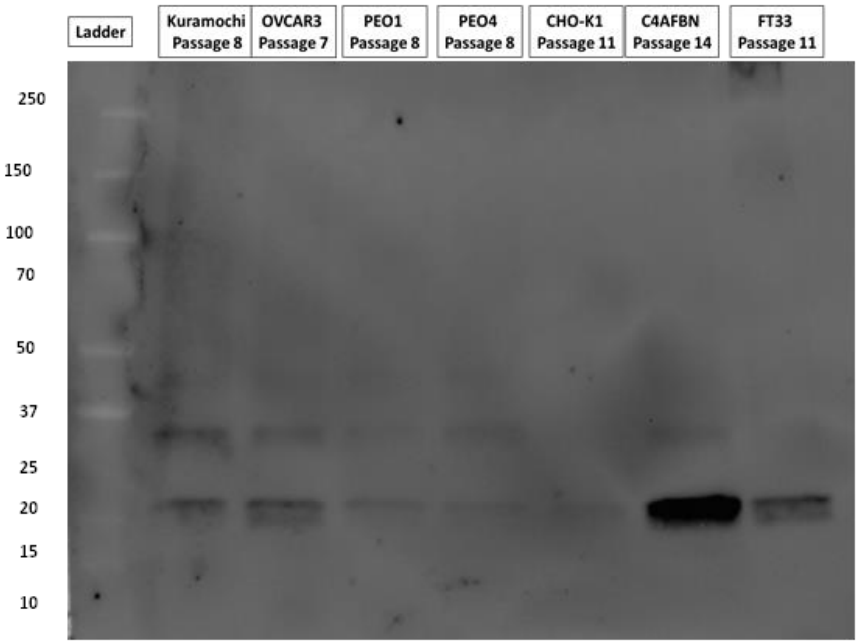

Figure 27 Western blot membrane labelled with 1:250 Mouse anti-CD81. *In ascending order from well "2", samples correspond to: Kuramochi, OVCAR3, PEO1, PEO4, CHO-K1, C4AFBN and FT33-TAg-RAS. Secondary antibody was a 1:2000 dilution of Rabbit anti-mouse.*

Results from the membrane in figure 23, show the presence of a band in all samples around the 20-25 kDa range, most likely binding to CD81, which would confirm the presence of exosomes in all samples collected from media obtained from all cell lines used in this thesis. Of note, the expression of CD81 in exosomes from the C4AFBN cell line was drastically greater that of the CHO-K1 cell line. Knowing that an equal number of exosomes were loaded into each membrane for all cell lines, we can gather that the level of CD81 expression was relatively low in exosome from both PEO1 and PEO4 cell lines, relative to the other human cell lines; of which the control cell line had the highest relative levels. Also observed in figure 23, was the presence of a secondary band in all samples, except for CHO-K1, observed around the 30kDa mark. However, the overall look of the membrane was blotchy, for which more repeats would be necessary to evaluate the utility of CD81 more critically as a marker in exosomes for the used cell lines; in addition, western blot analysis on whole cell lysate (WCL) from all of the studied cell lines would also be required. In addition, and as shown later in this chapter, anti-CD63 and anti-TSG101 antibodies, against known exosome marker proteins were trialled and found to give clearer results. Therefore, no further blots were probed with anti-CD81 antibodies.

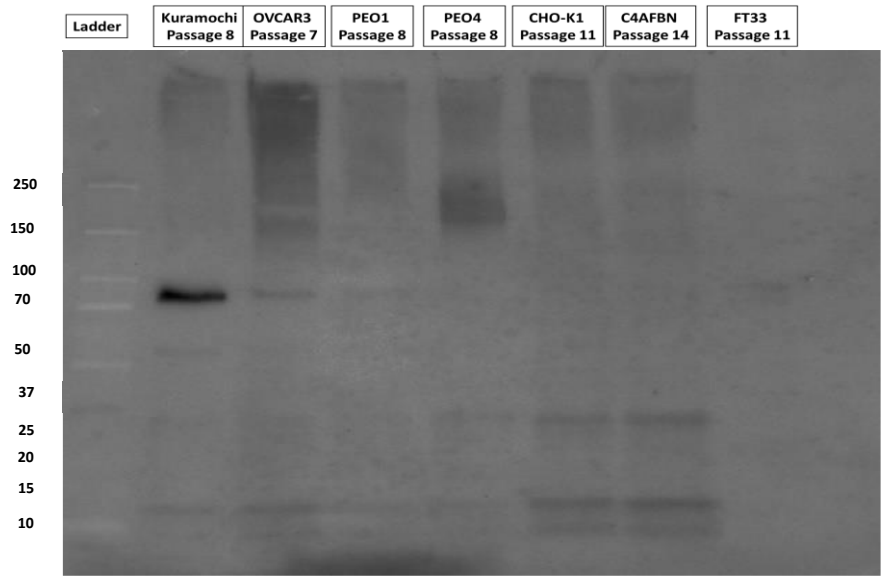

Figure 28 Western blot membranes labelled with 1:250 Rabbit Anti-MUC16. *In ascending order from well "2", samples correspond to: Kuramochi, OVCAR3, PEO1, PEO4, CHO-K1, C4AFBN and FT33-TAg-RAS. Secondary antibody was a 1:2000 dilution of Goat anti-rabbit.*

The membrane in figure 24 shows a duplicate western blot of exosome samples as Figure 32; however, this blot was probed with rabbit antibody against the previously discussed ovarian cancer marker CA125. Also, these exosomes samples were treated as discussed in the methods section for this chapter (d) Western Blot Analysis), with reducing agent added to the samples when loaded on the SDS-PAGE (unlike samples that were to be probed with antibodies against tetraspanin CD63 and CD81, which needed to be non-reduced). According to the product description, thick bands are expected to appear above the 250kDa mark as this protein is relatively large (1519kDa). Although we can clearly observe other unexpected positive signals of smaller than expected size, when focused on the >250kDa region, we can observe that across all cancer cell lines high molecular weight bands (likely CA125) are present in all samples, with higher levels in the cancer samples compared to exosomes from the control cell line. The results for this western blot are inconclusive, and upon investigating literature, western blot is not the best methodology for measuring exosomal CA125. However, the quality of our western blot results resemble that presented in a similar published study that measured CA125 on exosomes also purified by differential centrifugation from colorectal cancer cell lines (164). Prior to carrying out densitometry analysis on this preliminary western blot results, more repetitions would be necessary in order to draw significant conclusions; however, based on our preliminary results, it does appear that exosomal CA125 could help distinguish exosomes shed by ovarian cancer cells

compared to the control FT33 exosomes. Furthermore, probing with a loading control such as anti-actin is also needed to confirm equivalent protein loading across the samples.

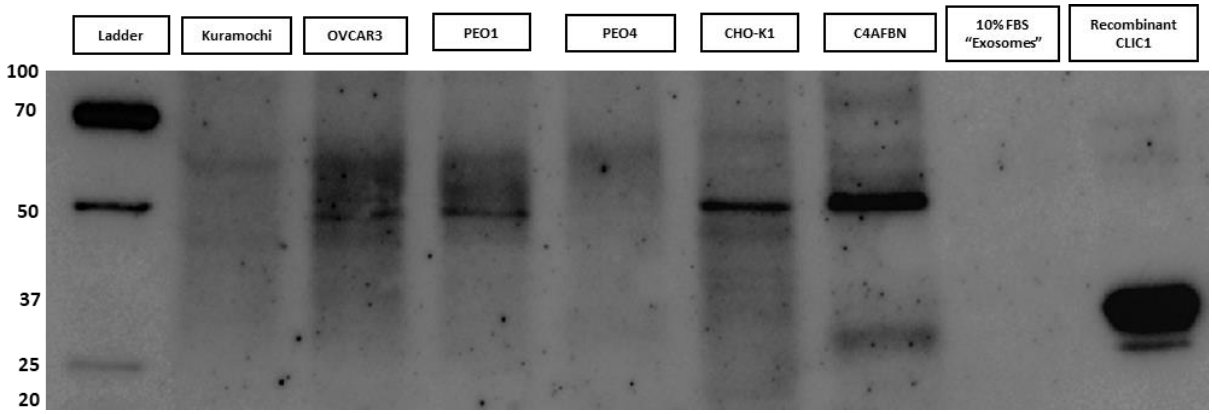

Figure 29 Western blot membranes labelled with 1:1000 mixture of CLIC1 and TSG-101 antibody. *In ascending order from well 2, samples correspond to: exosome from Kuramochi, OVCAR3, PEO1, PEO4, CHO-K1, C4AFBcell lines and "cell free sample" as well as recombinant CLIC1 Protein. Secondary antibody was a 1:2000 dilution of Goat anti-rabbit.*

Figure 29 presents results from a western blot carried out on exosomes collected from all cell lines except for the control cell line (FT33). These initial western blots were conducted alongside NTA to investigate the potential presence of contaminating vesicles derived from the serum supplement added to the cell growth media. Well 8, labelled "cell free sample", is an example of a cell-free blank control, which was prepared from media with 10% serum added, however, no cells were added, with the sample treated and processed in an equivalent manner as all other samples, following the usual media collection and exosome purification protocol. Our western blot findings clearly show that neither of the target proteins (TSG-101, 49kDa and CLIC1, 26kDa) are detected in the cell-free sample. These blank cell-free media samples were prepared as described in k) Preparation of negative media controls. This same process was repeated over various western blots, using cell-free samples, with all blank samples consistently showing no observable markers detected or present in the sample. These findings were also corroborated by the NTA results (See Nanoparticle Tracking Analysis of media only experimental controls.). These results show that the cell culturing model used in this thesis for the collection of exosomes from tissue culture is viable and suitable for use with our different cell lines, with no contaminating exosomes from the added bovine serum supplement.

h) Probing for Specific Protein Markers via Western Blot Analysis.

Below are 16 images grouped into four sets of four western blot membranes. Each set of four membranes displays exosome samples collected from three individual experiments (across three blots) and the fourth blot contains whole cell lysates from the respective 'originating' cell lines. Each set of four membranes was probed with an antibody against either a marker for exosome confirmation, (CD63 or TSG 101), or one of the two CLIC proteins of interest for this project (CLIC1 or CLIC4). The blots were then stripped and re-probed with an anti-actin antibody. As such, three biological replicates were analysed, with each membrane containing one distinct set of exosome samples purified from a different passage of cells. Each blot of exosomes contains one sample derived from each cell line, with the fourth blot containing a set of whole cell lysates inclusive of all cell lines and 50µg of recombinant CLIC1 and the final lane 50µg recombinant CLIC4 protein. *See* Table 16 *for a summary of the western blot loading schema.*

*Table 16 Layout of four different sets of samples used for western blot and densitometry analysis. **Note, lanes 9 & 10 were only used for the blots probed with anti – CLIC antibodies.*

	1	2	3	4	5	6	7	8	9**	10**
Membrane A (Exosome)	Protein Ladder (Bio-Rad)	Kuramochi (Passage 7)	OVCAR3 (Passage 6)	PEO1 (Passage 7)	PEO4 (Passage 7)	CHO-K1 (Passage 10)	C4AFBN (Passage 13)	FT33 (Passage 10)	50µg CLIC1	50µg CLIC4
Membrane B (Exosome)		Kuramochi (Passage 8)	OVCAR3 (Passage 7)	PEO1 (Passage 8)	PEO4 (Passage 8)	CHO-K1 (Passage 11)	C4AFBN (Passage 14)	FT33 (Passage 11)		
Membrane C (Exosome)		Kuramochi (Passage 9)	OVCAR3 (Passage 9)	PEO1 (Passage 9)	PEO4 (Passage 9)	CHO-K1 (Passage 12)	C4AFBN (Passage 15)	FT33 (Passage 11)		
Membrane D (Whole Cell Lysate)		Kuramochi WCL	OVCAR3 WCL	PEO1 WCL	PEO4 WCL	CHO-K1 WCL	C4AFBN WCL	FT33 WCL		

i) Western Blots labelled with Exosome markers.

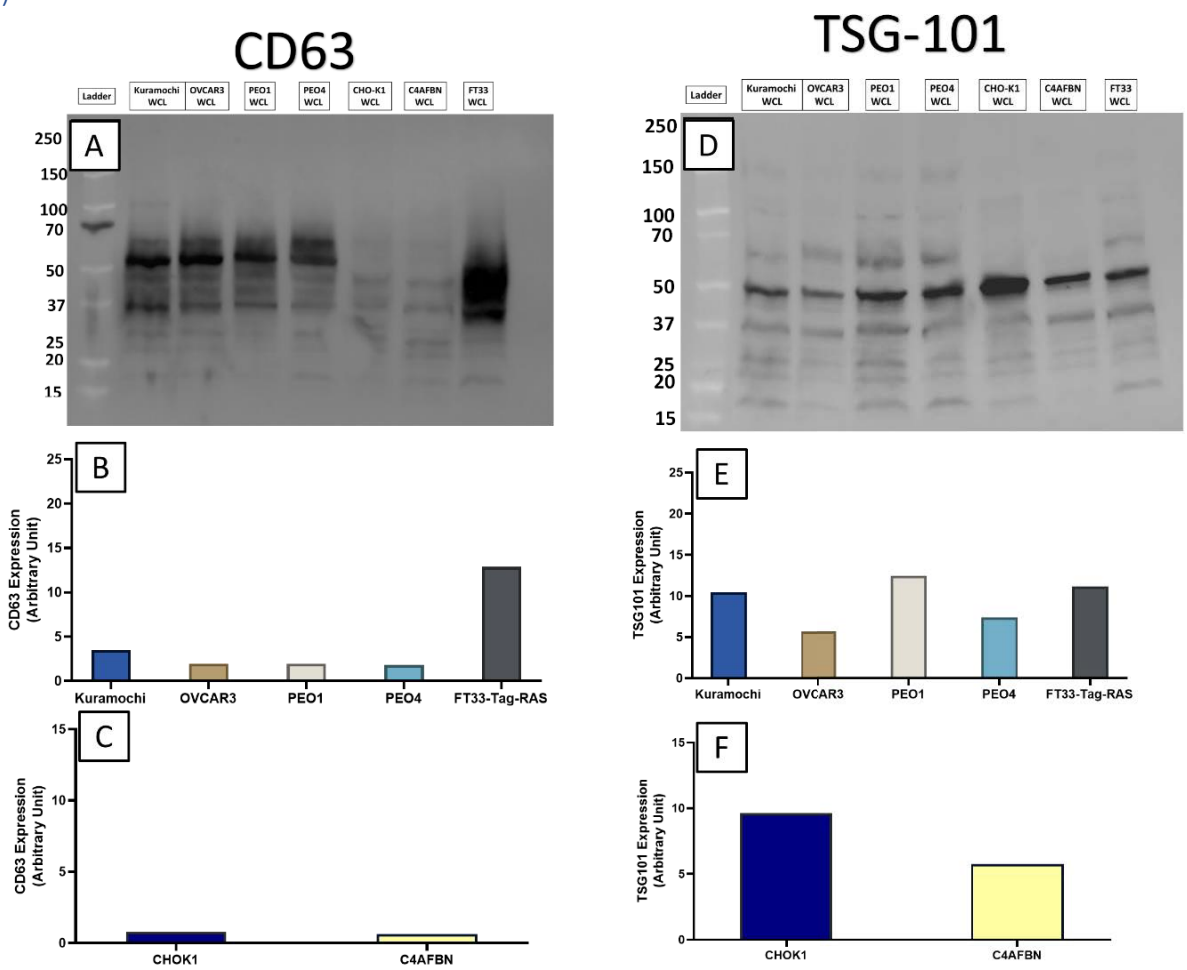

Figure 30 Western blot analysis of membranes loaded with whole cell lysates and labelled with CD63 and TSG101 antibodies. *Western blot of whole cell lysates for all cell lines tagged with two different exosome antibodies and their densitometry analysis. "A" displays the imaged western blot membrane with whole cell lysates tagged with mouse anti-CD63, while the secondary antibody was a 1:2000 dilution of rabbit anti-mouse. In ascending order from well "2", samples correspond to: Kuramochi, OVCAR3, PEO1, PEO4, CHO-K1, C4AFBN and FT33-TAg-RAS. "B" shows the densitometry analysis obtained from membrane "A" contrasting only the human cell lines, while "C" shows the same but for the two hamster cell lines. "D" displays the imaged western blot membrane with whole cell lysates tagged with mouse anti-TSG101, while the secondary antibody was a 1:2000 dilution of rabbit anti-mouse; and presents the same arrangement of samples as membrane "A". "E" shows the densitometry analysis of the signal obtained from the human cells in membrane "D", while "F" does so for the two hamster cell lines.*

Both membranes displayed in Figure 30 were used to produce the densitometry results using both different exosome antibodies CD63 and TSG101. Membrane A presents whole cell lysates analysed with ImageJ and the obtained values were then normalized to β-Actin to produce the data showed in the graphs labelled "B" and "C". These results show that the control cell line significantly expressed more CD63 when compared to all other cell lines. In contrast, both hamster cell lines expressed the lowest CD63 even when compared to all Human Ovarian cancer cell lines and show no significant difference between them. Membrane labelled "D" was tagged with anti-TSG101 and contains the same whole cell lysates as membrane "A", and with its obtained densitometry graphs "E" and "F" were

produced to show the human and hamster cell line findings correspondingly. Densitometry analysis from this membrane do not show a particular trend in either of the cell types; PEO1 cell line expressed the highest amount, while OVCAR3 presented the lowest amount of TSG101 expression.

Membranes that we loaded with exosome samples were similarly analysed using ImageJ, however, re-probing of these blots with actin (unsurprisingly) did not provide any usable results and hence normalisation against actin was not possible (blots not shown). Instead, the individual exosome blots were assumed to have equal loading based on the fact that each gel was loaded using an equal number of exosomes/well, as determined by NTA. However, as previously explained, the number of exosomes loaded for each replicate experiment did vary. Therefore, in order to allow comparison of the three blots to each other, the raw densitometry values were corrected against the corresponding number of particles loaded on each gel/membrane set. These corrected values were then used to plot graphs of the densitometry data for all exosome membranes.

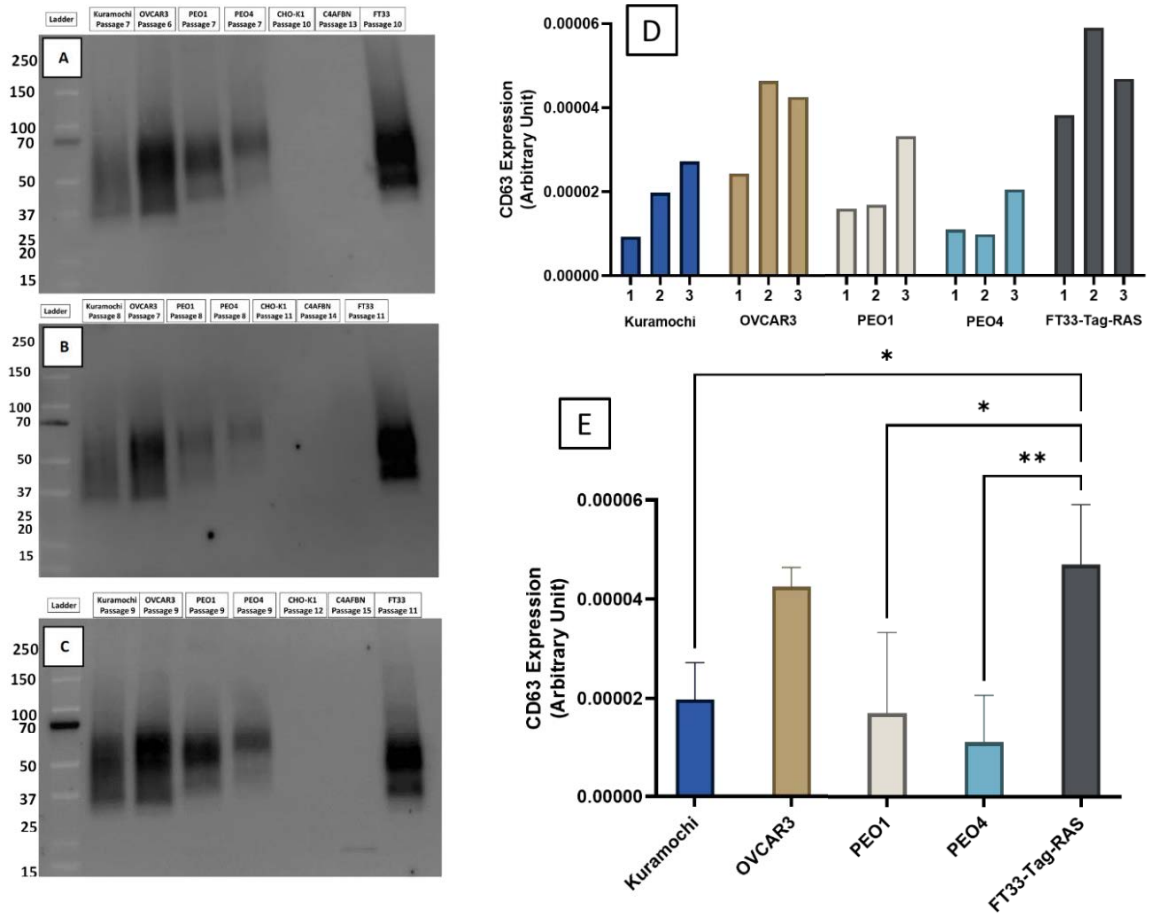

Figure 31 Western blot analysis of membranes loaded with exosomes and labelled with CD63 antibody. *Membranes A, B and C were loaded with exosome samples each from different cell passages, Lane 1 contained a molecular weight ladder and*

*in numerical order from well "2", samples correspond to: Kuramochi, OVCAR3, PEO1, PEO4, CHO-K1, C4AFBN and FT33-TAg-RAS. The secondary antibody was a 1:2000 dilution of Rabbit anti-mouse. The three Exosome membranes**, labelled with anti-CD63**, were analysed using ImageJ and the raw values obtained were corrected to the corresponding number of particles initially loaded. Graph labelled "D" shows individually these three corrected values for each of the cell lines, excluding the hamster cell lines from which no signal was detected. "E" is the analysis of variance between averages from the 3 repetitions shown in graph "D".*

Results from Figure 31 show that exosome samples from Hamster cell lines did not present any detectable CD63, even though CD63 was detected in the Hamster Whole cell lysates (Membrane A of figure 30). This indicates that CD63 likely is not abundant enough to be detected or not found on exosomes for CHO-K1 and C4AFBN cell lines. While for the exosome samples derived from human cell lines CD63 expression was clearly present for all cell lines, with the exosomes from both the control cell line and OVCAR3 presenting similarly the highest levels in contrast to Kuramochi, PEO1 and PEO4 (See graph D and E).

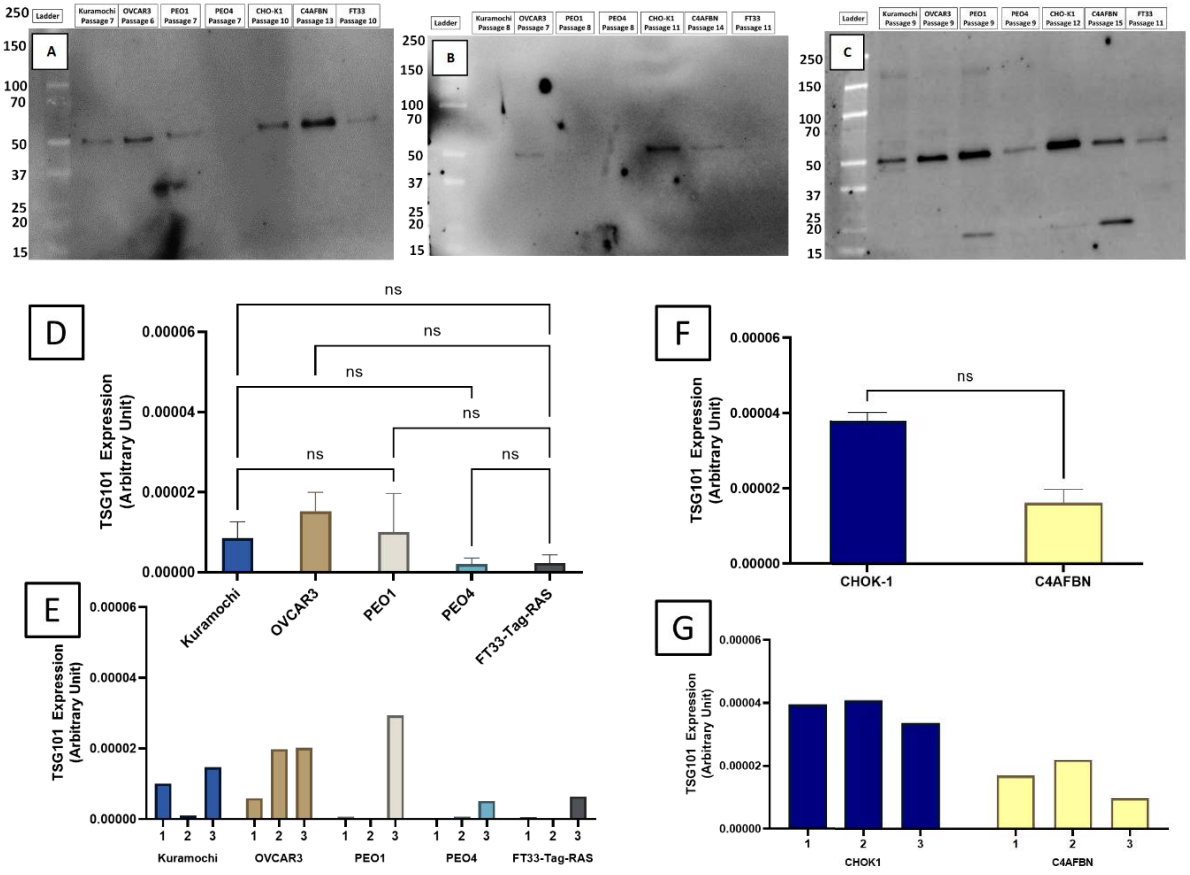

Figure 32 Western blot analysis of membranes loaded with exosomes and labelled with TSG101 antibody. *Membranes A, B and C were loaded with exosome samples each from different cell passages (Same as Figure 31), Lane 1 contained a molecular weight ladder and in numerical order from well "2", samples correspond to: Kuramochi, OVCAR3, PEO1, PEO4, CHO-K1, C4AFBN and FT33-TAg-RAS. The secondary antibody was a 1:2000 dilution of Rabbit anti-mouse. The three exosome membranes were **labelled with anti-TSG101**, then analysed using ImageJ after which the raw values obtained were corrected to the corresponding number of particles initially loaded. Graph labelled "D" the analysis of variance between averages from the 3 repetitions presented in graph "E"; which shows individually the three corrected values for all the human cell lines. Graphs "F" and "G" show the same variance analysis and individual corrected values for both ovary hamster cell lines.*

Membranes shown in Figure 32 (probed with anti-TSG101) were used to produce all graphs in the figure, which present results separately by their species of origin in graphs D and E from F and G (human and hamster correspondingly). Membranes A-C were also analysed as described for the CD63 membranes; their individual densitometry analysis displayed in graphs E and G of Figure 32, showed that the control cell line along with PEO4 were markedly the lowest. TSG 101 was present in exosomes from both hamster cell lines, where the wild type presented double that of C4AFBN. From the blots, it is clear that OVCAR3 consistently presented the highest level of exosomal TSG 101 compared with the other human ovarian cancer cell lines.

In summary, we can infer some significant outcomes from the densitometry protein analysis presented above. Mainly that the protein analysis carried out on the exosome samples, both CD63 and TSG101 can be used to confirm the presence of exosomes in the samples collected for all the human cells studied in this project. It is however important to note that these two markers do not seem to be equally expressed across the different exosome samples, therefore making it difficult to use them as loading controls for densitometry analysis.

j) Western Blot results for CLIC Proteins

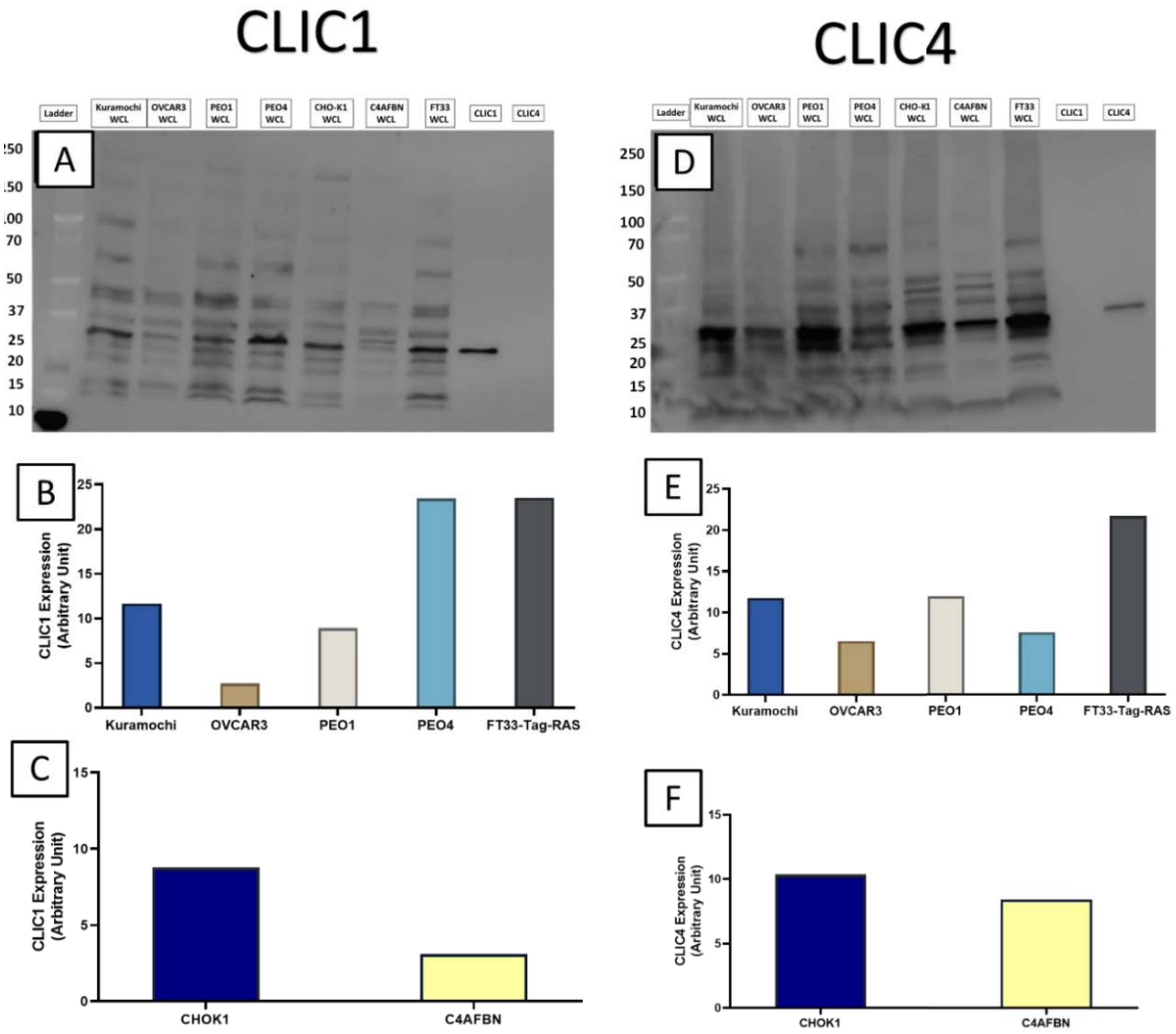

Figure 33 Western blot analysis of membranes loaded with whole cell lysates and labelled with CLIC1 and CLIC4 antibodies. *Western blot of whole cell lysates for all cell lines tagged with either anti-CLIC1 or anti-CLIC4 antibodies and their densitometry analysis. "A" displays the imaged western blot membrane with whole cell lysates tagged with mouse anti-CLIC1, while the secondary antibody was a 1:2000 dilution of rabbit anti-mouse. In ascending order from well "2", samples correspond to: Kuramochi, OVCAR3, PEO1, PEO4, CHO-K1, C4AFBN and FT33-TAg-RAS. "B" shows the densitometry analysis obtained from membrane "A" contrasting only the human cell lines, while "C" shows the same but for the two hamster cell lines. "D" displays the imaged western blot membrane with whole cell lysates tagged with mouse anti-CLIC4, similarly with the secondary antibody 1:2000 dilution of rabbit anti-mouse; as well as presenting the same set of samples as membrane "A". "E" shows the densitometry analysis of the signal obtained from the human cells in membrane "D", while "F" does so for the two hamster cell lines.*

The same whole cell lysate samples displayed in membranes of Figure 30 were loaded in the membranes in figure 33, however, were labelled in CLIC1 and CLIC4 specific antibodies. In a similar manner to the other whole cell lysate membranes, the raw densitometry data was analysed with ImageJ and corrected against the corresponding β-Actin intensity signal, not presented in this thesis. Membrane "A" was labelled with ant-CLIC1 antibody, and the data obtained was used to produce both graphs "B" and "C", which belong to the data obtained from the human and hamster cell lines correspondingly. Membrane labelled "D" was tagged

with anti-CLIC4 and contains the same whole cell lysates as past whole cell lysate membranes and was used to produce densitometry graphs “E” and “F” which show the human and hamster cell line findings correspondingly.

Results from these whole cell lysate membranes unexpectedly showed that Wild Type CHO-K1 expressed over double the amount of CLIC1 compared to C4AFBN. PEO4 and the control cell lines had at least double CLIC1 expression relative to the other human cell lines of which OVCAR3 was the lowest. CLIC4 whole cell lysate membrane analysis only clearly showed that the control cell drastically presented the most CLIC4 in comparison to all ovarian cancer cell lines; where in the case of Kuramochi and PEO1 it corresponded to nearly double, and in the case of OVCAR3 and PEO4 approximately four times.

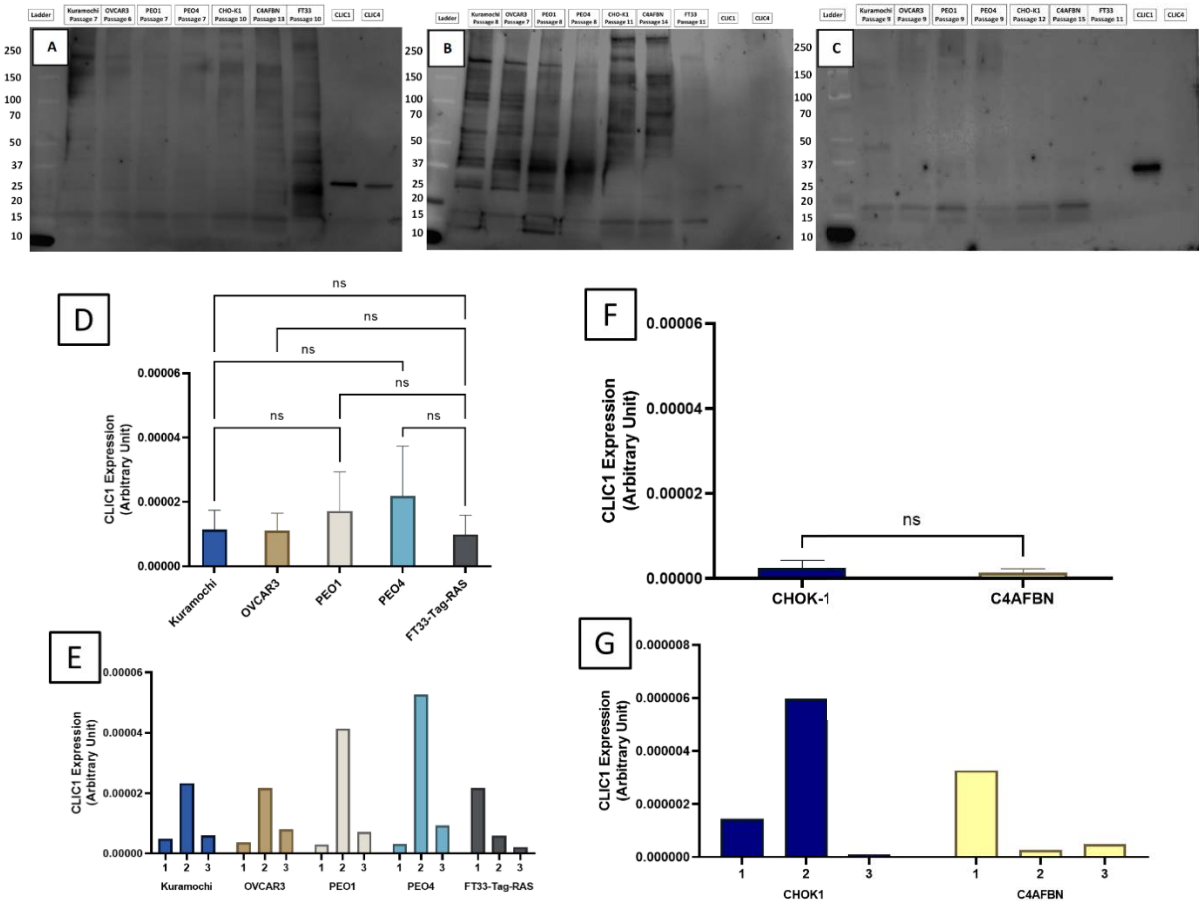

Figure 34 Western blot analysis of membranes loaded with exosomes and labelled with CLIC1 antibody. *Membranes A, B and C were loaded with exosome samples each from different cell passages (Same as Figure 31 and Figure 32), Lane 1 contains a molecular weight ladder and in numerical order from well “2”, samples correspond to: Kuramochi, OVCAR3, PEO1, PEO4, CHO-K1, C4AFBN and FT33-TAg-RAS. The secondary antibody was a 1:2000 dilution of Rabbit anti-mouse. The three exosome membranes were* ***labelled with anti-CLIC1****, then analysed using ImageJ after which the raw values obtained were corrected to the corresponding number of particles initially loaded. Graph labelled “D” shows the analysis of variance between averages from the 3 repetitions presented in graph “E”; which shows individually the three corrected values for all the human cell lines. Graphs “F” and “G” show the same variance analysis and individual corrected values for both ovary hamster cell lines.*

The membranes above in Figure 34 were labelled with anti-CLIC1 antibody and their densitometry analysis values, obtained by ImageJ, were used to produce both graphs in Figure 34. The intensity values of the exosome samples (Wells 2-8) were measured for the three exosome membranes (A-C) and were individually corrected against the corresponding number of particles loaded for each membrane (See graph E and G), to finally produce an average for the three sets of data to carry out the analysis of variance (See graphs D and F).

Results obtained from these membranes showed no notable difference in exosomal CLIC1 between CHO-K1 and C4AFBN. While for the human cell derived exosomes, interestingly PEO1 and PEO4 showed more exosomal CLIC1 than those from the control cell line; and although the exosomal CLIC1 from Kuramochi and OVCAR3 were also slightly greater than the control cell line, in the analysis of variance no significant differences were demonstrated between all human derived exosome samples.

A similar study investigating exosomal CLIC1 in a glioblastoma cancer compared three different cell lines; one wild type glioblastoma cell line, and the second was the same cell line modified to block CLIC1 expression, finally a healthy control cell line (88). They were able to display that CD63 and TSG101 were markedly expressed more in exosome samples when compared to their whole cell lysates, moreover, they were able to confirm the presence of CLIC1 in glioblastoma derived exosomes, where their wild type cancer cell line presented more exosomal CLIC1 than exosomes shed by the CLIC1 silenced cell line. Although their western blot findings align with our results when it comes to the exosome markers in terms of their expression in exosomes and whole cell lysates; our results do not agree, as our CLIC1 overexpressing cell line presented slightly less than the wild type, however, if we focus on comparing cancer vs healthy cell lines, we do see agreement in that exosomal CLIC1 is greater in cancerous cell lines.

We have shown that CLIC1 is carried by exosomes shed from a range of ovarian cancer cell lines, and our preliminary results indicate that in contrast exosomal levels of the cancerous cell lines, there is a trend for higher level of CLIC1 compared to those derived from the control cell line.

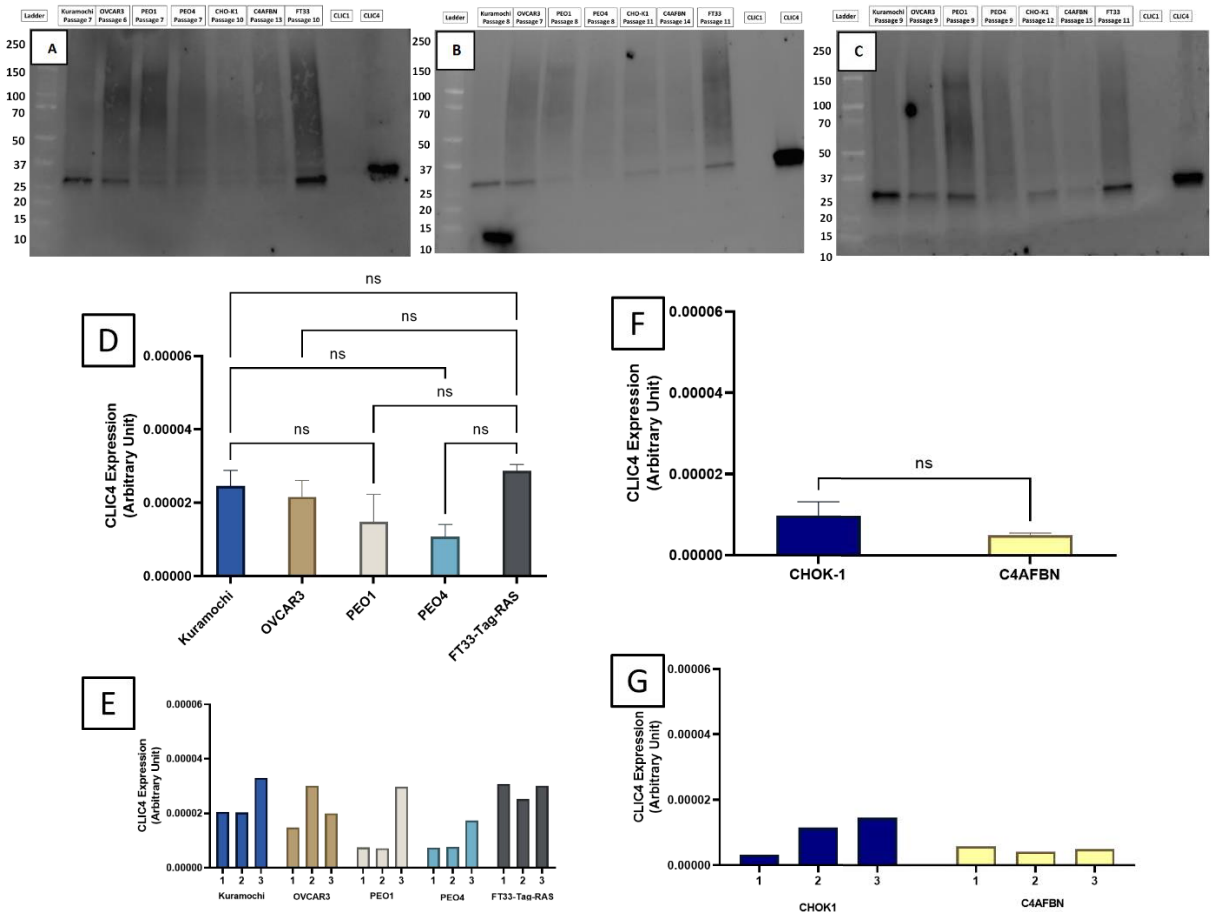

Figure 35 Western blot analysis of membranes loaded with exosomes and labelled with CLIC4 antibody. *Membranes A, B and C were loaded with exosome samples each from different cell passages (same samples as Figure 31, Figure 32 and Figure 34), Lane 1 loaded with a molecular weight ladder and in numerical order from well "2", samples correspond to: Kuramochi, OVCAR3, PEO1, PEO4, CHO-K1, C4AFBN and FT33-TAg-RAS. The secondary antibody was a 1:2000 dilution of Rabbit anti-mouse. The three Exosome membranes,* ***labelled with anti-CLIC4****, were analysed using ImageJ and the raw values obtained were corrected to the corresponding number of particles initially loaded. Graph labelled "E" shows individually these three corrected values for each of the cell lines, excluding the hamster cell lines from which no signal was detected. "D" is the analysis of variance between averages from the 3 repetitions shown in graph "D". Graphs "F" and "G" show the same variance analysis and individual corrected values for both ovary hamster cell lines.*

Similar to previously present exosome membranes, in Figure 35 we have presented the same arrangement of samples in three separate membranes which instead were labelled with anti-CLIC4 antibody. Membranes A-C correspond to the same sets of exosome samples as previous membranes. The densitometry analysis raw values were treated in the same way as described above with the CLIC1 membranes and were used to produce all the graphs in Figure 35; presenting analysis of variance results and individual readings from exosomes derived from human cell lines (graphs "D" and "E"), and the same for both hamster cell lines (graphs "F" and "G").

Results from the three exosome membranes showed no significant difference between CHO-K1 and C4AFBN for CLIC4 expression, although C4AFBN was slightly greater. Interestingly,

between the human cell lines, the control cell line along with Kuramochi and OVCAR3 expressed the most CLIC4 protein. Both PEO1 and PEO4 had similar CLIC4 expression of approximately half that of the control cell line, which consistently had the greatest level of exosomal CLIC4.

Distinctively, CLIC4 has more widely been studied in ovarian cancer, and previously has been found to be enriched in exosomes from ovarian cancer cell lines and ovarian cancer patient serum (165, 166, 167). We were unable to obtain results that align with that of previous research and begs for carrying out protein analysis on more exosome samples as well as samples derived from alternate controls and clinical samples.

Although we have highlighted significant trends of exosomal CLIC1 and CLIC4 expression observed in our western blots, it is important to evaluate the overall validity from results individually. Membranes "A" and "B" in Figure 34 and Figure 35 a significantly patchy background can be observed, which might have been due to the membranes drying out some point during the transfer or antibody labelling process. Because of this, to obtain more accurate densitometry results more repeats would be required for both proteins. In addition, in membrane "A" of Figure 34, well 10 was loaded with recombinant CLIC4 which in that case works as a negative control for the antibody being tested, despite this, we saw a positive signal in both positive (well 9) and negative controls. Due to the results obtained from other membranes labelled with anti-CLIC1 we suspect that during the loading of the wells, spillage likely occurred.

One of the reasons for the small number of experiments successfully carried out, was due to both the extensive time and manual work required to isolate exosome samples from cell media, as well as the fact that initially, we spent significant time refining an attempt to salvage as much sample as possible to allow for technical replicates as well as conducting other assays or western blot repetitions with any left-over sample. For this, we initially intended to label one transferred membrane with two different primary antibodies; we proposed pairing; CLIC1 with CD63 and CLIC4 with TSG101, which meant that for each exosome experiment only two membranes would be required. Because we had multiple artifacts and inconclusive results (weak signals) during most of our initial western blots with many sets of exosome samples (Not used for densitometry), we later opted to label each membrane with only one antibody. This allowed us to test each antibody individually to adjust the protocol accordingly. We

determined that 1:250 is a good working antibody dilution for testing our exosome samples; however anti-CD63 was the only antibody that did not work with any exosome samples during this fine-tuning stage, even though previously we had tested a 1:1000 dilution in a set of whole cell lysates and successfully showed signal. After some investigation we determined that adding reducing agent to the loading buffer damages the structure of the disulfide-bonded extracellular loop of the protein (168), which resulted in false negative results. After conducting the SDS-PAGE without the reducing agent for membranes intended for CD63 analysis, we started obtaining results such as those presented in Figure 31.

Summary and Conclusions:

Western blots were prepared with equal numbers of exosomes per sample but with equal volumes of whole cell lysates, as the same number of cells were lysed for each. For blots involving recombinant CLIC1 and CLIC4, 50ug of protein was loaded per well.

Initially, the study investigated various markers, including CD81, to confirm the presence of exosomes. CD81, with a molecular weight of 25 kDa, was found in all tested cell lines. However, the signal intensity varied among cell lines, with C4AFBN exhibiting the highest signal and PEO1 and PEO4 showing the lowest. More replicates would enhance the reliability of these results. However, we only tested one set of exosome samples with anti-CD81 antibody, and we would need additional replicates in order to obtain better value from the data. Additionally, we explored the presence of CA125 in exosomes, but the results were inconclusive due to unexpected signals at different sizes, including around 75 kDa in addition to the expected <250kDa; which interestingly was observed by a similar study that used the same antibody, however, on exosomes obtained from colorectal cancer cell lines. In a similar manner to CD63 only one set of samples were tested and would be of interest to try modifications to the method to see is better results may be achieved.

We successfully demonstrated that there was not presence of TSG-101 in “negative control” samples in a membrane that we labelled with both, anti-CLIC1 and anti-TSH-101. This can be observed in well 8 of figure 29. This supported the hypothesis and aligned with the NTA findings, suggesting that exosomes derived from foetal bovine serum (FBS) were relatively insignificant compared to those collected after growing cells for seven days.

The main markers CD63, TSG-101, CLIC1, and CLIC4 were tested in three complete sets of exosome samples from all cell lines, as well as one set of whole cell lysates. For the whole cell lysates, CD63 and TSG101 analysis showed no clear trend across cell types, with PEO1 showing the highest TSG101 expression and OVCAR3 the lowest CD63 expression was significantly higher in the control cell line compared to others, while hamster cell lines had the lowest CD63 expression. Analysis of CLIC1 in whole cell lysates revealed higher expression in Wild Type CHO-K1 compared to C4AFBN, with PEO4 and control cell lines also showing higher expression compared to other human cell lines. CLIC4 expression was highest in the control

cell line compared to all ovarian cancer cell lines, with Kuramochi and PEO1 showing nearly double expression and OVCAR3 and PEO4 approximately four times less expression.

The Western blot analysis of exosome samples revealed that CD63 expression was undetectable in exosomes from Hamster cell lines, although present in Hamster whole cell lysates, suggesting low abundance or absence of CD63 on exosomes from CHO-K1 and C4AFBN cell lines. However, exosome samples from human cell lines showed clear CD63 expression, with the control and OVCAR3 cell lines exhibiting the highest levels. TSG-101 analysis indicated lower levels in the control and PEO4 cell lines, with higher levels in exosomes from hamster cell lines compared to human cell lines. OVCAR3 consistently displayed the highest TSG-101 levels among the human ovarian cancer cell lines. These findings suggest that CD63 and TSG-101 protein analysis confirms the presence of exosomes in the studied human cell samples.

The study found no significant difference in exosomal CLIC1 between CHO-K1 and C4AFBN cell lines. However, exosomes derived from human cells, particularly PEO1 and PEO4, showed higher levels of CLIC1 compared to control cell lines. Exosomal CLIC1 levels in Kuramochi and OVCAR3 cells were also slightly elevated compared to controls, but no significant differences were observed among all human-derived exosomes. Similar research, conducted on exosomes from glioblastoma cell lines that investigated the disparity of exosomal PEO4 between cancerous and healthy cell lines, we consistently find that the presence of exosomal CLIC1 is notably higher in cancerous cell lines.

Regarding CLIC4 expression, no significant difference was found between CHO-K1 and C4AFBN cell lines. However, among human cell lines, the control line, along with Kuramochi and OVCAR3, showed the highest levels of exosomal CLIC4. Both PEO1 and PEO4 had similar CLIC4 expression levels, approximately half that of the control line. These findings diverge from previous research, indicating the need for further analysis with a larger sample size and diverse controls, including clinical samples.

Chapter 4

Conclusions and Future Studies

Cancer progression is driven by intercellular communication between cancer cells and its surrounding tissues, and in advanced stages any suitable metastatic site (102, 103, 104). A mechanism which facilitates communication outside paracrine signalling, occurs through exchange of bio-cargo via exosomes; which research has more recently demonstrated to be a driving signalling pathway for tumour growth, cell invasion, angiogenesis, drug resistance and metastasis across a spectrum of cancers including ovarian cancer (90, 91, 101). Investigating the rates of exosome shedding as well as contrasting the different levels of potential markers between cancerous and healthy exosomes derived from liquid biopsies, such as from serum or ascites fluid, potentially provides a minimally-invasive way to gain insight into ovarian cancer progression and diagnosis, allowing tracking of patient response to treatment, as well as screening for recurrence.

In recent years, CLIC1 overexpression has been linked to a range of cancers including ovarian (77), although most previous studies measured expression in serum and microarray of tumorous tissues. In a similar manner circulating CLIC4 has been linked to cancers including that of the ovary (84, 118). Both of these proteins have been detected and studied in exosomes from glioblastoma, gastric and ovarian cancer, which have a role in intercellular communication, and were found to drive tumour growth and angiogenesis (85, 87, 88, 165). The study of not only CLIC proteins but many other cargo biomarkers in exosomes has been of recent interest in cancer research as they allow for non-invasive screening and tracking of various cancers, and therefore simultaniously become a potential therapeutic target (101, 106, 107, 108, 109). Particularly in ovarian cancer, the number of exosomes in circulation has been directly linked to increased disease progression (169).

This compilation of knowledge prompted us to investigate the exosome mediated exchange of CLIC1 and CLIC4 proteins in order to see if relative levels between healthy and cancerous models matches findings from previous research, however, in this project the aim was to measure their expression on exosomes collected *in vitro* from a spectrum of human ovarian cancer cell lines and the control fallopian tube cell line; simultaniously, as a secondary aim we

wanted to use a simple CLIC1 control hamster cell line compared to equivalent cells that were modified as CLIC1 overexpressing cells, to see if the total number of shed exosomes is CLIC1 dependant. Thus, we collected exosomes from cell culture media for all cell lines after growing cells over a period of 7 days and purified the vesicles by differential ultracentrifugation. The defining factors for quality assesment of exosome samples in this study was determined by the ability to observe enrichment of significant protein markers CD63 and TSG-101 by western blot. The second method by which we analysed the quality and purity of exosomes was NTA and DLS which we carried prior to western blot analysis and which served to determine that the particles fell in the expected vesicle range. Since all of the protocols were established simultaneously, each exosome characterization method was deemed reliable by the ability to obtain consistent results from samples that meet the expected exosome results.

From our NTA results we can conclude that the *in vitro* model we arranged for collection of cell media, allows for the production of good quality high concentration exosome samples. In addition, although very time consuming, purifying exosomes by differential ultracentrifugation is cost-effective, and allowed for the production of exosome samples of relative concentration consistency across passages. Both DLS and NTA produced similar characterization of exosome diameter for all cell lines, however NTA produces more detailed results and allows to identify subpupolations of exosomes, in contrast to DLS where lower resolution of results pools particles under one greater population group. Overall, NTA proved to be the most beneficial for the purpose of our protein analysis study, as it uniquely provides particle concentration of samples. The sample quantification results did not find any significant difference between the number of exosomes shed by the control cell line relative to all 4 ovarian cancer cell lines, and did not align our hypothesis of greater number of exosomes for the ovarian cancer cell lines.

In addition, with the western blot analysis of our exosome samples we were able to confirm the presence of exosomes in our manually purified samples, by demonstrating the presence of CD63 and TSG101 in exosomes derived from all of our human cell lines, and therefore in follow up research, these markers would be ideal candidates if invesitgating supplementary cell lines. We have demonstrated a similarity to other research, that exosomal levels of CLIC1 of the control cell line presented relatively lower levels than that present in exosomes from

the ovarian cancer cell lines, while on the other hand, we found that exosomal CLIC4 presented the opposite trend instead; where the control cell line ranked highest although not by a drastic difference when compared to Kuramochi and OVCAR3 which approximately presented relatively double the expression than that of PEO1 and PEO4. Exosomes from the hamster cell lines demonstrated that the CLIC1 overexpressing cell line, had more exosomal CLIC1 protein compared to the wild type, however no significant difference was observed for the total number of shed exosomes; with this, a remaining enquiry would be to contrast the rate of exosome shedding between both cell lines, in order to investigate a putative CLIC1 involvement in exosome production machinery. Alternatively, to use exosomes derived from a CLIC1 knockdown cell model.

In this thesis we have displayed that CLIC1 and CLIC4 are measurable in exosomes derived from ovarian cancer cell lines as well as the healthy counterpart, with this we can infer that investigating the involvement of these secreted proteins in ovarian cancer progression could lead to better understading in the disease's pathophysiology. The next important points of research focus in order to build up from our findings would be, measuring CLIC protein levels in exosomes samples derived from clinical samples; and investigating the role that CLIC rich and CLIC depleted exosomes have regarding cell proliferation in ovarian cancer cell lines.

In ovarian cancer, the use of exosomes as a mechanism for delivery of platinum chemotherapy drug (Cisplatin) to resistant cells has been demonstrated to enhance the response both *in vitro* as well as in animal studies (170). Developing technologies that simultaneously distinguish exosomes shed by cancer cells while measuring a secondary marker, could lead to the development of a screening test for patients at risk. A screening test technology published in 2022 proved the possibility of doing so with chromatography paper (171).

In our opinion piece published in the journal Frontiers in Bioengineering and Biotechnology (172), we listed a number of techniques that would allow for exosome protein cargo analysis collected from human body fluids. These include; flow cytometry, protein microarray (EV Array), diagnostic magnetic resonance, nanoplasmonic sensing technology and microfluidics (173, 174, 175, 176, 177); the application and use of these technologies would extend past ovarian cancer into other cancers and potentially other diseases; however, early detection

prevails as the most promising approach that would lead to drastically improved patient survival in ovarian cancer.

The next logical step, would be to identically investigate exosomal CLIC1 and CLIC4 from control cell lines derived from healthy cell lines originated from the ovary and fallopian tube, as well as the relative number of exosomes shed by the new cell line. In addition, it would be of interest to investigate the potential role of exosomal CLIC1 in proliferation of one or various ovarian cancer cell lines; by setting up an in-vitro model to compare phenotypical changes to cell growth caused by the media supplementation of exosomes derived from a CLIC1 overexpressing cell line, exosomes derived from a CLIC1 silenced cell line and a wildtype cell line, model which was previously used by (Setti, 2015)(88), where they demonstrated that seeding exosomes from the CLIC1 overexpressing glioblastoma cell line resulted in increased cell proliferation of a drug resistant glioblastima cell line when compared to other exosomes and controls.

Sequentially, the next important milestone to investigate involves measuring CLIC protein levels in exosomes that are derived from a spectrum of clinical samples, as well as compared to healthy controls. A liquid biopsy allows for a potential non-invasive method for cancer diagnosis. Since exosomes can be found in a range of body fluids which include blood and ascites (178), contrasting clinically obtained exosomes and contrasting CLIC protein levels to our in vitro model is the next reasonable step. However, we agree that in future, growing the cells in serum-free conditions would undoubtedly eliminate contamination signals by ensuring the complete absence of media-derived exosomes. Furthermore, it is crutial to establish the detection limit of exosomes derived from serum samples (clinical) by means of western blot or other methods. A rigorous detection system is equally as important as the cargo analysis, and while considering that this research could lead to tracking for recurrence or even early diagnosis; then it becomes more essential to have the ability to carry out protein analysis even in samples with lower exosome counts. Exosomes derived from ascitic fluid have been demonstrated to drive growth and migration in ovarian cancer cells (162). Such research is worthy of pursuit and our study shows there remain a number of important questions needing to be answered and further investigated.

References

1. Doubeni CA, Doubeni AR, Myers AE. Diagnosis and Management of Ovarian Cancer. Am Fam Physician. 2016;93(11):937-44.
2. Jelovac D, Armstrong DK. Recent progress in the diagnosis and treatment of ovarian cancer. CA: A Cancer Journal for Clinicians. 2011;61(3):183-203.
3. Yee C, Dickson KA, Muntasir MN, Ma Y, Marsh DJ. Three-Dimensional Modelling of Ovarian Cancer: From Cell Lines to Organoids for Discovery and Personalized Medicine. Front Bioeng Biotechnol. 2022;10:836984.
4. Kurman RJ, Shih I-M. The origin and pathogenesis of epithelial ovarian cancer-a proposed unifying theory. The American journal of surgical pathology. 2010;34(3):433.
5. Bast RC, Hennessy B, Mills GB. The biology of ovarian cancer: new opportunities for translation. Nature Reviews Cancer. 2009;9(6):415-28.
6. Goff BA, Mandel L, Muntz HG, Melancon CH. Ovarian carcinoma diagnosis. Cancer. 2000;89(10):2068-75.
7. Burges A, Schmalfeldt B. Ovarian cancer: diagnosis and treatment. Dtsch Arztebl Int. 2011;108(38):635-41.
8. Akter S, Rahman MA, Hasan MN, Akhter H, Noor P, Islam R, et al. Recent Advances in Ovarian Cancer: Therapeutic Strategies, Potential Biomarkers, and Technological Improvements. Cells. 2022;11(4):650.
9. Sung H, Ferlay J, Siegel RL, Laversanne M, Soerjomataram I, Jemal A, et al. Global Cancer Statistics 2020: GLOBOCAN Estimates of Incidence and Mortality Worldwide for 36 Cancers in 185 Countries. CA: A Cancer Journal for Clinicians. 2021;71(3):209-49.
10. Health AIo, Welfare. Cancer data in Australia. Canberra: AIHW; 2022.
11. UK CR. Ovarian cancer survival statistics. 2015.
12. Chandra A, Pius C, Nabeel M, Nair M, Vishwanatha JK, Ahmad S, et al. Ovarian cancer: Current status and strategies for improving therapeutic outcomes. Cancer Medicine. 2019;8(16):7018-31.
13. Jelovac D, Armstrong DK. Recent progress in the diagnosis and treatment of ovarian cancer. CA Cancer J Clin. 2011;61(3):183-203.
14. Prat J. Staging classification for cancer of the ovary, fallopian tube, and peritoneum. Int J Gynaecol Obstet. 2014;124(1):1-5.
15. Simmons AR, Fourkala EO, Gentry-Maharaj A, Ryan A, Sutton MN, Baggerly K, et al. Complementary Longitudinal Serum Biomarkers to CA125 for Early Detection of Ovarian Cancer. Cancer Prev Res (Phila). 2019;12(6):391-400.
16. Nisenblat V, Bossuyt PM, Shaikh R, Farquhar C, Jordan V, Scheffers CS, et al. Blood biomarkers for the non-invasive diagnosis of endometriosis. Cochrane Database Syst Rev. 2016;2016(5):Cd012179.
17. Wang YF, Feng FL, Zhao XH, Ye ZX, Zeng HP, Li Z, et al. Combined detection tumor markers for diagnosis and prognosis of gallbladder cancer. World J Gastroenterol. 2014;20(14):4085-92.
18. Devarbhavi H, Kaese D, Williams AW, Rakela J, Klee GG, Kamath PS. Cancer antigen 125 in patients with chronic liver disease. Mayo Clin Proc. 2002;77(6):538-41.
19. Andersen MR, Goff BA, Lowe KA, Scholler N, Bergan L, Drescher CW, et al. Use of a Symptom Index, CA125, and HE4 to predict ovarian cancer. Gynecologic Oncology. 2010;116(3):378-83.
20. Srivastava S. Biomarkers in cancer screening and early detection: John Wiley & Sons; 2017.
21. Pruthi S, Gostout BS, Lindor NM. Identification and Management of Women With BRCA Mutations or Hereditary Predisposition for Breast and Ovarian Cancer. Mayo Clin Proc. 2010;85(12):1111-20.
22. Hunn J, Rodriguez GC. Ovarian cancer: etiology, risk factors, and epidemiology. Clin Obstet Gynecol. 2012;55(1):3-23.

23. Kuchenbaecker KB, Hopper JL, Barnes DR, Phillips KA, Mooij TM, Roos-Blom MJ, et al. Risks of Breast, Ovarian, and Contralateral Breast Cancer for BRCA1 and BRCA2 Mutation Carriers. Jama. 2017;317(23):2402-16.
24. Nelson HD, Pappas M, Zakher B, Mitchell JP, Okinaka-Hu L, Fu R. Risk assessment, genetic counseling, and genetic testing for BRCA-related cancer in women: a systematic review to update the U.S. Preventive Services Task Force recommendation. Ann Intern Med. 2014;160(4):255-66.
25. Nikolaidi A, Fountzilas E, Fostira F, Psyrri A, Gogas H, Papadimitriou C. Neoadjuvant treatment in ovarian cancer: New perspectives, new challenges. Front Oncol. 2022;12:820128.
26. Jayson GC, Kohn EC, Kitchener HC, Ledermann JA. Ovarian cancer. Lancet. 2014;384(9951):1376-88.
27. Yeung TL, Leung CS, Yip KP, Au Yeung CL, Wong ST, Mok SC. Cellular and molecular processes in ovarian cancer metastasis. A Review in the Theme: Cell and Molecular Processes in Cancer Metastasis. Am J Physiol Cell Physiol. 2015;309(7):C444-56.
28. Tewari D, Java JJ, Salani R, Armstrong DK, Markman M, Herzog T, et al. Long-term survival advantage and prognostic factors associated with intraperitoneal chemotherapy treatment in advanced ovarian cancer: a gynecologic oncology group study. J Clin Oncol. 2015;33(13):1460-6.
29. Jaaback K, Johnson N, Lawrie TA. Intraperitoneal chemotherapy for the initial management of primary epithelial ovarian cancer. Cochrane Database Syst Rev. 2016;2016(1):Cd005340.
30. Wright AA, Cronin A, Milne DE, Bookman MA, Burger RA, Cohn DE, et al. Use and Effectiveness of Intraperitoneal Chemotherapy for Treatment of Ovarian Cancer. J Clin Oncol. 2015;33(26):2841-7.
31. Xie T, Dickson K-A, Yee C, Ma Y, Ford CE, Bowden NA, et al. Targeting Homologous Recombination Deficiency in Ovarian Cancer with PARP Inhibitors: Synthetic Lethal Strategies That Impact Overall Survival. Cancers. 2022;14(19):4621.
32. Bast RC, Romero I, Mills GB. 37 - Molecular Pathogenesis of Ovarian Cancer. In: Mendelsohn J, Gray JW, Howley PM, Israel MA, Thompson CB, editors. The Molecular Basis of Cancer (Fourth Edition). Philadelphia: W.B. Saunders; 2015. p. 531-48.e2.
33. Iwabuchi H, Sakamoto M, Sakunaga H, Ma YY, Carcangiu ML, Pinkel D, et al. Genetic analysis of benign, low-grade, and high-grade ovarian tumors. Cancer Res. 1995;55(24):6172-80.
34. Risch HA, McLaughlin JR, Cole DE, Rosen B, Bradley L, Fan I, et al. Population BRCA1 and BRCA2 mutation frequencies and cancer penetrances: a kin-cohort study in Ontario, Canada. J Natl Cancer Inst. 2006;98(23):1694-706.
35. Kohler MF, Marks JR, Wiseman RW, Jacobs IJ, Davidoff AM, Clarke-Pearson DL, et al. Spectrum of mutation and frequency of allelic deletion of the p53 gene in ovarian cancer. J Natl Cancer Inst. 1993;85(18):1513-9.
36. Jia D, Nagaoka Y, Katsumata M, Orsulic S. Inflammation is a key contributor to ovarian cancer cell seeding. Sci Rep. 2018;8(1):12394.
37. Vang R, Levine DA, Soslow RA, Zaloudek C, Shih I-M, Kurman RJ. Molecular alterations of TP53 are a defining feature of ovarian high-grade serous carcinoma: a rereview of cases lacking TP53 mutations in The Cancer Genome Atlas Ovarian Study. International journal of gynecological pathology: official journal of the International Society of Gynecological Pathologists. 2016;35(1):48.
38. Cole AJ, Dwight T, Gill AJ, Dickson K-A, Zhu Y, Clarkson A, et al. Assessing mutant p53 in primary high-grade serous ovarian cancer using immunohistochemistry and massively parallel sequencing. Scientific Reports. 2016;6(1):26191.
39. Erickson BK, Conner MG, Landen CN, Jr. The role of the fallopian tube in the origin of ovarian cancer. Am J Obstet Gynecol. 2013;209(5):409-14.
40. Lee Y, Miron A, Drapkin R, Nucci MR, Medeiros F, Saleemuddin A, et al. A candidate precursor to serous carcinoma that originates in the distal fallopian tube. J Pathol. 2007;211(1):26-35.

41. Soong TR, Howitt BE, Horowitz N, Nucci MR, Crum CP. The fallopian tube, "precursor escape" and narrowing the knowledge gap to the origins of high-grade serous carcinoma. Gynecologic Oncology. 2019;152(2):426-33.
42. Crum CP, Drapkin R, Miron A, Ince TA, Muto M, Kindelberger DW, et al. The distal fallopian tube: a new model for pelvic serous carcinogenesis. Curr Opin Obstet Gynecol. 2007;19(1):3-9.
43. Cannistra SA. Cancer of the Ovary. New England Journal of Medicine. 2004;351(24):2519-29.
44. Singha B, Harper SL, Goldman AR, Bitler BG, Aird KM, Borowsky ME, et al. CLIC1 and CLIC4 complement CA125 as a diagnostic biomarker panel for all subtypes of epithelial ovarian cancer. Scientific reports. 2018;8(1):14725.
45. Lu R, Sun X, Xiao R, Zhou L, Gao X, Guo L. Human epididymis protein 4 (HE4) plays a key role in ovarian cancer cell adhesion and motility. Biochemical and biophysical research communications. 2012;419(2):274-80.
46. Nagy JA, Masse EM, Herzberg KT, Meyers MS, Yeo K-T, Yeo T-K, et al. Pathogenesis of ascites tumor growth: vascular permeability factor, vascular hyperpermeability, and ascites fluid accumulation. Cancer research. 1995;55(2):360-8.
47. Atallah GA, Abd. Aziz NH, Teik CK, Shafiee MN, Kampan NC. New Predictive Biomarkers for Ovarian Cancer. Diagnostics. 2021;11(3):465.
48. Press JZ, Wurz K, Norquist BM, Lee MK, Pennil C, Garcia R, et al. Identification of a preneoplastic gene expression profile in tubal epithelium of BRCA1 mutation carriers. Neoplasia. 2010;12(12):993-IN8.
49. Huddleston HG, Wong K-k, Welch WR, Berkowitz RS, Mok SC. Clinical applications of microarray technology: creatine kinase B is an up-regulated gene in epithelial ovarian cancer and shows promise as a serum marker. Gynecologic oncology. 2005;96(1):77-83.
50. Chang K, Pastan I. Molecular cloning of mesothelin, a differentiation antigen present on mesothelium, mesotheliomas, and ovarian cancers. Proceedings of the National Academy of Sciences. 1996;93(1):136-40.
51. Wei X, Li J, Xie H, Wang H, Wang J, Zhang X, et al. Chloride intracellular channel 1 participates in migration and invasion of hepatocellular carcinoma by targeting maspin. Journal of Gastroenterology and Hepatology. 2015;30(1):208-16.
52. Lucitti JL, Faber JE. A Chloride Intracellular Channel-4 (Clic4) and VEGF-A Signaling Pathway Regulates Maturation of the Collateral Circulation. Am Heart Assoc; 2013.
53. Yu W, Cui R, Qu H, Liu C, Deng H, Zhang Z. Expression and prognostic value of CLIC1 in epithelial ovarian cancer. Experimental and Therapeutic Medicine. 2018.
54. Elter A, Hartel A, Sieben C, Hertel B, Fischer-Schliebs E, Lüttge U, et al. A plant homolog of animal chloride intracellular channels (CLICs) generates an ion conductance in heterologous systems. J Biol Chem. 2007;282(12):8786-92.
55. Valenzuela SM, Alkhamici H, Brown LJ, Almond OC, Goodchild SC, Carne S, et al. Regulation of the membrane insertion and conductance activity of the metamorphic chloride intracellular channel protein CLIC1 by cholesterol. PLoS One. 2013;8(2):e56948.
56. Al Khamici H, Brown LJ, Hossain KR, Hudson AL, Sinclair-Burton AA, Ng JPM, et al. Members of the Chloride Intracellular Ion Channel Protein Family Demonstrate Glutaredoxin-Like Enzymatic Activity. PLoS ONE. 2015;10(1):e115699.
57. Littler DR, Harrop SJ, Goodchild SC, Phang JM, Mynott AV, Jiang L, et al. The enigma of the CLIC proteins: Ion channels, redox proteins, enzymes, scaffolding proteins? FEBS Lett. 2010;584(10):2093-101.
58. Birben E, Sahiner UM, Sackesen C, Erzurum S, Kalayci O. Oxidative stress and antioxidant defense. World Allergy Organ J. 2012;5(1):9-19.
59. Information NCfB. CLIC1 chloride intracellular channel 1 [Homo sapiens (human)] 2023 [updated 5th march 2023. Available from: https://www.ncbi.nlm.nih.gov/gene/1192#gene-expression.

60. Valenzuela SM, Martin DK, Por SB, Robbins JM, Warton K, Bootcov MR, et al. Molecular cloning and expression of a chloride ion channel of cell nuclei. J Biol Chem. 1997;272(19):12575-82.
61. Tulk BM, Schlesinger PH, Kapadia SA, Edwards JC. CLIC-1 functions as a chloride channel when expressed and purified from bacteria. J Biol Chem. 2000;275(35):26986-93.
62. Valenzuela SM, Mazzanti M, Tonini R, Qiu MR, Warton K, Musgrove EA, et al. The nuclear chloride ion channel NCC27 is involved in regulation of the cell cycle. The Journal of Physiology. 2000;529(3):541-52.
63. Chalothorn D, Zhang H, Smith JE, Edwards JC, Faber JE. Chloride intracellular channel-4 is a determinant of native collateral formation in skeletal muscle and brain. Circ Res. 2009;105(1):89-98.
64. Chou S-Y, Hsu K-S, Otsu W, Hsu Y-C, Luo Y-C, Yeh C, et al. CLIC4 regulates apical exocytosis and renal tube luminogenesis through retromer- and actin-mediated endocytic trafficking. Nature Communications. 2016;7(1):10412.
65. Fernández-Salas E, Suh KS, Speransky VV, Bowers WL, Levy JM, Adams T, et al. mtCLIC/CLIC4, an organellular chloride channel protein, is increased by DNA damage and participates in the apoptotic response to p53. Mol Cell Biol. 2002;22(11):3610-20.
66. Hernandez-Fernaud JRR, Elena; Casazza, Andrea; Neilson, Lisa J.; Pulleine, Ellie; Santi, Alice; Ismail, Shehab; Lilla, Sergio; Dhayade, Sandeep; MacPherson, Iain R.; McNeish, Iain; Ennis, Darren; Ali, Hala; Kugeratski, Fernanda G.; Khamici, Heba Al; Biggelaar, Maartje van den; Berghe, Peter V.E. van den ; Cloix, Catherine ; McDonald, Laura ; Millan, David ; Hoyle, Aoisha ; Kuchnio, Anna ; Carmeliet, Peter; Valenzuela, Stella M; Blyth, Karen ; Yin, Huabing ; Mazzone, Massimiliano ; Norman, Jim C; Zanivan, Sara. Secreted CLIC3 drives cancer progression through its glutathione-dependent oxidoreductase activity. Nature Communications. 2017;8.
67. Littler DR, Harrop SJ, Fairlie WD, Brown LJ, Pankhurst GJ, Pankhurst S, et al. The intracellular chloride ion channel protein CLIC1 undergoes a redox-controlled structural transition. J Biol Chem. 2004;279(10):9298-305.
68. Bezanilla F, Stefani E. [19] Gating currents. Methods in enzymology. 293: Elsevier; 1998. p. 331-52.
69. Gururaja Rao S, Patel NJ, Singh H. Intracellular Chloride Channels: Novel Biomarkers in Diseases. Front Physiol. 2020;11:96.
70. Ueno Y, Ozaki S, Umakoshi A, Yano H, Choudhury ME, Abe N, et al. Chloride intracellular channel protein 2 in cancer and non-cancer human tissues: relationship with tight junctions. Tissue barriers. 2019;7(1):1593775.
71. Xu T, Wang Z, Dong M, Wu D, Liao S, Li X. Chloride intracellular channel protein 2: prognostic marker and correlation with PD-1/PD-L1 in breast cancer. Aging (Albany NY). 2020;12(17):17305.
72. Dozynkiewicz MA, Jamieson NB, Macpherson I, Grindlay J, van den Berghe PV, von Thun A, et al. Rab25 and CLIC3 collaborate to promote integrin recycling from late endosomes/lysosomes and drive cancer progression. Dev Cell. 2012;22(1):131-45.
73. Ko J-H, Ko EA, Gu W, Lim I, Bang H, Zhou T. Expression profiling of ion channel genes predicts clinical outcome in breast cancer. Molecular Cancer. 2013;12(1):106.
74. Neveu B, Spinella JF, Richer C, Lagace K, Cassart P, Lajoie M, et al. CLIC5: a novel ETV6 target gene in childhood acute lymphoblastic leukemia. Haematologica. 2016;101(12):1534-43.
75. Wulfkuhle JD, Sgroi DC, Krutzsch H, McLean K, McGarvey K, Knowlton M, et al. Proteomics of human breast ductal carcinoma in situ. Cancer Res. 2002;62(22):6740-9.
76. Jia N, Dong S, Zhao G, Gao H, Li X, Zhang H. CLIC1 overexpression is associated with poor prognosis in pancreatic ductal adenocarcinomas. Journal of cancer research and therapeutics. 2016;12(2):892-6.
77. Qu H, Chen Y, Cao G, Liu C, Xu J, Deng H, et al. Identification and validation of differentially expressed proteins in epithelial ovarian cancers using quantitative proteomics. Oncotarget. 2016;7(50):83187.

78. Wang P, Zeng Y, Liu T, Zhang C, Yu P-W, Hao Y-X, et al. Chloride intracellular channel 1 regulates colon cancer cell migration and invasion through ROS/ERK pathway. World journal of gastroenterology: WJG. 2014;20(8):2071.
79. Wang P, Zhang C, Yu P, Tang B, Liu T, Cui H, et al. Regulation of colon cancer cell migration and invasion by CLIC1-mediated RVD. Molecular and cellular biochemistry. 2012;365:313-21.
80. Ye Y, Yin M, Huang B, Wang Y, Li X, Lou G. CLIC1 a novel biomarker of intraperitoneal metastasis in serous epithelial ovarian cancer. Tumor Biology. 2015;36(6):4175-9.
81. Zhao W, Lu M, Zhang Q. Chloride intracellular channel 1 regulates migration and invasion in gastric cancer by triggering the ROS-mediated p38 MAPK signaling pathway. Mol Med Rep. 2015;12(6):8041-7.
82. Suh KS, Crutchley JM, Koochek A, Ryscavage A, Bhat K, Tanaka T, et al. Reciprocal Modifications of CLIC4 in Tumor Epithelium and Stroma Mark Malignant Progression of Multiple Human Cancers. Clinical Cancer Research. 2007;13(1):121-31.
83. Al Khamici H, Sanchez VC, Yan H, Cataisson C, Michalowski AM, Yang HH, et al. The oxidoreductase CLIC4 is required to maintain mitochondrial function and resistance to exogenous oxidants in breast cancer cells. Journal of Biological Chemistry. 2022;298(9):102275.
84. Kong. CLIC4 mediates TGF-β1-induced fibroblast-to-myofibroblast transdifferentiation in ovarian cancer. Oncology Reports. 2009;22(03).
85. Zhao K, Wang Z, Li X, Liu J-l, Tian L, Chen J-q. Exosome-mediated transfer of CLIC1 contributes to the vincristine-resistance in gastric cancer. Molecular and cellular biochemistry. 2019;462(1-2):97-105.
86. Peretti M, Angelini M, Savalli N, Florio T, Yuspa SH, Mazzanti M. Chloride channels in cancer: Focus on chloride intracellular channel 1 and 4 (CLIC1 AND CLIC4) proteins in tumor development and as novel therapeutic targets. Biochimica et Biophysica Acta (BBA) - Biomembranes. 2015;1848(10):2523-31.
87. Geng HY, Feng ZJ, Zhang JJ, Li GY. Exosomal CLIC1 released by CLL promotes HUVECs angiogenesis by regulating ITGβ1-MAPK/ERK axis. Kaohsiung J Med Sci. 2021;37(3):226-35.
88. Setti M, Osti D, Richichi C, Ortensi B, Del Bene M, Fornasari L, et al. Extracellular vesicle-mediated transfer of CLIC1 protein is a novel mechanism for the regulation of glioblastoma growth. Oncotarget. 2015;6(31):31413-27.
89. Kowal J, Tkach M, Théry C. Biogenesis and secretion of exosomes. Current Opinion in Cell Biology. 2014;29:116-25.
90. Mathivanan S, Fahner CJ, Reid GE, Simpson RJ. ExoCarta 2012: database of exosomal proteins, RNA and lipids. Nucleic Acids Res. 2012;40(Database issue):D1241-4.
91. He C, Zheng S, Luo Y, Wang B. Exosome Theranostics: Biology and Translational Medicine. Theranostics. 2018;8(1):237-55.
92. Mittelbrunn M, Sánchez-Madrid F. Intercellular communication: diverse structures for exchange of genetic information. Nature Reviews Molecular Cell Biology. 2012;13(5):328-35.
93. El Andaloussi S, Mäger I, Breakefield XO, Wood MJA. Extracellular vesicles: biology and emerging therapeutic opportunities. Nature Reviews Drug Discovery. 2013;12(5):347-57.
94. De Toro J, Herschlik L, Waldner C, Mongini C. Emerging roles of exosomes in normal and pathological conditions: new insights for diagnosis and therapeutic applications. Front Immunol. 2015;6:203.
95. Schey KL, Luther JM, Rose KL. Proteomics characterization of exosome cargo. Methods. 2015;87:75-82.
96. Kalra H, Simpson RJ, Ji H, Aikawa E, Altevogt P, Askenase P, et al. Vesiclepedia: a compendium for extracellular vesicles with continuous community annotation. PLoS Biol. 2012;10(12):e1001450.
97. Witwer KW, Théry C. Extracellular vesicles or exosomes? On primacy, precision, and popularity influencing a choice of nomenclature. J Extracell Vesicles. 2019;8(1):1648167.
98. Kalluri R. The biology and function of exosomes in cancer. J Clin Invest. 2016;126(4):1208-15.

99. Raposo G, Stoorvogel W. Extracellular vesicles: Exosomes, microvesicles, and friends. Journal of Cell Biology. 2013;200(4):373-83.
100. Minciacchi VR, Freeman MR, Di Vizio D. Extracellular Vesicles in Cancer: Exosomes, Microvesicles and the Emerging Role of Large Oncosomes. Seminars in Cell & Developmental Biology. 2015;40:41-51.
101. Tai YL, Chen KC, Hsieh JT, Shen TL. Exosomes in cancer development and clinical applications. Cancer Science. 2018;109(8):2364-74.
102. Wortzel I, Dror S, Kenific CM, Lyden D. Exosome-Mediated Metastasis: Communication from a Distance. Developmental Cell. 2019;49(3):347-60.
103. Costa-Silva B, Aiello NM, Ocean AJ, Singh S, Zhang H, Basant, et al. Pancreatic cancer exosomes initiate pre-metastatic niche formation in the liver. Nature Cell Biology. 2015;17(6):816-26.
104. Peinado H, Alečković M, Lavotshkin S, Matei I, Costa-Silva B, Moreno-Bueno G, et al. Melanoma exosomes educate bone marrow progenitor cells toward a pro-metastatic phenotype through MET. Nature Medicine. 2012;18(6):883-91.
105. Yokoi A, Yoshioka Y, Yamamoto Y, Ishikawa M, Ikeda S-I, Kato T, et al. Malignant extracellular vesicles carrying MMP1 mRNA facilitate peritoneal dissemination in ovarian cancer. Nature Communications. 2017;8(1):14470.
106. Nilsson J, Skog J, Nordstrand A, Baranov V, Mincheva-Nilsson L, Breakefield XO, et al. Prostate cancer-derived urine exosomes: a novel approach to biomarkers for prostate cancer. Br J Cancer. 2009;100(10):1603-7.
107. Corcoran C, Friel AM, Duffy MJ, Crown J, O'Driscoll L. Intracellular and Extracellular MicroRNAs in Breast Cancer. Clinical Chemistry. 2011;57(1):18-32.
108. Li J, Sherman-Baust CA, Tsai-Turton M, Bristow RE, Roden RB, Morin PJ. Claudin-containing exosomes in the peripheral circulation of women with ovarian cancer. BMC Cancer. 2009;9(1):244.
109. Logozzi M, De Milito A, Lugini L, Borghi M, Calabrò L, Spada M, et al. High levels of exosomes expressing CD63 and caveolin-1 in plasma of melanoma patients. PLoS One. 2009;4(4):e5219.
110. Riches A, Campbell E, Borger E, Powis S. Regulation of exosome release from mammary epithelial and breast cancer cells - a new regulatory pathway. Eur J Cancer. 2014;50(5):1025-34.
111. Zhang W, Peng P, Kuang Y, Yang J, Cao D, You Y, et al. Characterization of exosomes derived from ovarian cancer cells and normal ovarian epithelial cells by nanoparticle tracking analysis. Tumor Biology. 2016;37(3):4213-21.
112. An T, Qin S, Xu Y, Tang Y, Huang Y, Situ B, et al. Exosomes serve as tumour markers for personalized diagnostics owing to their important role in cancer metastasis. J Extracell Vesicles. 2015;4:27522.
113. Nuzhat Z, Kinhal V, Sharma S, Rice GE, Joshi V, Salomon C. Tumour-derived exosomes as a signature of pancreatic cancer - liquid biopsies as indicators of tumour progression. Oncotarget. 2017;8(10):17279-91.
114. Sharma S, Zuñiga F, Rice GE, Perrin LC, Hooper JD, Salomon C. Tumor-derived exosomes in ovarian cancer - liquid biopsies for early detection and real-time monitoring of cancer progression. Oncotarget. 2017;8(61):104687-703.
115. Ortiz A, Gui J, Zahedi F, Yu P, Cho C, Bhattacharya S, et al. An Interferon-Driven Oxysterol-Based Defense against Tumor-Derived Extracellular Vesicles. Cancer Cell. 2019;35(1):33-45.e6.
116. Bobrie A, Krumeich S, Reyal F, Recchi C, Moita LF, Seabra MC, et al. Rab27a supports exosome-dependent and -independent mechanisms that modify the tumor microenvironment and can promote tumor progression. Cancer Res. 2012;72(19):4920-30.
117. Tang H-Y, Beer LA, Chang-Wong T, Hammond R, Gimotty P, Coukos G, et al. A Xenograft Mouse Model Coupled with In-depth Plasma Proteome Analysis Facilitates Identification of Novel Serum Biomarkers for Human Ovarian Cancer. Journal of Proteome Research. 2012;11(2):678-91.

118. Tang H-Y, Beer LA, Tanyi JL, Zhang R, Liu Q, Speicher DW. Protein isoform-specific validation defines multiple chloride intracellular channel and tropomyosin isoforms as serological biomarkers of ovarian cancer. Journal of proteomics. 2013;89:165-78.
119. Elias KM, Emori MM, Papp E, Macduffie E, Konecny GE, Velculescu VE, et al. Beyond genomics: Critical evaluation of cell line utility for ovarian cancer research. Gynecologic Oncology. 2015;139(1):97-103.
120. Motoyama T. [Biological characterization including sensitivity to mitomycin C of cultured human ovarian cancers (author's transl)]. Nihon Sanka Fujinka Gakkai Zasshi. 1981;33(8):1197-204.
121. Hamilton TC, Young RC, McKoy WM, Grotzinger KR, Green JA, Chu EW, et al. Characterization of a human ovarian carcinoma cell line (NIH:OVCAR-3) with androgen and estrogen receptors. Cancer Res. 1983;43(11):5379-89.
122. Beaufort CM, Helmijr JC, Piskorz AM, Hoogstraat M, Ruigrok-Ritstier K, Besselink N, et al. Ovarian cancer cell line panel (OCCP): clinical importance of in vitro morphological subtypes. PLoS One. 2014;9(9):e103988.
123. Cortez AJ, Tudrej P, Kujawa KA, Lisowska KM. Advances in ovarian cancer therapy. Cancer chemotherapy and pharmacology. 2018;81:17-38.
124. Byrne AT, Ross L, Holash J, Nakanishi M, Hu L, Hofmann JI, et al. Vascular endothelial growth factor-trap decreases tumor burden, inhibits ascites, and causes dramatic vascular remodeling in an ovarian cancer model. Clin Cancer Res. 2003;9(15):5721-8.
125. Wolf CR, Hayward IP, Lawrie SS, Buckton K, McIntyre MA, Adams DJ, et al. Cellular heterogeneity and drug resistance in two ovarian adenocarcinoma cell lines derived from a single patient. International Journal of Cancer. 1987;39(6):695-702.
126. Stordal B, Timms K, Farrelly A, Gallagher D, Busschots S, Renaud M, et al. BRCA1/2 mutation analysis in 41 ovarian cell lines reveals only one functionally deleterious BRCA1 mutation. Molecular Oncology. 2013;7(3):567-79.
127. Karst AM, Levanon K, Drapkin R. Modeling high-grade serous ovarian carcinogenesis from the fallopian tube. Proceedings of the National Academy of Sciences. 2011;108(18):7547-52.
128. Karst AM, Drapkin R. Ovarian Cancer Pathogenesis: A Model in Evolution. Journal of Oncology. 2010;2010:1-13.
129. Hahn WC, Counter CM, Lundberg AS, Beijersbergen RL, Brooks MW, Weinberg RA. Creation of human tumour cells with defined genetic elements. Nature. 1999;400(6743):464-8.
130. Dragovic RA, Gardiner C, Brooks AS, Tannetta DS, Ferguson DJ, Hole P, et al. Sizing and phenotyping of cellular vesicles using Nanoparticle Tracking Analysis. Nanomedicine. 2011;7(6):780-8.
131. Malloy A. Count, size and visualize nanoparticles. Materials Today. 2011;14(4):170-3.
132. Szatanek R, Baj-Krzyworzeka M, Zimoch J, Lekka M, Siedlar M, Baran J. The Methods of Choice for Extracellular Vesicles (EVs) Characterization. International Journal of Molecular Sciences. 2017;18(6):1153.
133. Théry C, Amigorena S, Raposo G, Clayton A. Isolation and Characterization of Exosomes from Cell Culture Supernatants and Biological Fluids. Current Protocols in Cell Biology. 2006;30(1):3.22.1-3..9.
134. Zeringer E, Barta T, Li M, Vlassov AV. Strategies for isolation of exosomes. Cold Spring Harb Protoc. 2015;2015(4):319-23.
135. Yakubovich EI, Polischouk AG, Evtushenko VI. Principles and Problems of Exosome Isolation from Biological Fluids. Biochemistry (Moscow), Supplement Series A: Membrane and Cell Biology. 2022;16(2):115-26.
136. Livshits MA, Khomyakova E, Evtushenko EG, Lazarev VN, Kulemin NA, Semina SE, et al. Isolation of exosomes by differential centrifugation: Theoretical analysis of a commonly used protocol. Scientific Reports. 2015;5(1):17319.
137. Chhoy P, Brown CW, Amante JJ, Mercurio AM. Protocol for the separation of extracellular vesicles by ultracentrifugation from in vitro cell culture models. STAR Protocols. 2021;2(1):100303.

138. Chiu YJ, Cai W, Shih YR, Lian I, Lo YH. A Single-Cell Assay for Time Lapse Studies of Exosome Secretion and Cell Behaviors. Small. 2016;12(27):3658-66.
139. Koliopanos A, Friess H, Kleeff J, Shi X, Liao Q, Pecker I, et al. Heparanase expression in primary and metastatic pancreatic cancer. Cancer Res. 2001;61(12):4655-9.
140. Koo TH, Lee J-J, Kim E-M, Kim K-W, Kim HD, Lee J-H. Syntenin is overexpressed and promotes cell migration in metastatic human breast and gastric cancer cell lines. Oncogene. 2002;21(26):4080-8.
141. Liu R-T, Huang C-C, You H-L, Chou F-F, Hu C-CA, Chao F-P, et al. Overexpression of tumor susceptibility gene TSG101 in human papillary thyroid carcinomas. Oncogene. 2002;21(31):4830-7.
142. King HW, Michael MZ, Gleadle JM. Hypoxic enhancement of exosome release by breast cancer cells. BMC Cancer. 2012;12(1):421.
143. Li L, Li C, Wang S, Wang Z, Jiang J, Wang W, et al. Exosomes Derived from Hypoxic Oral Squamous Cell Carcinoma Cells Deliver miR-21 to Normoxic Cells to Elicit a Prometastatic Phenotype. Cancer Res. 2016;76(7):1770-80.
144. Kalluri R, LeBleu VS. The biology, function, and biomedical applications of exosomes. Science. 2020;367(6478):eaau6977.
145. Chen CD, Wang CS, Huang YH, Chien KY, Liang Y, Chen WJ, et al. Overexpression of CLIC1 in human gastric carcinoma and its clinicopathological significance. Proteomics. 2007;7(1):155-67.
146. Wang JW, Peng SY, Li JT, Wang Y, Zhang ZP, Cheng Y, et al. Identification of metastasis-associated proteins involved in gallbladder carcinoma metastasis by proteomic analysis and functional exploration of chloride intracellular channel 1. Cancer Lett. 2009;281(1):71-81.
147. Kim A, Ng WB, Bernt W, Cho N-J. Validation of Size Estimation of Nanoparticle Tracking Analysis on Polydisperse Macromolecule Assembly. Scientific Reports. 2019;9(1).
148. Hoo CM, Starostin N, West P, Mecartney ML. A comparison of atomic force microscopy (AFM) and dynamic light scattering (DLS) methods to characterize nanoparticle size distributions. Journal of Nanoparticle Research. 2008;10(S1):89-96.
149. Quek C, Bellingham SA, Jung C-H, Scicluna BJ, Shambrook MC, Sharples RA, et al. Defining the purity of exosomes required for diagnostic profiling of small RNA suitable for biomarker discovery. RNA Biology. 2017;14(2):245-58.
150. Chan MY, Dowling QM, Sivananthan SJ, Kramer RM. Particle Sizing of Nanoparticle Adjuvant Formulations by Dynamic Light Scattering (DLS) and Nanoparticle Tracking Analysis (NTA). Springer New York; 2017. p. 239-52.
151. Théry C, Witwer KW, Aikawa E, Alcaraz MJ, Anderson JD, Andriantsitohaina R, et al. Minimal information for studies of extracellular vesicles 2018 (MISEV2018): a position statement of the International Society for Extracellular Vesicles and update of the MISEV2014 guidelines. J Extracell Vesicles. 2018;7(1):1535750.
152. Escola J-M, Kleijmeer MJ, Stoorvogel W, Griffith JM, Yoshie O, Geuze HJ. Selective Enrichment of Tetraspan Proteins on the Internal Vesicles of Multivesicular Endosomes and on Exosomes Secreted by Human B-lymphocytes. Journal of Biological Chemistry. 1998;273(32):20121-7.
153. Mathieu M, Névo N, Jouve M, Valenzuela JI, Maurin M, Verweij FJ, et al. Specificities of exosome versus small ectosome secretion revealed by live intracellular tracking of CD63 and CD9. Nature Communications. 2021;12(1).
154. Kobayashi M, Salomon C, Tapia J, Illanes SE, Mitchell MD, Rice GE. Ovarian cancer cell invasiveness is associated with discordant exosomal sequestration of Let-7 miRNA and miR-200. Journal of Translational Medicine. 2014;12(1):4.
155. Lee AH, Ghosh D, Quach N, Schroeder D, Dawson MR. Ovarian Cancer Exosomes Trigger Differential Biophysical Response in Tumor-Derived Fibroblasts. Scientific Reports. 2020;10(1).
156. Young TW, Mei FC, Rosen DG, Yang G, Li N, Liu J, et al. Up-regulation of Tumor Susceptibility Gene 101 Protein in Ovarian Carcinomas Revealed by Proteomics Analyses. Molecular & Cellular Proteomics. 2007;6(2):294-304.

157. Colombo M, Moita C, Van Niel G, Kowal J, Vigneron J, Benaroch P, et al. Analysis of ESCRT functions in exosome biogenesis, composition and secretion highlights the heterogeneity of extracellular vesicles. Journal of Cell Science. 2013;126(24):5553-65.
158. Kowal J, Arras G, Colombo M, Jouve M, Morath JP, Primdal-Bengtson B, et al. Proteomic comparison defines novel markers to characterize heterogeneous populations of extracellular vesicle subtypes. Proceedings of the National Academy of Sciences. 2016;113(8):E968-E77.
159. Zhang Y, Qian H, Xu A, Yang G. Increased expression of CD81 is associated with poor prognosis of prostate cancer and increases the progression of prostate cancer cells in vitro. Exp Ther Med. 2020;19(1):755-61.
160. Signorelli D, Ghidotti P, Proto C, Brambilla M, De Toma A, Ferrara R, et al. Circulating CD81-expressing extracellular vesicles as biomarkers of response for immune-checkpoint inhibitors in advanced NSCLC. Front Immunol. 2022;13:987639.
161. Kumar D, Gupta D, Shankar S, Srivastava RK. Biomolecular characterization of exosomes released from cancer stem cells: Possible implications for biomarker and treatment of cancer. Oncotarget. 2015;6(5):3280-91.
162. Mitra A, Yoshida-Court K, Solley TN, Mikkelson M, Yeung CLA, Nick A, et al. Extracellular vesicles derived from ascitic fluid enhance growth and migration of ovarian cancer cells. Scientific Reports. 2021;11(1).
163. Chen X, Zhou J, Li X, Wang X, Lin Y, Wang X. Exosomes derived from hypoxic epithelial ovarian cancer cells deliver microRNAs to macrophages and elicit a tumor-promoted phenotype. Cancer Letters. 2018;435:80-91.
164. Xiao Y, Li Y, Yuan Y, Liu B, Pan S, Liu Q, et al. The potential of exosomes derived from colorectal cancer as a biomarker. Clinica Chimica Acta. 2019;490:186-93.
165. Liang B, Peng P, Chen S, Li L, Zhang M, Cao D, et al. Characterization and proteomic analysis of ovarian cancer-derived exosomes. Journal of proteomics. 2013;80:171-82.
166. Sinha A, Ignatchenko V, Ignatchenko A, Mejia-Guerrero S, Kislinger T. In-depth proteomic analyses of ovarian cancer cell line exosomes reveals differential enrichment of functional categories compared to the NCI 60 proteome. Biochemical and Biophysical Research Communications. 2014;445(4):694-701.
167. Peng P, Zhang W, Cao D, Yang J, Shen K. The proteomic comparison of peripheral circulation-derived exosomes from the epithelial ovarian carcinoma (EOC) patients and non-EOC subjects. Translational Cancer Research. 2019;8(2):452-65.
168. Jamshad M, Rajesh S, Stamataki Z, McKeating JA, Dafforn T, Overduin M, et al. Structural characterization of recombinant human CD81 produced in Pichia pastoris. Protein Expr Purif. 2008;57(2):206-16.
169. Szajnik M, Derbis M, Lach M, Patalas P, Michalak M, Drzewiecka H, et al. Exosomes in plasma of patients with ovarian carcinoma: potential biomarkers of tumor progression and response to therapy. Gynecology & obstetrics (Sunnyvale, Calif). 2013:003.
170. Zhou G, Gu Y, Zhu Z, Zhang H, Liu W, Xu B, et al. Exosome Mediated Cytosolic Cisplatin Delivery Through Clathrin-Independent Endocytosis and Enhanced Anti-cancer Effect via Avoiding Endosome Trapping in Cisplatin-Resistant Ovarian Cancer. Front Med (Lausanne). 2022;9:810761.
171. Kasetsirikul S, Tran KT, Clack K, Soda N, Shiddiky MJA, Nguyen N-T. Low-cost electrochemical paper-based device for exosome detection. The Analyst. 2022;147(16):3732-40.
172. Hossain KR, Escobar Bermeo JD, Warton K, Valenzuela SM. New Approaches and Biomarker Candidates for the Early Detection of Ovarian Cancer. Front Bioeng Biotechnol. 2022;10:819183.
173. Orozco AF, Lewis DE. Flow cytometric analysis of circulating microparticles in plasma. Cytometry Part A. 2010;77(6):502-14.
174. Shao H, Chung J, Balaj L, Charest A, Bigner DD, Carter BS, et al. Protein typing of circulating microvesicles allows real-time monitoring of glioblastoma therapy. Nature medicine. 2012;18(12):1835-40.

175. Jørgensen M, Bæk R, Pedersen S, Søndergaard EK, Kristensen SR, Varming K. Extracellular Vesicle (EV) Array: microarray capturing of exosomes and other extracellular vesicles for multiplexed phenotyping. Journal of extracellular vesicles. 2013;2(1):20920.
176. Im H, Shao H, Park YI, Peterson VM, Castro CM, Weissleder R, et al. Label-free detection and molecular profiling of exosomes with a nano-plasmonic sensor. Nature biotechnology. 2014;32(5):490-5.
177. Sullivan R, Maresh G, Zhang X, Salomon C, Hooper J, Margolin D, et al. The emerging roles of extracellular vesicles as communication vehicles within the tumor microenvironment and beyond. Frontiers in Endocrinology. 2017;8:194.
178. Lässer C. Exosomal RNA as biomarkers and the therapeutic potential of exosome vectors. Expert opinion on biological therapy. 2012;12(sup1):S189-S97.